FINAL REPORT

NASA CONTRACT NAG 8-149

PROJECT JOVE

AUGUST, 1994

Dr. M.J. Lyell, P.I.
Mechanical & Aerospace Engr. Dept.
Box 6106
West Virginia University
Morgantown, WV 26505-6106
(304) 293-3111

FINAL REPORT

NASA CONTRACT NAG 8-149
PROJECT JOVE

AUGUST, 1994

Dr. M.J. Lyell, P.I.
Mechanical & Aerospace Engr. Dept.
Box 6106
West Virginia University
Morgantown, WV 26505-6106
(304) 293-3111

CONTENTS

PROJECT OVERVIEW:

This final report for Project JOVE (NASA Contract NAG8-149) presents the results of work performed. Efforts under this contract involved a research component, an education component, and an outreach component.

Early on, the research effort under JOVE was concerned with identifying specific research activities of interest to both the principal investigator and NASA technical interests. In the work of this principal investigator, the research efforts were concerned with the behavior of fluid dynamics in a microgravity environment; in particular, the free surface/interface behavior of fluid configurations. Earlier work centered on the behavior of "slab" configurations. More recent efforts have looked at the finite length fluid column behavior under forcing. It is emphasized that the multiplicity of research tasks was considered to be open-ended (ie., there's always more research to be done).

Indeed, part of the agenda of the JOVE project has been to involve more university researchers in research of interest to NASA. To this end, it was understood that the principal investigator would seek additional sources of funding. The proposals which were written to do this are listed in the following chapter on Project Accomplishments.

A new focus for Year 4 of the JOVE project was the effort to identify practical applications of free surface fluid mechanics which would have applications in microgravity fluid mechanics or be relevant to another aspect of the NASA mission and be also of some commercial interest. The thrust was to seek not only novel

application area(s) in which research would contribute to the technology, but also to identify problems which are accessible via a fully computational fluid dynamics methodology. This is a departure from the previous JOVE efforts, which involved primarily theoretical formulations. The results of this investigation are listed in Section A of this volume of the final report.

Research results on the interface shape and stability of the slab configuration are given in the additional volume labeled "SUPPLEMENT I ---- INTERFACE BEHAVIOR OF A MULTI-LAYER FLUID CONFIGURATION SUBJECT TO ACCELERATION IN A MICROGRAVITY ENVIRONMENT". (This volume is essentially the thesis work done by a graduate student who was supported by the contract, and who received a masters degree in mechanical engineering.)

With regard to the research investigations which focused on the interface behavior of the fluid cylinder in microgravity, the results may be perused as follows. The problem of the response of a finite length fluid column to forcing along the longitudinal axis of the column was accomplished via Laplace transform techniques. This work is presented in Section B of this volume of the final report. The results of the investigation on the interface stability of an infinite length fluid column subject to periodic accelerations oriented perpendicular to the longitudinal axis of the column are found in Section B also.

Nonlinear behavior was taken into account in one of the investigations of finite length fluid column interface behavior in microgravity. In this case, the focus was on the nonlinear corrections to the normal modes of free oscillation of the finite length fluid column. It was not necessary that the fluid column be

restricted to the slender column limit case. The analysis was inviscid and incompressible, and the perturbations were assumed irrotational. Also, the disturbances were restricted to those which are axisymmetric. Additional details and results on this problem are found in "SUPPLEMENT II ---- NONLINEAR EFFECTS ON THE NATURAL MODES OF OSCILLATION OF A FINITE LENGTH INVISCID FLUID COLUMN". This is in another spiral volume of the final report. (This volume is essentially the first draft of the dissertation of a Ph.d. student who has been supported by the JOVE contract.)

With regard to the problem of the interface stability of the finite length fluid column subject to both periodic disturbances and a static acceleration oriented normal to the longitudinal axis of the column, the full theoretical formulation of the problem, including the static deformation, has been made. The numerical investigation is underway, and when finished, results will be submitted for publication. A discussion may be found in Section C of this volume of the final report.

The educational efforts of this program have involved the instruction and supervision of graduate students (2 masters level and 1 ph.d level), and the teaching of a graduate course specialized to include free surface/interface behavior in microgravity. These will be listed in the JOVE accomplishments. A syllabus for the graduate class is attached in Section E of this volume of the final report.

The outreach efforts of this project consisted primarily of lectures/talks given to the general public. However, one of the outreach events involved a "workshop style" presentation to middle school-junior high age girls. The workshop introduced the girls to

the world of an aerospace engineer, and involved some hands-on demonstrations of flight principles. Spacecraft and microgravity were part of this. (The workshop was co-sponsored by the WV chapter of the Association for Women in Science (AWIS) , the WV Dept. of Education--Office of Sex Equity, the AAUW, and the Southern West Virginia Community College).

JOVE ACCOMPLISHMENTS

RESEARCH:

REFEREED JOURNAL ARTICLES PUBLISHED:

(1.) M.J. Lyell, "Fluid column stability in the presence of periodic accelerations", AIAA Journal, Vol. 31, p. 1519-21, 1993.

(2.) M.J. Lyell, "Axial forcing of a finite length liquid column", Phys. Fluids , Vol. 3, p. 1828-31, 1991.

(3.) M.J. Lyell and M. Roh, "The effect of time-dependent accelerations on interface stability in a multi-layered configuration", AIAA Journal, Vol. 29, p. 1894-1990, 1991.

Manuscript in Preparation: to be submitted to Physics of Fluids by Sept. 30, 1994, entitled, "Nonlinear corrections to interface shape and oscillation frequencies of a finite length inviscid liquid column in microgravity", by M.J. Lyell and L. Zhang.

OTHER PUBLICATIONS:

(1.) M.J. Lyell and L.Zhang, "On the nonlinear dynamics of liquid bridges", Proceedings, 12th U.S. National Congress of Applied Mechanics, 1994. (Conference held in Seattle, WA, in June, 1994.)

(2.) M.J. Lyell, "Interface stability of a fluid column subject to periodic acceleration oriented normal to the longitudinal axis of the column", presented at the World Space Congress, held Washington, D.C., Aug. 1992, PAPER NUMBER IAF-92-0914.

(3.) M.J. Lyell, "Interface stability of a liquid column in the presence of periodic accelerations oriented normal to the longitudinal axis", Bull. Am. Phys. Soc., Vol. 37, 1992.

(4.) M.J. Lyell and M. Roh, "Instabilities in a multi-slab fluid configuration due to time-dependent acceleration normal to the fluid-fluid interface in a microgravity environment", 29th AIAA Aerospace Science Conference (held Jan., 1991, Reno, NV), AIAA PAPER 91-1019.

(5.) M. Roh and M.J. Lyell, "Investigation of Interface in a Multiple Layer Slab Configuration--Utilizing WVNET Computational Resources", WVNET Conference 1990 Proceedings, p. 27-39, 1990.

TEACHING:

GRADUATE STUDENTS:

(1.) Ms. L. Zhang

Ph.d. Candidate, MAE

Research Area: fluid mechanics/non-linear oscillations.

Dissertation Topic: Nonlinear corrections to the natural oscillations of a finite length inviscid liquid column in microgravity.

Anticipated graduation date: Dec. 1994.

(2.) Ms. K. Perkins

MSAE Candidate

Research Area: Fluid mechanics , ferrofluids, free surfaces.

Thesis topic: Wave dynamics in ferrofluids.

Anticipated degree date: Dec. 1995.

(3.) Mr. Michael Roh

MSME Degree awarded May, 1991.

Research area: Fluid mechanics.

Thesis topic: Stability of fluid layer configurations subject to time-varying acceleration with application to microgravity fluid mechanics.

COURSES:

(1.) MAE 399 --SPECIAL TOPICS GRADUATE COURSE

entitled "Fluid dynamics of free surfaces/ interfacial fluid mechanics" .

Course formally taught to 1 student in Fall semester, 1993.

Syllabus for this course in Section E of this volume of the final report.

OUTREACH:

(1.) Event: Workshop and Question and Answer Panel.
March, 1994 , at WV Southern Community College, Williams, WV.
65-80 participants (middle school-junior high girls).
workshop on "Up, up, and Away, The World of an Aerospace Engineer".

(2.) Event: Lecture/ film / handouts
Oct., 1991, at Cheat Lake Junior HS, Morgantown (Cheat Lake area) , WV.
80 participants.
handout on space suit designs.

(3.) Event: Invited speaker at Sigma Xi meeting.
Dec., 1990, at Marshall Univ., Huntington, WV.
25-30 participants.
"general lecture" to audience with diverse scientific backgrounds.

SECTION A

Investigation of Potential Research Topics of Scientific and Commercial Interest Relevant to Microgravity Fluid Mechanics

Abstract

The goal of this project is to investigate new areas of research pertaining to free surface-interface fluids mechanics and/or microgravity which have potential commercial applications. This paper presents an introduction to ferrohydrodynamics (FHD), and discusses some applications. Also, computational methods for solving free surface flow problems are presented in detail. Both have diverse applications in industry and in microgravity fluids applications. Three different modeling schemes for FHD flows are addressed and the governing equations, including Maxwell's equations are introduced. In the area of computational modeling of free surface flows, both Eulerian and Lagrangian schemes are discussed. The state of the art in computational methods applied to free surface flows is elucidated. In particular, adaptive grids and rezoning methods are discussed.

Table of Contents

Chapter I
Overview

The goal of this project was to investigate new areas pertaining to microgravity which have potential commercial applications. The two topics studied for this project were state of the art computational methods for solving free surface flow problems and ferrohydrodynamic free surface flows.

Free surface and interface flows do indeed have many commercial applications in diverse areas. These include crystal growth, melting and solidification, capillary flows, wave propagation, and metal and glass forming processes.

Ferrohydrodynamics deals with fluid dynamics that occurs in a magnetic fluid as a result of an applied magnetic field. A ferrofluid is a colloidal suspension of solid magnetic particles in a typically Newtonian parent liquid. These fluids also have many applications, including rotary shaft seals, cooling processes, and sink-float separation processes.

A number of interesting phenomena are exhibited by magnetic fluids in response to applied magnetic fields. These include a normal field instability, in which a pattern of spikes appears on the fluid surface. Also, in thin layers of ferrofluid, there exists the spontaneous formation of labyrinthine patterns. In rotary fields, a body couple is generated which is manifested as anti-symmetric stress. In addition, ferrofluids with temperature-dependent magnetic moment allow for enhanced convective cooling.

Ferrohydrodynamics is a fairly new area of study, since the onset of research in this field began in the 1960s. There is still much to be discovered in this area, and linking ferrofluids with free surface flow problems can lead to many interesting new developments.

Chapter II of this paper gives a brief introduction into ferrohydrodynamics. This section also discusses some of the many applications involving ferrofluids.

There are three primary modeling schemes which are appropriate in analyzing ferrofluid motion--(1) restriction to inviscid flow, (2) viscous flow with a symmetric stress tensor, and (3) viscous flow with a non-symmetric stress tensor. Situations are given in which each scheme would be applicable. In addition, the main governing equations for ferrofluid motion in each modeling type and the equations for the magnetic field conditions (including Maxwell's equations) are included in the discussion.

Chapter III discusses state of the art computational methods for solving free surface flow problems. Found in this chapter is a discussion on Eulerian and Lagrangian computational methods for solving free surface problems, with several examples given in detail. Also discussed is the efficacy of finite differences versus finite element formulations.

Chapter IV gives conclusions regarding this project. Suggestions are provided for future research ideas arising from the investigation of free surface flows and ferrohydrodynamics.

Chapter II

Introduction to Ferrohydrodynamics

Ferrohydrodynamics (FHD) deals with the mechanics of fluid movement that is influenced by an applied magnetic field. In FHD, there is usually no electric current flowing in the fluid, as opposed to magnetohydrodynamics (MHD). (In MHD flows the body force acting on the fluid is the Lorentz force that results when electric current flows at an angle to the direction of an applied magnetic field). A ferrofluid is a colloidal suspension of solid magnetic particles in typically a Newtonian parent liquid such as kerosene. In a true ferrofluid, the colloid suspension never settles out because the particles are small enough (3-15 nm) that thermal agitation keeps them suspended. In addition, particles are coated with a dispersant that provides for short range repulsion and prevents agglomeration of the particles. A typical ferrofluid contains 10^{23} particles per cubic meter and is opaque to visible light. Ferrofluids are not found in nature, but are the result of laboratory synthesis. Ferrofluids retain their fluid nature even in intense magnetic fields (Rosenweig, 1985, and Cowley and Rosenweig, 1967).

The body force in FHD flows is due to a polarization force. This requires that the magnetic particles in the ferrofluid align in the presence of an applied magnetic field. The particles in a colloidal ferrofluid have an embedded magnetic moment. When the magnetic field is absent, these particles are randomly oriented,

and the fluid has no net magnetization. When ordinary field strengths are applied, thermal agitation partially overcomes the tendency of the dipole moments to align with the applied field. However, as the magnitude of the magnetic field increases, the particles become more aligned with the direction of the field. In the presence of very intense magnetic fields, the particles may align completely, and the magnetization is said to be saturated.

Applications of ferrofluids are diverse. These include zero leakage rotary shaft seals used in computer disk drives, vacuum feed throughs, and pressure seals for compressors and blowers. Also widely available are liquid cooled speakers that use drops of ferrofluid to conduct heat away from the speaker coils. In the medical field, the use of a magnetic field can direct the path of a drop of ferrofluid in the body, which allows for the directing of drugs to a target site. In addition, ferrofluids can be employed as a tracer of blood flow in non-invasive circulatory measurements. In other areas, high volumes of ferrofluids are utilized in sink-float separation processes that use the artificial high specific gravity imparted to a pool of ferrofluid subjected to a magnetic field. This process is used to separate scrap metals and is also used to sort diamonds. Ferrofluids are also being considered as a possible candidate for ink in high-speed, silent printers.

Modeling of physical problems which involve ferrofluids typically utilize on of three modeling approaches:

1) inviscid flow

2) viscous flow with a symmetric stress tensor

3) viscous flow with a non-symmetric stress tensor.

Inviscid flows

This approach is utilized when there exists no shearing stresses in the flow. This is the case when flow configurations have no bulk motion or when the flow is irrotational (Cowley and Rosenweig, 1967). Such problems include wave motion on a surface and/or the study of interfacial processes.

The governing equations for these flows include:

The Continuity equation

$$\nabla \cdot \underline{u} = 0 \tag{2.1a}$$

The Momentum equation

$$\frac{\partial \underline{u}}{\partial t} + \underline{u} \cdot \nabla \underline{u} = -\frac{1}{\rho} P^* + \mu_0 M \nabla H \tag{2.1b}$$

where $\underline{u}$ is the velocity vector, μ_0 is the magnetic permeability of free space, P^* is the modified pressure, M is the magnitude of the magnetization of the fluid, $\underline{M}$, and H is the magnitude of the magnetic field vector applied to the fluid, $\underline{H}$. The modified pressure P^* is given by

$$P^* = P(\rho, T) + \mu_0 \int_0^H \left(v \frac{\partial M}{\partial v}\right)_{H,T} dM + \mu_0 \int_0^H M \, dH \tag{2.2}$$

$$P^* = P(\rho, T) + P_s + P_m$$

The magnetostrictive pressure is given by P_s, and the fluid magneto

pressure by P_m.

If the flow is irrotational, the velocity can be expressed in terms of the potential, ϕ, with

$$\underline{u} = \nabla\phi \tag{2.3}$$

Substitution of this expression for the velocity into the continuity equation leads to the Laplace Equation

$$\nabla^2 \phi = 0 \tag{2.4}$$

The magnetic field is governed by Maxwell's equations, which are the following:

$$\nabla \times \underline{E} = - \frac{\partial \underline{B}}{\partial t} \tag{2.5}$$

where $\underline{E}$ is the electric field and $\underline{B}$ is the magnetic induction field which is defined as

$$\underline{B} \equiv \mu_0 (\underline{H} + \underline{M}) \tag{2.6}$$

and

$$\underline{M} = (\mu - 1) \underline{H} \tag{2.7}$$

where μ is the magnetic permeability of the fluid.

$$\nabla \cdot \underline{D} = \rho_f \tag{2.8}$$

where $\underline{D}$ is the electric displacement and ρ_f is the free charge due to electricity.

$$\nabla \times \underline{H} = \underline{J_f} + \frac{\partial \underline{D}}{\partial t} \quad (2.9)$$

where $\underline{J_f}$ is the electric current.

$$\nabla \cdot \underline{J_f} = - \frac{\partial \rho_f}{\partial t} \quad (2.10)$$

$$\nabla \cdot \underline{B} = 0 \quad (2.11)$$

If there is no electric field/electric current, then Maxwell's equations reduce to:

$$\nabla \times \underline{H} = \underline{0} \quad (2.12)$$

$$\nabla \cdot \underline{B} = 0 \quad (2.13)$$

It follows that with $\underline{B}$ proportional to $\underline{H}$, or for uniform $\underline{M}$,

$$\nabla \cdot \underline{H} = 0 \quad (2.14)$$

Since the magnetic field is irrotational, $\underline{H}$ can be expressed as

$$H = -\nabla \psi \tag{2.15}$$

where ψ is the magnetic field potential. Substitution into equation 2.14 yields

$$\nabla^2 \psi = 0 \tag{2.16}$$

Typical boundary conditions at an interface and/or free surface include:

The Kinematic Condition

The kinematic condition relates the interface deflection to the motion of the adjacent fluid. When the surface position changes with time, the location of the interface can be represented as

$$z = z_0(x, y; t)$$

If a Monge function is defined by $Fe(x, y, z; t) \equiv z - z_0(x, y; t)$, then the kinematic equation at the interface is

$$\frac{\partial Fe}{\partial t} + \underline{u_1} \cdot \nabla Fe = \frac{\partial Fe}{\partial t} + \underline{u_2} \cdot \nabla Fe = 0 \tag{2.17}$$

Normal Force Balance

$$P_1^* + \frac{1}{2}\mu_0 M_{n_1}^2 = P_2^* + \frac{1}{2}\mu_0 M_{n_2}^2 + \sigma \nabla \cdot \hat{n} \tag{2.18}$$

where subscripts 1 and 2 denote fluid properties above and below the interface. The surface tension of the interface is denoted by σ. The outward normal to the interface is given by $\underline{n} = \nabla Fe/|\nabla Fe|$

Also, other boundary conditions which depend on the configuration of the problem are needed. These involve constraints on the magnetic field and fluid variables.

Viscous flows with a symmetric stress tensor

When considering viscous flows with $\underline{M}$ and $\underline{H}$ collinear, the viscous stress tensor, $\underline{T}$, is symmetric. A ferrofluid will always have a symmetric stress tensor if it is superparamagnetic, which means the solid particles instantaneously align with the magnetic field ($\underline{M}$ and $\underline{H}$ are collinear). The equation for the viscous stress tensor is given by

$$T = - P \delta_{ij} + \eta \left(\frac{\partial u_i}{\partial x_j} + \frac{\partial u_j}{\partial x_i}\right) + \delta_{ij} \lambda \left(\frac{\partial u_i}{\partial x_i}\right) \qquad (2.19)$$

The equation for the magnetic stress tensor is

$$\underline{T_m} = - \left[\int_0^H \mu_0 \left(\frac{\partial \upsilon M}{\partial \upsilon}\right)_{H,\theta} dH + \frac{1}{2} \mu_0 H^2\right] \delta_{ij} + B_i H_j \qquad (2.20)$$

Flow configurations involving incompressible viscous fluids and a symmetric viscous stress tensor are governed by the

continuity equation and the conservation of momentum equation as well as Maxwell's equations. In this case, the conservation of momentum equation is given by

$$\rho \frac{D\underline{u}}{Dt} = -\nabla P + \rho \underline{g} + \eta \nabla^2 \underline{u} - \nabla[\mu_0 \int_0^H [\frac{\partial(\upsilon M)}{\partial \upsilon}]_{H,\theta} dH] + \mu_0 M \nabla H \qquad (2.21)$$

The equation assumes that the flow is incompressible and isothermal with constant viscosity, η. Here, θ is the temperature of the fluid and $\upsilon = \rho^{-1}$. Also, the body force term of gravity is included in equation (2.21) and also could be included in equation (2.1b) if so desired.

Additional boundary conditions arise at the interface/free surface for viscous flow problems. These include the continuity of the tangential velocity components at the interface and the implementation of a tangential stress balance at the interface.

Viscous flows with a non-symmetric stress tensor

Up to this point, the magnetization $\underline{M}$ has been collinear with the magnetic field, $\underline{H}_0$, which is the case in static equilibrium. If superparamagnetism in the ferrofluid is obtained, collinearity is an adequate assumption, because the direction of $\underline{M}$ rotates freely within the magnetic particle. Conversely, in

paramagnetic fluids, the particles in the fluid have a magnetic moment that is locked to the orientation of the particle. If $\underline{\mathbf{H}}$ changes direction, $\underline{\mathbf{M}}$ responds by particle rotation, which is a much slower process because it is resisted by fluid viscous-drag torque. The result constitutes a body couple of $\mu_0 \underline{\mathbf{M}} \times \underline{\mathbf{H}}$. When this body couple is present, the viscous stress tensor is no longer symmetric.

This phenomenon occurs in several cases. For example, if a beaker of magnetic fluid is subjected to a rotating magnetic field, a non-symmetric stress tensor will result. In addition, any flow that possesses vorticity and is subject to a steady magnetic field will have some degree of antisymmetric stress present. Also, this phenomenon occurs in cases in which a steady field is imposed on a ferrofluid moving across a stationary flat plate. The result in this third case is that the velocity in the fluid in the boundary layer adjacent to the plate becomes coupled to the field. The boundary flow is rotational, tending to reorient the magnetic particles of the ferrofluid in the magnetic field. Thus relative rotation of particles and the carrier liquid results. However, if the field is parallel to the plate and perpendicular to the flow, there is no coupling, because the particles can rotate freely with their axes parallel to the field direction.

A system may not only exchange linear momentum with its surroundings, but it can also exchange angular momentum. The rate of linear momentum gained from the surroundings is accounted for by the body force $\underline{\mathbf{F}}$. In addition, the surroundings may transmit

angular momentum through a body couple, $\underline{G}$. A surface traction exists

$$\underline{t_n} = \hat{n} \cdot \underline{T} \tag{2.22}$$

per unit area of the surface, (where $\underline{T}$ is the fluid's stress tensor), which is either accumulated within the system, or is removed to the surroundings as linear momentum. The surroundings also exert on the surface of the system a couple $\underline{c_n}$ per unit area.

Let $\underline{L}$ denote the total local density of angular momentum. Then $\underline{L}$ is written

$$\underline{L} = \underline{r} \times \underline{u} + \underline{s} \tag{2.23}$$

where $\underline{r} \times \underline{u}$ is the external angular momentum and $\underline{s}$ is the internal angular momentum, or spin. The spin field describes the rotation of the magnetic particles in the ferrofluid and the viscous fluid that is entrained by the particles.

Coupling exists between internal and external forms of angular momentum. The integral form of the equation balancing the total angular momentum is

$$\frac{D}{Dt}\int_V \rho\,(\underline{s} + \underline{c} \times \underline{u})\,dV = \int_V (\rho\underline{G} + \underline{r} + \rho\underline{F})\,dV + \int_S (\underline{c_n} + \underline{r} \times \underline{t_n})\,dS \tag{2.24}$$

c_n accounts for the presence of a surface-couple density acting on the surface, and is expressed by the following:

$$\underline{c_n} = \hat{n} \cdot (\hat{i}\, c_x + \hat{j}\, c_y + \hat{k}\, c_z) = \hat{n} \cdot \underline{\underline{c}} \qquad (2.25)$$

The expression in parentheses is the couple stress tensor $\underline{\underline{c}}$. This couple can arise from viscous diffusive transport of internal momentum.

Thus, the differential equation governing the change in total angular momentum is

$$\rho \frac{D}{Dt} (\underline{s} + \underline{r} + \underline{u}) = \rho \underline{G} + \underline{r} \times \rho \underline{F} + \nabla \cdot \underline{\underline{c}} + \underline{r} \times (\nabla \underline{\underline{T}}) + \underline{A} \qquad (2.26)$$

where

$$\underline{A} = \epsilon_{ijk}\, \hat{e}_i\, T_{jk}$$

ϵ_{ijk} = +1 if ijk = 123, 231, or 312

-1 if ijk = 321, 132, or 213

0 if i = j, i = k, or j = k

Chapter III

Computational Methods For Solving Free Surface Flows

Free surface flows can be divided into three main areas: (1) those concerned with wave motion on the surface, (2) bulk fluid motion in a configuration which involves a free surface, and (3) interfacial processes on the two-dimensional free surface itself. Solid boundaries can further complicate the configuration, giving rise to finite domain problems involving both free and fixed boundaries.

Computational solutions techniques will change, depending on whether the flow is viscous or inviscid, steady or unsteady, and whether the analysis is linear or nonlinear.

The governing equations for free surface/interfacial flow problems include:

The Continuity equation

$$\frac{\partial \rho}{\partial t} + \nabla \cdot \rho \underline{u} = 0 \qquad (3.1a)$$

or

$$\nabla \cdot \underline{u} = 0 \qquad (3.1b)$$

in the case in which the fluid is incompressible.

Conservation of Momentum equation

$$\rho\left(\frac{\partial \underline{u}}{\partial t} + \underline{u} \cdot \nabla \underline{u}\right) = -\nabla P + \rho \underline{g} + \mu \nabla^2 u \qquad (3.2)$$

for viscous, incompressible flows. If the flow is inviscid, the last term on the right side of the equation is absent.

Boundary Conditions for inviscid flows

1. If the flow is inviscid, the normal velocity components at an interface must be equated.
2. The normal force balance for free surface flows is

$$\Delta P = \sigma \nabla \cdot \hat{n} \qquad (3.3)$$

where n is the unit outward normal to the interface, σ is the surface tension and ΔP denotes the difference in pressures of the fluids above and below the interface.

$$P = P_0 - \rho \frac{\partial \phi}{\partial t} - \frac{\rho}{2} \nabla\phi \cdot \nabla\phi - \rho g z \qquad (3.4)$$

on $z = 1 + \eta$

where ϕ is the velocity potential obtained from $\underline{u} = \nabla \phi$, and η is the shape of the interface.

3. The Kinematic Condition

Define $Fe = z - \eta(x,y,t)$, then

$$\frac{\partial Fe}{\partial t} + \underline{u} \cdot \nabla Fe = 0 \qquad (3.5)$$

This ensures that particles on an interface remain on the interface.

Boundary Conditions for Viscous Flows

1. Velocity components corresponding to upper and lower regions must be equated.
2. The kinematic condition (the same equation as for inviscid flows).
3. A normal and tangential stress balance must be utilized.

If the configuration of the problem is temperature dependent, then the Conservation of Energy equation must also be utilized.

$$\rho c_p \frac{D\theta}{Dt} = k \nabla^2 \theta \qquad (3.6)$$

where θ is the temperature, k is the thermal conductivity of the fluid, and c_p is the specific heat of the fluid at constant pressure. Note that contribution from viscous heating and any potential thermal source have been neglected

These above equations illustrate in general the system which must be solved. However, additional thermal and fluid boundary conditions specific to the particular configuration would be needed in order to formulate the problem properly. Once formulated, the problem would be solved via techniques of computational fluid mechanics.

From the literature search, a database was formed by culling articles published in Journal of Computational Physics and International Journal of Numerical Methods in Fluids and further references obtained from selected journals. This database is

included in the report as Appendix E. From these references, it was determined that the type of computational grid used in free surface problems can be either Eulerian or Lagrangian in nature. In an Eulerian grid, the cells remain fixed in the domain of the problem and fluid movement through the cells is tracked. In contrast, Lagrangian grids have cells that move along with the fluid so that the same cell in the mesh is associated with the same fluid element. The choice of using either method is application specific and both configurations are widely used.

Eulerian Methods

It has also been discovered that Eulerian methods can be further divided into three categories:

1. Fixed Grid Methods
2. Adaptive Grid Methods
3. Mapping Methods

In the fixed grid method, the grid does not change in the domain of the problem. Finite difference methods have been mainly used for fixed grids because these are predominantly utilized for the simplest types of flow configurations. The two basic ways of tracking the interface are surface tracking methods (Marker and Cell) and volume tracking methods (Volume of Fluid). These methods are detailed in Appendix A and B.

Surface tracking involves specifying a set of marker particles on the surface. The particles move according to the governing equations of the flow--usually the Navier-Stokes equations and the continuity equation. In volume tracking, however, each interface

cell is specified by a fractional volume of fluid in the cell. A function is defined that denotes which cells have fluid, which ones are partially filled, and which ones are empty. The surface cells are those that are adjacent to empty cells.

In general, the moving interface does not coincide with a grid line in fixed grid methods. In this case, special book-keeping procedures must be included in the algorithm in order to handle this. It is difficult to calculate the position of the interface accurately.

Some advantages to using fixed grids are:

1. It is possible for interfaces to undergo large deformations with little loss of accuracy.
2. It is straightforward to handle multiple interfaces.

Adaptive grid methods involve moving meshes where the motion of the grid is linked to the deformation of the interface. They are still considered Eulerian because the domain remains fixed. These methods are much more versatile in that either steady or unsteady flow can be handled. The main reasons for using adaptive grids are:

1. The grid can be moved in the interior of the solution domain so that local accuracy can be attained, if desired.
2. In moving boundary problems, the grid can conform to geometry changes in the problem.

Finite elements are preferred for adaptive grids because they are more efficient in handling complex geometrical configurations. A disadvantage of this method is that if there are large

distortions in the free surface, the grid can become twisted, causing the solution to the field variables to be highly difficult.

Further exposition of adaptive grids can be found in Appendix C.

In the mapping method, an unknown, irregularly shaped flow domain is transformed onto a fixed and regularly shaped computational domain. By utilizing this technique, it becomes fairly easy to obtain a finite difference mesh for which boundaries coincide with mesh lines. The mapping function is an explicit unknown and must be determined along with the field variables. However, it is quite difficult to determine, in the general case, what the appropriate mapping function is. Appendix D presents some details on mapping methods for the specific problem of a bubble moving in an unbounded liquid.

Lagrangian Methods

Lagrangian methods are well suited for free surface problems because they allow material interfaces to be specifically delineated and precisely followed. In addition, interface boundary conditions can be easily applied.

Lagrangian methods can be categorized in two ways:

1. Strictly Lagrangian methods
2. Lagrangian methods with rezoning

In strictly Lagrangian methods, the computation grid topology is fixed and it moves along with the fluid. Clearly, these cases should only be used for limited evolution times so that mesh tangling does not occur.

A well known Lagrangian scheme of type 1 is a method proposed by Hirt et al (1970), referred to as LINC (Lagrangian Incompressible). This technique is used for transient two-dimensional flow of viscous and incompressible free surface configurations. This method employs a finite volume discretization with quadrilateral cells. Positions, velocities, and body accelerations are defined at the vertices. The pressures and stress tensors are stored at the center of each cell. The pressure of a given cell is derived by the constraint that the volume of each cell remains constant when vertices are moved to a different position. As a result, a Poisson-like equation is developed.

Lagrangian methods with rezoning are introduced when the computational mesh become severely distorted. In this case, a new mesh is developed and information from the old mesh is transferred to the new one. Typically, this procedure calls for a Lagrangian phase followed by a rezoning phase where mesh points are moved to the prescribed positions. If rezoning occurs at every time step, the process is called continuous rezoning. However, if rezoning occurs after many time steps, but before the mesh becomes tangled, the process is called general rezoning.

Rezoning of the Lagrangian boundary vertices simplifies further the treatment of strongly distorted interfaces. This involves tangential rezoning, which equalizes the spacing of vertices along an interface, and normal rezoning, which eliminates the interface distortion that cannot be resolved with the employed grid structure. Newer Lagrangian methods can track an interface

through large distortions with the use of rezoning even with surface tension effects included.

A further issue raised in the literature concerns the efficacy of finite difference techniques versus finite element methods. It is noted that the choice of method depends on the configuration of the problem. Finite differences are preferred when fixed grids and mapping methods are employed. Finite elements, however, are more suited to moving boundary problems where adaptive grids are used. Also, finite elements are more efficient when complicated geometries of the flow exist.

Chapter IV

Conclusions and Recommendations

The combination of the topics of ferrohydrodynamics and free surface fluid dynamics proves to be highly relevant to commercial research applications. There also exists a considerable amount of new computational methods for solving free surface fluid mechanics problems, which could be utilized in ferrohydrodynamic applications.

The area of ferrohydrodynamics is a relatively new area of fluid mechanics. Use of ferrofluids allows for control of the fluid configuration by the applied magnetic field. This has both current and potential applications in a terrestrial environment as well as a microgravity environment.

It is recommended that future work in this area focus on the formulation of specific research problems which are scientifically important and whose results would be of interest to industry.

It is anticipated that future proposals will be written in this area.

Appendix A

The Marker and Cell Technique

This method is used for problems involving time dependent motion of viscous, incompressible fluids in a two-dimensional configuration. The fluid can be bounded in part by walls of an irregular box or by lines of reflective symmetry. Initial and boundary conditions are supplied.

The solution methodology utilizes primarily finite difference approximations applied to Naiver-Stokes equations. The dependent variables are pressure and two velocity components.

The finite differences apply to space and time. The region is divided into small rectangular cells where field variables are given by single, average values. Time changes are represented by a sucession of field variables separated by small increments of time.

The complete velocity field in known at the beginning of the cycle. The coordinates of the marker particles are known (these show which regions have fluid and which do not). The pressures are found such that the rate of change of velocity divergence vanishes everywhere. The two components of acceleration are found, multiplied by time, incremented per cycle, and the change in velocity is added to the old values. The marker particles are moved according to the velocity components. Adjustments are made for passing marker particles across cell boundaries. Velocity modifications are made when a cell, previously full, is emptied, or

vice versa. The marker particles do not participate in the calculation, but they do show fluid element trajectories and relative position of fluids.

The equations utilized are

Continuity

$$\frac{\partial u}{\partial x} + \frac{\partial v}{\partial y} = 0 \qquad \text{(A.1)}$$

and

Conservation of Momentum

$$\frac{\partial u}{\partial t} + \frac{\partial u^2}{\partial x} + \frac{\partial uv}{\partial y} + \frac{\partial P}{\partial x} = \nu(\nabla^2 u) + g_x \qquad \text{(A.2a)}$$

$$\frac{\partial v}{\partial t} + \frac{\partial uv}{\partial x} + \frac{\partial v^2}{\partial y} + \frac{\partial P}{\partial y} = \nu(\nabla^2 v) + g_y \qquad \text{(A.2b)}$$

where, here, P is the ratio of pressure to constant density. The fluid is divided into small regions with local field variables. They are given indices i and j which count cell center positions along the horizontal and vertical directions.

Cell boundaries are labeled with 1/2 integer values of indices. The rectangular cells have dimensions of δx and δy.

Superscripts are used to number the time cycle and δt is the time increment per cycle.

The finite difference approximations for the continuity and momentum equations are

$$\frac{U^{n+1}_{i+\frac{1}{2}}}{\delta t} = \frac{(u_{i,j})^2-(u_{i+1,j})^2 + (u_{i+\frac{1}{2},j-\frac{1}{2}})(v_{i+\frac{1}{2},j+\frac{1}{2}})}{\delta x} - \frac{(u_{i+\frac{1}{2},j+\frac{1}{2}})(v_{i+\frac{1}{2},j+\frac{1}{2}}}{\delta y} + \nu\left(\frac{U_{i+\frac{1}{2},j} + U_{i-\frac{1}{2},j} - 2\,U_{i,j}}{\delta x^2} + \frac{U_{i+\frac{1}{2},j+1} + U_{i+\frac{1}{2},j-1} - 2\,U_{i+\frac{1}{2},j}}{\delta y^2}\right) + \frac{P_{i,j} - P_{i+1,j}}{\delta x} + g_x \qquad \text{(A.3)}$$

$$\frac{V^{n+1}_{i,j} - V_{i,j}}{\delta t} = \frac{(U_{i+\frac{1}{2},j+\frac{1}{2}})(V_{i-\frac{1}{2},j+\frac{1}{2}}) - (U_{i+\frac{1}{2}j+\frac{1}{2}})(V_{i+\frac{1}{2},j+\frac{1}{2}})}{\delta x} + \frac{(V_{i,j})^2 - (V_{i,j+1})^2}{\delta y} + \nu\left(\frac{V_{i+1,j+\frac{1}{2}} + V_{i-1,j+\frac{1}{2}} - 2\,V_{i,j+\frac{1}{2}}}{\delta x^2} \frac{V_{i,j+\frac{1}{2}} + V_{i,j-\frac{1}{2}} - 2\,V_{i,j+\frac{1}{2}}}{\delta y^2}\right) + \frac{P_{i,j} - P_{i,j+1}}{\delta y} \qquad \text{(A.4)}$$

Define

$$D_{i,j} = \frac{(U_{i+\frac{1}{2},j} - U_{i-\frac{1}{2},j})}{\delta x} + \frac{(V_{i,j+\frac{1}{2}} - V_{i,j-\frac{1}{2}})}{\delta y} \qquad (A.5)$$

So the continuity equation is

$$D_{i,j} = 0 \qquad (A.6)$$

From the momentum equations we obtain

$$\begin{aligned} \frac{D^{n+1}_{i,j} - D_{i,j}}{\delta t} = & - Q_{i,j} - \frac{P_{i+1,j} + P_{i-1,j} - 2\,P_{i,j}}{\delta x^2} \\ & - \frac{P_{i,j+1} + P_{i,j-1} - 2\,P_{i,j}}{\delta y^2} \\ & + \nu \left(\frac{D_{i+1,j} + D_{i-1,j} + 2\,D_{i,j}}{\delta x^2} \right. \\ & \left. + \frac{D_{i,j+1} + D_{i,j-1} - 2\,D_{i,j}}{\delta y^2} \right) \end{aligned} \qquad (A.7)$$

We want $D^{n+1}_{i,j}$ to disappear for every cell at the end of a cycle. This leads to

$$\frac{P_{i+1,j} + P_{i-1,j} - 2\,P_{i,j}}{\delta x^2} + \frac{P_{i,j+1} + P_{i,j-1} - 2\,P_{i,j}}{\delta y^2} = - R_{i,j} \qquad (A.8)$$

where

$$R_{i,j} = Q_{i,j} - \frac{D_{i,j}}{\delta t} - \nu \left(\frac{D_{i+1,j} + D_{i-1,j} - 2\,D_{i,j}}{\delta x^2} + \frac{D_{i,j+1} + D_{i,j-1} - 2\,D_{i,j}}{\delta y^2} \right) \tag{A.9}$$

and

$$Q_{i,j} = (U_{i+1,j})^2 + (U_{i-1,j})^2 - 2\,(U_{i,j})^2 + (V_{i,j+1})^2 + V_{i,j-1})^2 - 2\,V_{i,j} + \frac{2\left[(U_{i+\frac{1}{2},j+\frac{1}{2}})\,(V_{i+\frac{1}{2},j+\frac{1}{2}}) + (U_{i-\frac{1}{2},j-\frac{1}{2}})\,(V_{i-\frac{1}{2},j-\frac{1}{2}})\right]}{\delta x\,\delta y} + \frac{2\left[(-U_{i+\frac{1}{2},j+\frac{1}{2}})\,(V_{i+\frac{1}{2},j-\frac{1}{2}}) + (U_{i-\frac{1}{2},j+\frac{1}{2}})\,(V_{i-\frac{1}{2},j+\frac{1}{2}})\right]}{\delta x\,\delta y} \tag{A.10}$$

First, $R_{i,j}$ is found for every cell, then $P_{i,j}$ is obtained for the cells. Finally, the new velocity components are found from the momentum equation.

To account for the free surface, the new position of the surface must be calculated. This calculation can be done because of the coordinate system of marker particles which follow the motion of the elements throughout the fluid. The marker particles are placed in cells with fluid, and they move with the local velocity. Cells with no marker particles are said to have no fluid in them and cell with marker particles that are adjacent to empty cells are called surface cells.

Boundary Conditions

There two types of walls: free slip and no slip walls. For a free slip wall, normal velocity reverses and tangential velocity remains the same. However, for a no slip wall, the opposite is

true. Also, in a free slip wall the pressure is

$$P' = P \pm g_x \delta x \tag{A.11}$$

for a vertical wall, and

$$P' = P \pm g_y \delta y \tag{A.12}$$

for a horizontal wall.

For a no slip wall,

$$P' = P_1 \pm g_x \delta x \pm \left(\frac{2\nu u_1}{\delta x}\right) \tag{A.13}$$

for a vertical wall, and

$$P' = P_1 \pm g_y \delta y \pm \left(\frac{2\nu v_1}{\delta y}\right) \tag{A.14}$$

for a horizontal wall.

At the free surface, D = 0 for surface cells. The pressure boundary condition is derived from either the disappearance of the normal stress component or from equating it to the applied external pressure.

Appendix B

The Volume of Fluid (VOF) Method

This method involves the introduction and use of a function F that has a value of one at any point occupied by a fluid and zero otherwise. The average value of F in a cell represents the fractional volume of the cell occupied by the fluid. Cells with values between one and zero must contain a free surface. The normal direction of the boundary lies in the direction in which F values change most rapidly.

The time dependence of F is governed by the equations

$$\frac{\partial F}{\partial t} + u \frac{\partial F}{\partial x} + v \frac{\partial F}{\partial y} = 0 \qquad \text{(B.1)}$$

F moves along with the fluid, and it is the partial differential equation analog of the marker particles. In this case, F is a flag identifying cells containing fluid.

The method follows a region of fluid rather than surfaces, has minimum storage requirements, and there are no problems with intersecting surfaces.

If the flow is incompressible, then the conservation of mass equation

$$\frac{\partial u}{\partial x} + \frac{\partial v}{\partial y} = 0 \qquad \text{(B.2)}$$

must be implemented. If limited compressibility is desired, then

$$\frac{1}{c^2}\frac{\partial P}{\partial t} + \frac{\partial u}{\partial x} + \frac{\partial v}{\partial y} = 0 \qquad \text{(B.3)}$$

will hold, where C is the speed of sound in the fluid.

For specificity, consider the conservation of momentum equation to be given by the Naiver-Stokes equations.

Discrete values of dependent variables, including F (the fractional volume of fluid) are used in the VOF technique. The free surface cells are the ones which contain a nonzero value of F and have empty cells neighboring them.

There are three steps for advancing a solution through one increment of time, δt. First, approximations of the Naiver-Stokes equations compute the first guess for new time level velocities using initial conditions or previous time-level values for all advective, viscous, and pressure accelerations. Secondly, the pressures are adjusted in each cell and consequent velocity changes are added to velocities computed in the first step. This is done to satisfy continuity. Finally, F must be updated to denote new fluid configurations. These steps are repeated to advance a solution through any desired time interval. At each step, boundary conditions are imposed at all mesh and free surface boundaries.

This method improves on the old MAC method by using a more accurate form of the continuity and momentum equations. In MAC, continuity and momentum equations were combined so that the convective flux term could be written in divergence form ($\nabla \underline{u}\,\underline{u}$ instead of $\underline{u} \cdot \nabla \underline{u}$). This ensured conservation of momentum in the difference approximations. This does not, however, ensure accuracy

in a variable mesh. It is better to use the form for advective flux.

An iterative process is used to adjust velocities and pressures in each cell in order to satisfy continuity. In each cell with fluid, the pressure is changed to either push out fluid or to bring it into the cell. This must be dome in a number of passes through the mesh. In cells containing a free surface, the pressure is assumed to be specified. The surface cell pressure is set equal to the value found by linear interpolation between the pressure at the surface and a pressure in the fluid.

In the VOF technique, the boundary of the surface cells is approximated by a straight line through the cell. The slope of the line is determined and it is moved across the cell to a position that intersects the known amount of fluid in the cell.

Appendix C

Adaptive Grid Methods

Adaptive grid methods involve moving meshes where the motion of the grid is linked to the movement of the interface. To demonstrate this process, consider the problem solved by Cuvelier and Driessen (J. Fluid Mech., 1986) involving the thermocapillary free boundaries in crystal growth. The governing equations are the Naiver-Stokes equations coupled with the heat equation. Boundary conditions include the normal and tangential stress conditions, continuity of thermal flux, conservation of volume, and the condition that the normal component of velocity is zero at the free surface. The goal of this problem is to find the shape of the free boundary, ϕ, a velocity vector, u, and a pressure field that satisfies all of the equations describing the configuration. The boundary condition that is relaxed is

$$(Oh\ Re)^2\ \sigma_v = \frac{1}{R} - B_0\ \phi \qquad (C.1)$$

which is the normal force condition. Oh is the Ohnesorge number, equal to

$$Oh = \frac{\mu}{(\rho_0\ \gamma_0\ L)^{\frac{1}{2}}}$$

Re is the Reynolds number, equal to

$$Re = \frac{L\ u\ \rho_0}{\mu}$$

Bo is the Bond number, equal to

$$Bo = \frac{g \rho_0 L^2}{\gamma_0}$$

An auxiliary problem is defined by finding the solution {u,p,T} satisfying all of the remaining boundary conditions. The relaxed boundary condition is used to adjust the function ϕ.

The function ϕ will now be compared with the free boundary of the static problem, ϕ_*. If $\Psi = \phi + \phi_*$, then Ψ satisfies the following equation

$$\left(\frac{\Psi'}{[1 + \phi_*^2]^{\frac{1}{2}}}\right)' + B_0 \Psi = G \qquad (C.2)$$

$\Psi'(0) = \Psi(1) = 0$

with G given by

$$G = -(Oh\ Re)^2\ (\sigma_v(p_0 u)) - \int_0^1 \sigma_v(p_0 u)\, dx_1 + \frac{1}{R\phi} - \frac{1}{R\phi_*} - \frac{\phi' - \phi_*'}{[1 + \phi_*'^2]^{\frac{1}{2}}} \qquad (C.3)$$

The algorithm is based on the following: the free boundary ϕ is iteratively approximated by a sequence ϕ^0, ϕ^1, ...ϕ^l defined by

(i) $\phi^0 = \phi^*$ the static free boundary

(ii) assume $\phi^1, \phi^2, \ldots$ are known

(iii) solve the auxiliary problem with ϕ^l; the solution is denoted by $\{u^l, p^l, T^l\}$

(iv) Solve problem (2) with $G^l = G(\phi^l, u^l, p^l, T^l)$

The solution is denoted by ψ^l.

(v) $\phi^{l+1} = \phi_* + \psi^l$

The auxiliary problem is nonlinear, so it must be solved iteratively. The Newton Raphson method is used to linearize the nonlinear terms.

Appendix D

Mapping Methods

Mapping methods make it possible to transform an irregularly shaped flow domain into a fixed, regularly shaped computational domain. This makes it easy to implement a finite difference mesh for which the boundaries coincide with a mesh line. This method also maintains a sharp resolution of the interface.

The general algorithm for mapping methods is as follows:

1. The governing equations of the flow are introduced and boundary conditions are implemented.
2. An equation for the surface is set up. This is regarded as an unknown function.
3. The equations are non-dimensionalized.
4. The coordinate transformation occurs. This solves the problem of the difficulty of having an implicit unknown function of the surface. It also insures that the boundary lies on a coordinate line. The governing equations and the boundaries are solved under the assumption that the surface is now a known function. Next, the pressure is restored on the basis of the calculated stream function of velocity function. When all of the other functions are known, the calculation of the original free surface is the final step.

An example of this method is given by Christov and Volkov (J. Fluid Mech., 1985) in their study of the steady viscous flow past a stationary, deformable bubble.

Consider an unbounded volume of viscous incompressible liquid having a velocity U_∞ at infinity. There is a resting bubble in the flow.

The 2-D Naiver-Stokes equations in spherical coordinates are introduced in a stream function-vorticity formulation.

The first boundary condition states that at infinity, liquid moves with a uniform velocity U_∞ in the z direction.

$$\Psi(r, \theta) \to \frac{1}{2} U_\infty r^2 \sin^2\theta \qquad \text{(D.1a)}$$

$$\xi \to 0 \quad at \quad r \to \infty \qquad \text{(D.1b)}$$

The other boundary conditions are

$$\Psi(r, \theta) \to \frac{1}{2} U_\infty r^2 \sin^2\theta - \frac{g V}{4\pi V_\infty}(1 + \cos\theta) \times [1 - \exp(\frac{rV_\infty}{p}(1 - \cos\theta))] \qquad \text{(D.2)}$$

$$\xi(r, \theta) \to - \frac{gVU_\infty}{4\pi V^2} \frac{\sin\theta}{r}(1 + \frac{V}{rU_\infty}) \exp[\frac{rV_\infty}{\nu}(1 - \cos\theta)] \qquad \text{(D.3)}$$

g = acceleration due to gravity, V = volume of the bubble

$$r = R(\theta) \qquad \text{(D.4)}$$

Let the equation of the surface be

Next, the equations are non-dimensionalized. Because r = $R(\theta)$ is unknown, many obstacles arise in solving the problem. To overcome this problem, the coordinate transformation takes place.

The transformation used to simplify the problem is

$$r = \eta\, R(\theta) \quad , \quad \theta = \theta \tag{D.5}$$

These are substituted into all the equations. A Finite difference method can now be used to solve for the function $R(\theta)$.

Appendix E

Database of Articles Collected
Pertaining to Free Surface Flow

Free Surface Flow During the Filling of a Cylinder, Abdullah, Z. and Salcudean, M. International Journal for Numerical Methods in Fluids. vol. 11, p. 151-168, 1990.
Key words:
Free surface flows Filling of molds Flow Visualization
Mathematical modeling Control volume method

A High Resolution Godunov-Type Scheme in Finite Volumes for the 2D Shallow-Water Equations, Alcrudo, Francisco and Garcia-Navarro, Pilar. International Journal for Numerical Methods in Fluids, vol. 16, p. 489-505, 1993.
Key words:
Two-dimensional modeling Finite volumes MUSCL approach
Upwind differencing

Numerical Solution of the Generalized Serre Equations with the Maccormiack Finite Difference Scheme, Antunes Do Carmo, J.S, Seabra Santos, F.J. and Almeida, A.B. International Journal for Numerical Methods in Fluids, vol. 16, p.725-738, 1993.
Key words:
Serre equations Maccormack's Method Solitary Waves
Sudden releases

Flair: Flux Line-Segment Model for Advection and Interface Reconstruction, Ashgurz, N., and Poo, J.Y. Journal of Computational Physics, vol. 93, p. 449-468, 1991.
Key words:
Cell volume fraction approach Line segments Capillary forces

Adaptive Zoning for Singular Problems in Two Dimensions Brackbill, J.U. and Saltzman, J.S. Journal of Computational Physics, vol. 46, p. 342-268, 1982.
Winslow's method Adaptive mesh

A Continuum Method for Modeling Surface Tension, Brackbill, J.U., Kothe, D.B., and Zemach, C. Journal of Computational Physics, vol. 100, p. 335-354, 1992.
Key words:
Surface tension Fluid interfaces Continuum method

Modelling the Initial Motion of Large Cylindrical and Spherical Bubbles, Bugg, J.D. and Rowe, R.D. International Journal for Numerical Methods in Fluids, vol. 13, p. 109-129, 1991.
Key words:
Bubbles Finite difference Initial motion

Application of a Vortex Method to Free Surface Flows
Chen, Liyong and Vorus, William. International Journal of Numerical Methods in Fluids, vol. 14, p. 1289-1310, 1992.
Key words:
Vortex method Free surface flows Body-wave interactions

Numerical Investigation of the Steady Viscous Flow Past a Stationary Deformable Bubble, Christov, C.I. and Volkov, P.K. Journal of Fluid Mechanics, vol. 138, p. 341-364, 1983.
Key words:
Moving Boundaries Coordinate transformation Steady Viscous Deformable bubble

Explicit Streamline Method for Steady Flows of Non-Newtonian Matter: History Dependence and Free Surfaces, Chung, S.G. and Kuwahara, K. Journal of Computational Physics, vol. 104, p. 444-450, 1993.
Key words:
Finite difference method Non-Newtonian matter History dependence Free surface

An Orthogonal Mapping Technique for the Computation of a Viscous Free-Surface Flow, Cliffe, K.A., Tavener, S.J., and Wheeler, A.A. International Journal for Numerical Methods in Fluids, vol. 15, p. 1243-1258, 1992.
Key words:
Free surface Viscous flow Finite element method Orthogonal mapping

Thermocapillary Free Boundaries in Crystal Growth, Cuvelier, C., and Driessen, J.M. Journal of Fluid Mechanics, vol. 169, p. 1-26, 1986.
Key words:
Two-dimensional flow Thermocapillary flow Steady Crystal growth Finite element method

A Newton's Method Scheme for Solving Free-Surface Flow Problems, Dandy, David S. and Leal, Gary L. International Journal for Numerical Methods in Fluids, vol. 9, p. 1469-1486, 1989.
Key words:
Bubble Intermediate Reynolds number Newton's method

An Efficient Surface-Integral Algorithm Applied to Unsteady Gravity Waves, Dold, J.W. Journal of Computational Physics, vol. 103, p. 90-115, 1992.
Key words:
Unsteady motion Two-dimensional flow Cauchy's integral theorem Numerical instabilities

Three-Dimensional Streamlined Finite Elements: Design of Extrusion Dies, Ellwood, Kevin,R, Papanastasiou, T.C. and Wilkes, J.O. International Journal for Numerical Methods in Fluids, vol. 14, p. 13-24, 1992.
Key words:
Streamlined Finite elements Extrusion Free surface flows Die design Three-dimensional flows Three-dimesional finite elements

Consistent vs. Reduced Integration Penalty Method for Incompressible Media Using Several Old and New Elements, Engleman, M.S. and Sani, R.L. International Journal for Numerical Methods in Fluids, vol. 2, p. 25-42, 1982.
Key words:
Penalty Method Incompressible flow Reduced quadrature Finite elements

Finite Element Method for Time-Dependent Incompressible Free Surface Flow, Frederiksen, C.S. and A.M. Watts. Journal of Computational Physics, vol. 39, p. 292-304, 1981.
Key words:
Finite element method Time dependent flow Vertically moving plate Circulation in rectangular channel

Flux Difference Splitting for Open-Channel Flows, Glaister, P. International Journal for Numerical Methods in Fluids, vol. 16, p. 629-654, 1993.
Key words:
Shallow-water equations Subcritical and supercritical flows Open channels

A Finite Difference Technique for Solving the Newtonian Jet Swell Problem, Han, Chin-Tsu, Tsai, Chin-Chin, Yu, Tsai-An, and Liu, Ta-Jo. International Journal for Numerical Methods in Fluids, vol. 15, p. 773-789, 1992.
Key words:
Finite difference method Newtonian jet swell

Lagrangian Finite Element Method for Free Surface Navier-Stokes Flow Using Fractional Step Method, Hayashi, Masahiro, Hatanaka, Katsumori, and Kawahara, Mutsuto. International Journal for Numerical Methods in Fluids, vol. 13, p. 805-840, 1991.
Key words:
Finite element method Lagrangian description Fractional Step Navier-Stokes equations Linear interpolation Free surface

Numerically Induced Phase Shift in the KdV Soliton
Herman, R.L., and Knickerbocker, C.J. Journal of Computational Physics, vol. 104, p. 50-55, 1993.
Key words:
KdV equation Finite difference Phase shift Perturbation theory

Vol.ume of Fluid (VOF) Method for the Dynamics of Free Boundaries, Hirt, C.W. and Nichols, B.D. Journal of Computational Physics, vol. 39, p. 201-225, 1981.
Key words:
Fractional volume of fluid Incompressible Finite difference

A Lagrangian Method for Calculating the Dynamics of an Incompressible Fluid with Free Surface, Hirt, C.W., Cook, J.L., and Butler, T.D. Journal of Computational Physics, vol. 5, p. 103-124, 1970.
Key words:
Transient flow Viscous Incompressible Lagrangian coordinates

The Effect of Surface Contamination on Thermocapillary Flow in a Two-Dimensional Slot, Homsy, G.M. and Meiburg, E. Journal of Fluid Mechanics, vol. 139, p. 443-459, 1984.
Key words:
Insoluble surfactants Steady thermocapillary flow
Interfacial tension Lubrication theory

The Numerical Solution of the Thin Film Flow Surrounding A Horizontal Cylinder Resulting from a Vertical Cylindrical Jet, Hunt, Ronald. International Journal for Numerical Methods in Fluids, vol. 14, p. 539-556, 1992.
Key words:
Thin film flows Free boundary problems Parabolic equations

Numerical Methods for Tracking Interfaces, Hyman, James M. Physica 12D p. 396-407, 1984.
Key words:
Front tracking Interface tracking Surface tracking Volume tracking

Numerical Solution of the Eulerian Equations of Compressible Flow by a Finite Element Method Which Follows the Free boundary and the Interfaces, Jamet, P. and Bonnerot, R. Journal of Computational Physics, vol. 18, p. 21-45, 1975.
Key words:
Eulerian equations Compressible flow Finite elements

Finite Element Method for Shallow Water Equation Including Open Boundary Condition, Kodama, Toshio, Kawasaki, Tomoyuki, and Kawahara, Mutsuto. International Journal for Numerical Methods in Fluids, vol. 13, p. 939-953, 1991.
Key words:
Finite element method Shallow water equations Open boundary Parameter identification Tokyo Bay

A Total Linearization Method for Solving Viscous Free Boundary Flow Problems By The Finite Element Method, Kruyt, N.P., Cuvelier, C., Segal, A., and Van Der Zanden, J. International Journal for Numerical Methods in Fluids, vol. 8, p. 351-363, 1988
Key words:
Navier-Stokes equations Finite element method Viscous flow Free boundary flow

Turbulent Free Surface Flow Simulation Using a Multilayer Model, Lai, C.J. and Yen, C.W. International Journal for Numerical Methods in Fluids, vol. 16, p. 1007-1025, 1993
Key words:
Multilayer model Free surface Recirculating flow Curvilinear co-ordinates Non-staggered grid Depth correction

Variational Formulation of Three-Dimensional Viscous Free-Surface Flows: Natural Imposition of Surface Tension Boundary Conditions, Lee-Wing Ho and Anthony T. Patera. International Journal for Numerical Methods in Fluids, 1991.
Key words:
Curvature Finite Element method Free surface flow
Navier-Stokes equations Spectral element method Surface tension
Three-dimensional Variational form Viscous incompressible flow

Die Design: An Implicit Formulation for the Inverse Problem, Legat, Vincent, and Marchal, Jean-Marie. International Journal for Numerical Methods in Fluids, vol. 16, p. 29-42, 1993.
Key words:
3D extrusion Moving boundaries Die design Remeshing
Finite elements Free surfaces

An Efficient Three-Dimensional Semi-Implicit Finite Element Scheme for Simulation of Free Surface Flows, Li, Y.S. and Zhan, J.M. International Journal for Numerical Methods in Fluids, vol. 16, p. 187-198, 1993.
Key words:
Three-dimensional Finite Element Free surface flows

A General Numerical Method for the Solution of Gravity Wave Problems. Part 1: 2-D Steep Gravity Waves in Shallow Water, Liao, S.J. International Journal for Numerical Methods in Fluids, vol. 12, 727-745, 1991.
Key words:
Non-linear gravity waves Velocity potential
Transformation from non-linear to linear

Finite Element Simulation of Flow in Deforming Regions, Lynch, Daniel and Gray, William, Journal of Computational Physics, vol. 36, p. 135-153, 1980.
Key words:
Finite element technique Multidimensional flow Moving boundaries
Galerkin's method

A Finite Element Analysis of A Free Surface Drainage Problem of Two Immiscible Fluids, Masatake Mori and Makoto Natori International Journal for Numerical Methods in Fluids, vol.9, p. 569-582, 1989.
Key words:
Flow analysis Free surface problem Finite element method
Blast furnace

A Consistent Boundary Element Method For Free Surface Hydrodynamic Calculations, Medina, Daniel E., Liggett, James A., Birchwood, Richard A., and Torrance, Kenneth E. International Journal for Numerical Methods in Fluids, vol. 12, p. 835-857, 1991.
Key words:
Boundary element Free surface Hydrodynamic

A Computational Method for Simulating Transient Motions of an Incompressible Inviscid Fluid with a Free Surface, Nakayama, Tsukasa. International Journal for Numerical Methods in Fluids, vol. 10, p. 683-695, 1990.
Key words:
Boundary element method Taylor series expansion Water waves

The solution of Viscous Incompressible Jet and Free-Surface Flows Using Finite-Element Methods, Nickell, R.E., Tanner, R.I., and Caswell, B. Journal of Fluid Mechanics, vol. 65, p. 189-206, 1974.
Key words:
Finite element Viscous Incompressible Steady flow
Galerkin formulation Stress singularities

Two-dimensional Sloshing Analysis By Lagrangian Finite Element Method, Okamoto, Takashi and Kawahara, Mutsuto, International Journal for Numerical Methods in Fluids, vol.11, p. 453-477, 1990.
Key words:
Finite element method Lagrangian description Velocity correction
Sloshing analysis

Rimming Flow: Numerical Simulation of Steady, Viscous, Free-surface Flow with Surface Tension, Orr, F.M. and Scriven, L.E. Journal of Fluid Mechanics, vol. 84, p. 145-165, 1978.
Key words:
Rotating cylinder Finite elements Steady flow viscous
Surface tension Capillary forces

A Front Tracking Method for Viscous, Incompressible Multi-fluid Flows, Ozen Unverdi, Salih and Tryggvason, Gretar. Journal of Computational Physics, vol. 100, p. 25-37, 1992.
Key words:
Unsteady flow Multi-fluid flow Fluid interfaces Front tracking
Two-dimensional flow Three-dimensional flow

Nonlinear Oscillations of Inviscid Free Drops, Patzek, T.W., Benner, R.E., Basaran, O.A., and Scriven, L.E. Journal of Computational Physics, vol. 97, p. 489-515, 1991.
Key words:
Inviscid oscillations Liquid drops Galerkin's weighted residuals Dynamic responses

A Hybrid Finite-Boundary Element Method for Inviscid Flows with Free Surfaces, Pelekasis, N.A., Tsamopoulis, J.A. and Mangolis, G.D. Journal of Computational Physics, vol. 101, p. 231-251, 1992.
Key words:
Inviscid flow Liquid drops Boundary and finite element combination

On the Nature of Boundary Conditions for Flows with Moving Free Surfaces, Renardy, Michael and Renardy, Yukiko. Journal of Computational Physics, vol. 93, p. 325-355, 1991.
Key words:
Perturbations Plane parallel flow Moving free surface

A Method for Incorporating Free Boundaries With Surface Tension in Finite Element Fluid-Flow Simulators, Ruschak, Kenneth. International Journal for Numerical Methods in Engineering, vol. 15 p. 639-648, 1980.
Kew words:
Finite elements Steady Two-dimensional flow Newtonian fluid Inertial, viscous, surface tension, and gravitational effects

Numerical Solution of Free-Boundary Problems in Fluid Mechanics Part 1. The Finite Difference Technique, Ryskin, G. and Leal, L.G. Journal of Fluid Mechanics, vol. 148, p. 1-17, 1984.
Key words:
Two-dimensional flow Finite differences Curvilinear coordinates

Finite Element Analysis of Creeping Flows Using Marker Particles, Shiojima, Takeo, Shimazaki, Yoh, and Daiguji, Hisaaki International Journal for Numerical Methods in Fluids, vol. 11, p. 397-404, 1990.
Key words:
Numerical analysis Finite element method Transient flow Creeping flow Power-law fluid

Numerical Method for Unsteady Viscous Hydrodynamical Problem with Free Boundaries, Shopov, Peter, Minev, Peter, and Bazhlekov, Ivan B. International Journal for Numerical Methods in Fluids, vol. 14, p. 681-705, 1992.
Key words:
Unsteady Navier-Stokes Equations Finite elelment method Viscous Multiphase flow

Interaction of a Deformable Bubble with a Rigid Wall at Moderate Reynolds Numbers, Shopov, Peter, J., Minev, Peter,D., Bazhlekov, Ivan, B., and Zapryanov, Zaphyan, D. Journal of Fluid Mechanics, vol. 219, p. 241-271, 1990.
Key words:
Unsteady flow Viscous flow Deformable gas bubble Finite element Moderate Reynolds numbers Buoyancy force

Separating Flow Near a Static Contact Line: Slip at a Wall and Shape of a Free Surface, Silliman, William J. and Scriven, L.E. Journal of Computational Physics, vol. 34, p. 287-313, 1980.
Key words:
Slip-coefficient boundary condition Galerkin Finite Elements Surface tension Die swell

Dispersion and Group Velocity in Numerical Schemes for Three-Dimensional Hydrodynamic Equations, Song, Yuhe and Tang, Tao. Journal of Computational Physics, vol. 105, p. 72-82, 1993.
Key words:
Dispersion and group velocity Three-dimensional flow

Thermocapillary convection in a rectangular cavaity: asymptotic theory and numerical simulation, Strani, M., Piva, R., and Graziani, G. Journal of Fluid Mechanics, vol. 130, p. 347-376 1983.
Key words:
Steady flow Newtonian fluid Rectangular enclosure Thermocapillary flow Surface tension gradients

Numerical Solution of Eigenvalue Problem Using Spectral Techniques, Su, Y.Y. and Khomami, B. Journal of Computational Physics, vol. 100, p. 297-305, 1992.
Key words:
Spectral methods Interfacial conditions Eigenvalue problem Newtonian fluid Poiseuille flow

Generalization of Physical Component Boundary Fitted Co-Ordinate Method for the Analysis of Free Surface Flow, Takizawa, Akihiko, Koshizuka, Seichi, and Kondo, Shunsuke. International Journal for Numerical Methods in Fluids, vol. 15, p. 1213-1237, 1992.
Key words:
Physical component Lie derivative Physical curvilinear space Riemennian geometry Lagrangian front tracking Free surface

Computing Brine Transport in Porous Media with an Adaptive Grid Method, Trompert, R.A., Verwer, J.G. and Blom, J.G. International Journal for Numerical Methods in Fluids, vol. 16, p. 43-63, 1993.
Key words:
Finite differences Adaptive Grid methods
Local uniform grid refinement Method of Lines Brine transport
Fluid flow/solute transport in porous media

Marangoni Convection in Weld Pools with a Free Surface, Tsai, M.C. and Sindo, Kou. International Journal for Numerical Methods in Fluids, vol. 9, p. 1503-1516, 1989.
Key words:
Welding Free Surface Marangoni convection

Solution of Free-boundary Problems Using Finite Element/Newton Methods and Locally Refined Grids: Application to Analysis of Solidification Microstructure. Tsiveriotis, K. and Brown, R.A. International Journal for Numerical Methods in Fluids, vol. 16, p. 827-843, 1993.
Key words:
Local mesh refinement Free boundary Finite element method
Co-ordinate mapping Solidification

Boundary-Conforming Mapping Applied to Computations of Highly Deformed Solidification Interfaces, Tsiveriotis, K. and R.A. Brown. International Journal for Numerical Methods in Fluids, vol. 14, p. 981-1000, 1992.
Key words:
Co-ordinate mapping Finite element method Free boundary Solidification

Transient Finite Element Method for Calculating Steady State Three-Dimensional Free Surfaces, Wambersie, O. and Crochet, M.J. International Journal for Numerical Methods in Fluids, vol. 14, p. 343-360, 1992.
Key words:
Free Surfaces Extrusion Conjugate gradients Finite elements
Three dimensional Free surfaces

Surface Tension and Buoyancy-Driven Flow in a Non-Isothermal Liquid Bridge, Zhang, Yiqiang and Alexander, J. Iwan D.
International Journal of Numerical Methods in Fluids, vol. 14, p. 197-215, 1992.
Key words:
Thermocapillary Flow Buoyancy Free surface Finite difference Picard iteration ADI

Appendix F
Database of Articles Related to Ferrohydrodynamics

Effects of Viscosity and Non-Uniform Heating on the Break-Up of a Cylindrical Layer of Fluid. V.I. Arkhipenko, Yu.D. Barkov, V.G. Bashtovoi, M.S. Krakov, and M.I, Pavlinov. Magnetohydrodynamics. vol. 17 no. 3, p. 232-237, 1981
Key words:
Viscous Heating Magnetized liquid Instability Thermocapillary convection

Study of the Deformation of Ferrofluid Droplets in a Magnetic Field. J.C. Bacri and D. Salin. J. Physique Lett. vol. 43, p. L179-L184, 1982.
Key words:
Deformation Weak magnetic field Agglomerates

Instability of Ferrofluid Magnetic Drops Under Magnetic Field, J.C. Bacri and D. Salin. J. Physique Lett. vol. 43, p. L649-L654, 1982.
Key words:
Ferrofluid drops Instability

Lesser Known Applications of Ferrofluids. R.L. Bailey. J. Magnetism Magnetic Mater. vol. 39, p. 178-182, 1983.
Key words:
Applications Commercial

Axisymmetric Shapes of Charged Drops in an External Electric Field. O.A. Basaran and L.E. Scriven. Physics of Fluids A. vol. 1, p. 799-809, 1989.
Key words:
Charged drops Galerkin's Method Electric field

Solitary and Cnoidal Waves in Ferrofluid, V.G. Bashtovoi and R.A. Foigel. Magnitnaya Gidrodinamika. vol. 2, p. 55-60, 1983.
Key words:
Cylindrical column Solitary wave Cnoidal wave KdV equation

Instabilities of Magnetic Fluids Leading to a Rupture in Continuity. B. Berkovsky and V. Bashtovoi. IEEE Trans. Mag. vol. MAG-16, p. 288-297, 1980.
Key words:
Magnetic fluid Instability Rupture in continuity

Magnetic Fluid as a Continuum with Internal Degrees of Freedom. IEEE Trans. Mag. vol. MAG-16, p.329-342, 1980.
Key words:
Thermomechanics Dynamic magnetization

Magnetohydrostatic Equilibria of Ferrofluid Drops in External Magnetic Fields. A.G. Boudouvis, J.L. Puchalla, and L.E. Scriven. Chem. Eng. Comm. vol. 67, p. 129-144, 1988.
Key words:
Drop Wetting Capillarity Fringing Finite element

Multifurcation of Patterns in Ferrofluids, A.G. Boudouvis, and L.E. Scriven. J. Magnetism Magnetic Mater. vol. 85, p. 155-158, 1990.
Key words:
Ferrofluid interface Normal field instability Hexagonal and triangular patterns

Sensitivity Analysis of Hysteresis in Deformation of Ferrofluid Drops, A.G. Boudouvis and L.E. Scriven. J. Magnetism Magnetic Mater. vol. 122, p. 254-258, 1993.
Key words:
Ferrofluid drops Hysteresis Wetting

Interfacial Instability in Viscous Ferrofluids, J.P. Brancher. IEEE Trans. Mag. vol. MAG-16, p. 1331-1336, 1980.
Key words:
Viscous Infinitessimal waves Instability Interface

Equilibrium of a Magnetic Liquid Drop. J.P. Brancher and D. Zouaoui. J. Magnetism Magnetic Mater. vol. 65, p. 311-314, 1987.
Key words:
Ferrofluid drop Cone formation

Agglomeration Formation in a Magnetic Fluid. R.W. Chantrell. J. Appl. Phys. vol. 3, p. 2742-2744, 1982.
Key words:
Agglomeration Particle size Magnetization

Interfacial Stability of a Ferromagnetic Fluid. M.D. Cowley and R.E. Rosenweig. J. Fluid Mech. vol. 30, p. 671-688, 1967.
Key words:
Normal magnetic field Stability Interfacial tension Magnetization

Flows and Wave Propagation in Ferrofluids. R.A. Curtis. Phys.of Fluids. vol. 14, p. 2096-2102, 1971.
Key words:
Waves Temperature dependence Thermal stability Perturbations

Applications of Ferrofluids as an Accoustic Transducer Material, P.S. Dubbleday. IEEE Trans. Mag. vol. MAG-16, p. 372-374, 1980
Key words:
Electroaccoustic Transconduction

Convective Instability of Ferromagnetic Fluids, B.A. Finlayson. J. Fluid Mech. vol. 40, p. 753-769, 1970.
Key words:
Convective instability Vertical magnetic field Temperature gradient Galerkin Method Free boundary Rigid boundary

Form of Surface Instability of a Ferromagnetic Fluid, A. Gailitis, Magnitnaya Gidrodinamika. vol. 5, p. 68-70, 1969.
Key words:
Free surface Instability Hexagonal patterns

Surface Phenomena in Ferrohydrodynamics, V.V. Gogosov, V.A. Naletova, and N.G. Taktarov. Acta Astronautica. vol.7, p. 489-497, 1980.
Key words:
Free surface Magnetic surfactant Damping coefficients Surface waves

New Methods for Sealing, Filtering, and Lubricating with Magnetic Field, M. Goldowsky. IEEE Trans. Mag. vol. MAG-16, p. 382-386, 1980.
Key words:
Sealing Filtering Lubrication Magnetic field

Thermal Convection in a Horizontal Layer of Magnetic Fluid. K. Gotoh and M. Yamada, J. Phys. Soc. Japan. vol. 51, p. 3042-3048, 1982.
Key words:
Linear stability Ferromagnetic boundaries Vertical magnetic field Galerkin Method

Frictional Torque in Ferrofluids, Katja Henjes. J. Magnetism Magnetic Mater. vol. 119, P. L311-L316, 1982.
Key words:
Vorticity Frictional torque Rotational viscosity Magnetic relaxation time

Some Simple flows of a Paramagnetic Fluid, J.T. Jenkins, J. Physique vol. 32, p. 931-938, 1971.
Key words:
Paramagnetic fluid Shearing flow Rotating magnetic field

Numerical Calculations for Ferrofluid Seals, Zou Jibin and Lu Yongping, IEEE Trans. Mag. vol. 28, p. 3367-3371, 1992.
Key words:
Seal Seal capacity Magnetic circuit parameters

Some applications of Ferrofluid Magnetic Colloids, Robert Kaiser and Gabor Miskolczy. IEEE Trans. Mag. vol. MAG-6, p. 694-698, 1970.
Key words:
Applications

Thermomechanical Instability and Chaotic State. D. Kobou and H. Yamaguchi. J. Magnetism Magnetic Mater. vol. 122, p. 290-293, 1993.
Key words:
Heat Ferrofluid Layer Chaotic properties Rigid and free boundaries

Flow Regimes for a Magnetic Suspension Under a Rotating Magnetic Field, R. Mailfert and A. Martinet. J. Physique. vol. 34, p. 197-201, 1973.
Key words:
Rotating magnetic field Magnetization

Long Wave Equations in Magnetic Fluids, S.K. Malik and M. Singh. Magnitnaya Gidrodinamika, vol. 4, p. 17-21, 1990.
Key words:
Nonlinear wave packet 3-D Long waves K-P equation Rayleigh-Taylor instability

Wave Propagation in Thermo-Viscous Magnetofluid Dynamics, A. Morrow. Physics Letters, vol.79A, p. 84-86, 1980.
Key words:
Wave propagation Thermo-viscous fluids Entropy waves Alfven waves Magneto-accoustic waves

Some Viscous Flows of a Saturated Ferrofluid Under the Combined Influence of Thermal and Magnetic Field Gradients, Joseph Neuringer. Int. J. Non-linear Mech. vol. 1, p. 123-137, 1966.
Key words:
Flowing Viscous Incompressible Heated Varying magnetic field

Taylor-Vortex Flow of Ferrofluids in the Presence of General Magnetic Fields. M. Niklas and H. Muller-Krumbhaar. J. Magnetism Magnetic Mater. vol. 81, p. 29-38, 1987.
Key words:
Concentric rotating cylinders Linear analysis Time dependent magnetic fields Instability

A Review of Damping Applications of Ferrofluids, K. Raj and R. Moskowitz. IEEE Trans. Mag. vol. MAG-16, p. 358-363, 1980.
Key words:
Dampers Rotary dampers Applications

Commercial Applications of Ferrofluids, K. Raj and R. Moskowitz. J. Magnetism Magnetic Mater. vol. 85, p. 233-245, 1990.
Key words:
Sealing Damping Hydrodynamic bearings

Fluid Magnetic Buoyancy, R.E. Rosenweig. AIAA Journal, vol. 4, p. 1751-1758, 1966.
Keywords:
Buoyant levitation Bernoulli relationship

Labyrinthe Instability in Magnetic and Dielectric Fluids, R.E. Rosenweig. J. Magnetism Magnetic Mater. vol. 39, p. 127-132, 1983.
Key words:
Labyrinthe instability Thin layers Uniform fields

Ferrohydrodynamics, R.E. Rosenweig. Cambridge University Press, 1985.

Magnetic Fluids as Drug Carriers: Target Transport by a Magnetic Field, E.K. Runge and A.N. Rusetski. J. Magnetism Magnetic Mater. vol. 122, p. 335-339, 1993.
Key words:
Biomedical application Drug localization

Theory of Agglomeration of Ferromagnetic Particles in Magnetic Fluids, K. Sano and M. Doi. J. Phys. Soc. Japan. vol. 52 p. 2810-2815, 1983.
Key words:
Agglomeration Weak magnetic field Van de Waals attraction

Thermal Convection in Ferrofluids Under a Free Surface, L. Shwab. J. Magnetism Magnetic Mater. vol. 85, p. 199-202, 1990.
Key words:
Flat layers Stability Vertical temperature gradient Free surface

Thermoconvective Instability of a Horizontal Layer of Ferrofluid in a Strong Vertical Magnetic Field. Peter T. Stiles and Michael Kagan. J. Magnetism Magnetic Mater. vol. 85, p. 196-198, 1990.
Key words:
Benard convection Vertically magnetized

Nonlinear Waves in Conductive Magnetizable Fluid, I. Tarapov, N.F. Patsegon. IEEE Trans. Mag. vol. MAG-16, p. 309-316, 1980.
Key words:
Non-uniform magnetization One-dimensional shock wave

Magnetostatic Instabilities in Plane Layers of Magnetizable Liquids. A.O. Tsebers and M. Maiorov. Magnetohydrodynamics vol. 16, p. 21-28, 1980.
Key words:
Instability Labyrinthe Free surface Plane Layers Thin films Normal magnetic fields

Comblike Instability in Thin Layers in a Magnetic Fluid, A.O. Tsebers and M. Maiorov. Magnetohydrodynamics vol. 16 p. 126-130, 1980.
Key words:
Comblike instability Vertical thin layers

Dynamics of Magnetostatic Instabilities. A.O. Tsebers. Magnetohydrodynamics vol. 17, p. 113-122, 1981.
Key words:
Thin plane layers Spiral instability Free boundary Perturbations

Instability of a Free Surface of a Magnetofluid in a Tangentially Rotating Magnetic Field. A.O. Tsebers. Magnetohydrodynamics, vol. 17, p. 242-249, 1981.
Key words:
Surface instabilities Uniform rotating magnetic field Free surface Waves

Mathematical Theory of Non-linear Waves on the Surface of a Magnetic Fluid. Evan Twombly and J.W. Thomas. IEEE Trans. Mag. vol. Mag-16, p. 214-220, 1980.
Key words:
Strong magnetic field Surface waves Bifurcation

Response of Magnetic Fluids to Mechanical, Magnetic, and Thermal Forces, P.D.D Verma. IEEE Trans. Mag. vol. MAG-16, p.317-325, 1980.
Key words:
Mechanical Thermal forces Steady rotation Paramagnetic fluid Flow through annulus Helical flow Heat conduction

Ferrohydrodynamic Thrust Bearings, J.S. Walker and J.D. Buckmaster. Int. J. Eng. Sci. vol. 17, p. 1171-1182, 1979.
Key words:
Thrust bearings Lubricant

Spherical Couette Flow in Magnetic Fluid, H. Yamaguchi and J. Kobori. Magnitnaya Gidrodinamika, vol. 3, p. 21-25, 1990.
Key words:
Rotation Concentric spheres Stability Taylor-Goerther vortices

Ferrohydrodynamic Torque Driven Flows, Markus Zahn. J. Magnetism Magnetic Mater. vol. 85, p. 181-186, 1990.
Key words:
Traveling wave magnetic field Non-collinear magnetization and magnetic field Phase lag

SECTION B

Interface Response of the Finite Length Liquid Column to Longitudinal Forcing and Interface Stability of the Infinite Liquid Column to Forcing Normal to the Column Axis

Axial forcing of an inviscid finite length fluid cylinder

M. J. Lyell
Department of Mechanical and Aerospace Engineering, West Virginia University, Morgantown, West Virginia 26506-6101

(Received 8 August 1990; accepted 7 March 1991)

Current interest in microgravity materials processing has focused attention upon the finite fluid column. This configuration is used in the modeling of float zones. In this Brief Communication, the incompressible inviscid finite length fluid column is subjected to an axial, time-dependent disturbance. The response of the fluid system and the resulting interface location are determined via Laplace transform methods.

The presence of vibrations will affect the fluid dynamical environment in which materials processing occurs. Experiments performed on Spacelab D1 investigated the effect of g-jitter on the stability of finite fluid columns. It was found that long columns are particularly sensitive to residual accelerations and impulses.[1] The analytical effort has been concerned with the *axial* forcing of *slender* liquid bridges.[2-5] In these analyses, a one-dimensional "slice" model has been used. Such a restriction is invalid in the situation in which the liquid column is not slender, yet whose height and radius are within the static stability limits for fluid columns. The work of Sanz[6,7] has addressed the problem of the *unforced* modes of oscillation of a nonslender finite fluid column.

In this work, the problem of the *axially forced* finite fluid column is investigated, with the axial forcing considered periodic in time. The analysis is linear, inviscid, incompressible, and axisymmetric. It utilizes Laplace transform techniques. The direction of the imposed body force is taken parallel to the longitudinal axis, and in the negative $\hat{e}_z$ direction. The undisturbed column is cylindrical, and is surrounded by an inert gas.

Quantities will be nondimensionalized as follows:

$$R\tilde{\mathbf{x}}=\mathbf{x},\quad \omega_f^{-1}\tilde{t}=t,\quad R\omega_f\tilde{\mathbf{u}}=\mathbf{u},\quad \rho\omega_f^2R^2\tilde{p}=p, \tag{1}$$

and R is the radius of the column. The forcing frequency is ω_f. Pressure and velocity fields are indicated by p and $\mathbf{u}$, respectively. The density of the column is given by ρ. A tilde indicates dimensionless quantities.

Equations are to be rendered nondimensional through the use of (1). This results in

$$\nabla\cdot\mathbf{u}=0, \tag{2a}$$

$$\frac{\partial\mathbf{u}}{\partial t}+\mathbf{u}\cdot\nabla\mathbf{u}=-\nabla p-\mathrm{Fr}\,g(t)\hat{e}_z \tag{2b}$$

and the nondimensional interface equation is

$$f_e=r-1-\mathrm{Fr}\,f(z,t) \tag{2c}$$

with $f(z,t)$ representing the functional form of the perturbation to the interface. The tildes have been dropped for convenience. The nondimensional parameter Fr is a Froude type number, and is given by $(G_0/R\omega_f^2)$. It is taken to be a small parameter. Pressure and velocity are expanded in terms of Fr about a state of zero mean motion. This results in the linearized system of governing equations

$$\nabla\cdot\mathbf{u}=0, \tag{3a}$$

$$\frac{\partial(\nabla\phi)}{\partial t}=-\nabla p-g(t)\hat{e}_z \tag{3b}$$

with $\mathbf{u}=\nabla\phi$. For definiteness, $g(t)$ is chosen to be $\sin(t)$.

The boundary conditions at the upper and lower disks are that the normal component of the velocity be zero. Also, an anchored triple-contact line assumption at both disks will further restrict the interface behavior. These are

$$\left.\frac{\partial\phi}{\partial z}\right|_{z=\Lambda}=0,\quad \left.\frac{\partial\phi}{\partial z}\right|_{z=-\Lambda}=0, \tag{4a}$$

$$f(\Lambda,t)=f(-\Lambda,t)=0. \tag{4b}$$

The constant Λ acts as a slenderness parameter, and is given by $(L/2R)$. As the fluid is incompressible, volume must be conserved, and so

$$\int_{-\Lambda}^{\Lambda}f(z,t)dz=0. \tag{4c}$$

Because of axisymmetry

$$\left.u_r\right|_{r=0}=0,\quad \left.\frac{\partial w}{\partial r}\right|_{r=0}=0. \tag{4d}$$

At the fluid column/inert gas interface, both the kinematic and normal force balance conditions must be imposed. These are given by

$$\frac{-\partial f}{\partial t}+\frac{\partial\phi}{\partial z}=0, \tag{4e}$$

$$\Delta p=\left(\frac{-1}{B_0}\right)\left(\frac{\partial^2 f}{\partial z^2}+f\right), \tag{4f}$$

and are evaluated on $r=1$ (Δp indicates the change in pressure across the interface). The nondimensional parameter B_0 is given by $(\rho R^3\omega_f^2/\gamma)$. Gamma denotes the surface tension. Note that Eqs. (4e) and (4f) have been linearized [and are at $O(\mathrm{Fr})$].

Both the system of equations (3) and the boundary/interface conditions (4) are Laplace-transformed with respect to time. The time dependence is replaced by a pa-

 0899-8213/91/071828-04$02.00

rameter s. The initial velocity perturbation is taken to be zero. The initial position of the interface is taken to be that of the undisturbed cylindrical column $f_o = 1$. This is realistic for the case of a zero mean gravity, which is the case in the present investigation. This yields

$$sU = -\nabla P - [1/(s^2+1)]\hat{e}_r \tag{5a}$$

$$sF = \frac{\partial \Phi}{\partial r}. \tag{5b}$$

The upper-case representation indicates the Laplace transformed variables.

The velocity potential is found to be

$$\Phi(r,z,s) = \sum_{n=1}^{\infty} A_n(s) I_0(k_n r)\cos[k_n(z+\Lambda)], \tag{6}$$

with $k_n = (n\pi/2\Lambda)$. Here, $A_n(s)$ indicates the unknown coefficients and I_0 represents the modified Bessel function.

Use of the kinematic condition yields

$$sF = \sum_{n=1}^{\infty} A_n(s) k_n I_1(k_n)\cos[k_n(z+\Lambda)] \quad \text{on} \quad r=1. \tag{7a}$$

However, use of the normal force balance condition yields a forced ordinary differential equation for $F(z,s)$ at $r = 1$,

$$\frac{\partial^2 F}{\partial z^2} + F = \left(\frac{B_0}{(s^2+1)}\right) z + B_0 K(s) + \sum_{n=1}^{\infty} B_0 s A_n(s) I_0(k_n)\cos[k_n(z+\Lambda)]. \tag{7b}$$

Note that s appears as a parameter. Also, $K(s)$ is a constant of integration. The solution of Eq. (7b) is

$$F(z,s) = a(s)\cos(z) + b(s)\sin(z) + B_0 K(s) + \left(\frac{B_0}{(s^2+1)}\right) z + \sum_{n=1}^{\infty} B_0\left(\frac{s A_n(s) I_0(k_n)\cos[k_n(z+\Lambda)]}{(1-k_n^2)}\right). \tag{7c}$$

Both forms given for $F(z,s)$ must be consistent, and must allow for the remaining boundary conditions to be satisfied. In order to determine the forms of the coefficients "$a(s)$" and "$b(s)$," it is advantageous to expand the functions $\sin(z)$, $\cos(z)$, and (z) in terms of $\cos[k_n(z+\Lambda)]$. These are found in the literature:[6,7]

$$A_{2m} = [2\sin(\Lambda)/\Lambda]\{s/[(1-k_{2m}^2)k_{2m} I_1(k_{2m}) - B_0 I_0(k_{2m}) s^2]\} a(s), \tag{8}$$

$$A_{2m-1} = \left[\left(\frac{2\cos(\Lambda)}{\Lambda}\right) s b(s) + B_0\left(\frac{-2}{\Lambda}\right)\left(\frac{s}{(s^2+1)}\right) \times \left(\frac{(1-k_{2m-1}^2)}{k_{2m-1}^2}\right)\right] (D_{2m-1})^{-1}, \tag{9}$$

with

$$D_{2m-1} = [(1-k_{2m-1}^2)k_{2m-1} I_1(k_{2m-1}) - B_0 I_0(k_{2m-1}) s^2].$$

The conservation of volume requires that

$$a(s)[\sin(\Lambda)/\Lambda] + B_0 K(s) = 0. \tag{10a}$$

Finally, the anchored triple-contact line condition is imposed. This yields a forced set of algebraic equations in the coefficients "$a(s)$" and "$b(s)$," of the form

$$(a11)a(s) + (a12)b(s) = c1, \tag{10b}$$

$$(a21)a(s) + (a22)b(s) = c2, \tag{10c}$$

with $a11 = a21$, $a22 = -a12$, and $c2 = -c1$, and with

$$(a11) = \cos(\Lambda) - \frac{\sin(\Lambda)}{\Lambda} + s^2\left(\frac{2\sin(\Lambda)}{\Lambda}\right) \times \sum_{m=0}^{\infty} \frac{B_0 I_0(k_{2m})}{[(1-k_{2m}^2)D_{2m}]}, \tag{10d}$$

$$(a12) = -\sin(\Lambda) + s^2\left(\frac{2\cos(\Lambda)}{\Lambda}\right) \times \sum_{m=0}^{\infty} \frac{B_0 I_0(k_{2m-1})}{[(1-k_{2m-1}^2)D_{2m-1}]}, \tag{10e}$$

$$(c1) = \left(\frac{B_0}{(s^2+1)}\right)\Lambda\left[1 + \left(\frac{2s^2}{\Lambda^2}\right) \times \sum_{m=0}^{\infty} \frac{B_0 I_0(k_{2m-1})}{(k_{2m-1}^2 D_{2m-1})}\right], \tag{10f}$$

and with

$$D_q = [k_q(1-k_q^2)I_1(k_q) - B_0 I_0(k_q)s^2].$$

It is found that

$$a(s) = 0 \text{ and } b(s) = (c1/a12). \tag{10g}$$

Recall that the expression for A_{2m} contained the factor $a(s)$. Thus A_{2m} will be identically zero, and only the odd modes will contribute to the motion. This reflects the nature of the forcing, i.e., "z" is an odd function with respect to the mean plane between the disks.

The form of the Laplace-transformed perturbation interface $F(z,s)$ is given by

$$F(z,s) = b(s)\sin(z) + B_0\left(\frac{1}{(s^2+1)}\right) z + \sum_{m=0}^{\infty} \frac{s A_{2m-1}(s) B_0 I_0(k_{2m-1})\cos[k_{2m-1}(z+\Lambda)]}{(1-k_{2m-1}^2)}, \tag{11}$$

with the A_{2m-1} as previously determined. Taking the inverse Laplace transform of Eq. (11) will yield the expression for $f(z,t)$.

In order to gain insight into the form of the perturbation interface in the presence of a periodic body force directed along the longitudinal axis of the column, the series will be severely truncated. Only one term in each series will be retained. The inversion will then be done analytically.

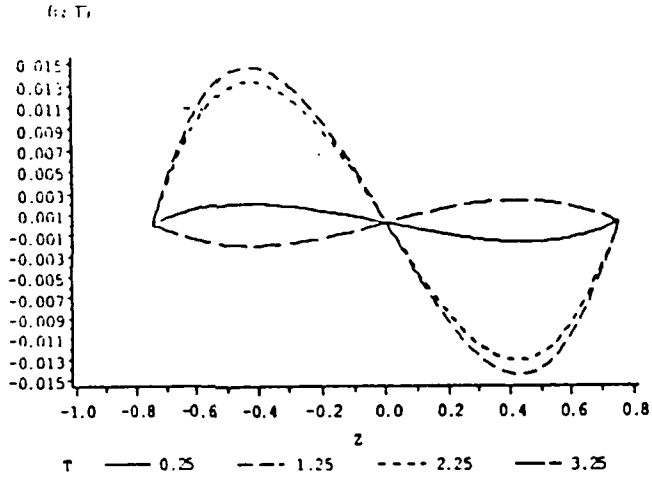

FIG. 1. Deformation $f(z,t)$ versus time, for time = 0.25, 1.25, 2.25, 3.25. $B_0 = 0.50$ and $\Lambda = 0.75$.

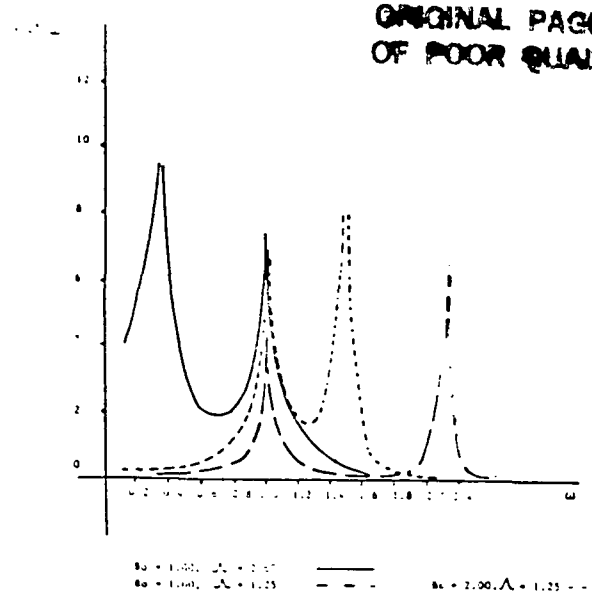

FIG. 2. Transfer function $F(z^*,\omega)$, $z^* = -\Lambda/2$, for the cases ($\Lambda = 2.60$, $B_0 = 1.00$), ($\Lambda = 1.25$, $B_0 = 1.00$), and ($\Lambda = 1.25$, $B_0 = 2.00$).

Then

$$f(z,t) = \sin(z)b(t) + B_0(z)\sin(t) + \cos[k_1(z+\Lambda)] \times \left(\frac{-2\cos\Lambda}{\Lambda(1-k_1^2)}\right)\left(\alpha \int_0^t b(\tau)\sinh[\alpha(t-\tau)]d\tau + b(t)\right) + \cos[k_1(z+\Lambda)]\left(\frac{2B_0}{\alpha\Lambda k_1^2}\right) \times \left(\int_0^t \sin(\tau)\sinh[\alpha(t-\tau)]d\tau + \alpha\sin(t)\right), \tag{12}$$

with

$$\alpha^2 = \left(\frac{k_1(1-k_1^2)I_1(k_1)}{B_0 I_0(k_1)}\right), \quad b(t) = \mathcal{L}^{-1}(b(s)),$$

$$\delta^2 = \left[1 + \left(\frac{2\,\text{cotan}\,\Lambda}{\Lambda(1-k_1^2)}\right)\right], \quad \text{and } \beta^2\delta^2 = \alpha^2.$$

The inverse Laplace transform for $F(z,s)$ [see Eq. (11)] was taken numerically for different values of (B_0,Λ). Graphical results are presented in Fig. 1 for the case $(B_0 = 0.5, \Lambda = 0.75)$ at successive (nondimensional) times of 0.25, 1.25, 2.25, and 3.25. The maximum value of $f(z,t)$ at each of these times is 0.0019, 0.0145, 0.0131, and 0.002, respectively. The value of the parameter Λ indicates that the column is not slender. Note the sinusoidal form of the interface deformation. This is observed for the case of the axially directed forcing.[1]

The equation for $F(z,s)$ [Eq. (11)] can be viewed as a transfer function. Setting $s = i\omega$, values of F may be plotted in frequency space. This is done, and the results are shown in Fig. 2 for $\Lambda = 2.60$, $B_0 = 1.00$, and $\Lambda = 1.25$ with $B_0 = 1.00$ and 2.00. The curve for the slender column ($\Lambda = 2.60$) may be compared with a similar type graph found in Ref. 4 (Fig. 3 in that work). It is seen that a spike in both graphs occur about the resonant frequency at $\omega = 0.34$. The long column is shown to be sensitive to lower-frequency disturbances ($\omega < 1$), as indicated by the relatively large functional values [for $F(z,s)$] in this work and in Ref. 4. Note that the numerical value of $F(z^*,\omega)$ (with $z^* = -\Lambda/2$) compares well with that of the defined transfer function perturbation amplitude in Ref. 4.

It was found that nonslender columns are not similarly sensitive to these low-frequency disturbances. This is shown graphically in Fig. 2 for $\Lambda = 1.25$, $B_0 = 1.00$, and $B_0 = 2.00$. Note the low numerical values of $F(z^*,\omega)$ as compared with that of the case $\Lambda = 2.60$, $B_0 = 1.00$.

The work of Sanz[6] determined the nondimensional natural frequency $\tilde{\omega}_{nat}$ of the fluid column for a range of Λ values. In that work, time was nondimensionalized by $(\rho R^3/\gamma)^{1/2}$. It can be shown that this results in the following equivalence $(\omega_f^2/\omega_{nat}^2) = B_0(1/\tilde{\omega}_{nat}^2)$.

The perturbation interface was determined (numerically) in a number of cases for which the (B_0,Λ) values corresponded to eigenvalues of the unforced system. In these cases, the inviscid finite length fluid column was found to be very sensitive to forcing.

Various orders of magnitude for the vibration level have appeared in the literature.[8] The range of interest of parameter B_0 can be constructed for fluid cylinders of a given density and radius. The interface shape can be obtained for specific values of B_0 and Λ.

ACKNOWLEDGMENTS

The author would like to thank Dr. F. Leslie, Dr. N. Ramachandran, and Ms. C. M. Winter for helpful discussions.

This work was performed as part of Project JOVE (NAG8-149) for NASA Marshall Spaceflight Center.

J. Martinez, Acta Astron. 15, 449 (1987).
[2]J. Meseguer, J. Cryst. Growth 62, 577 (1983).
[3]Y. Zhang and J. I. D. Alexander, Phys. Fluids A 2, 1966 (1990).
[4]J. Meseguer, Appl. Microgravity Tech. I, 136 (1988).
[5]J. Meseguer, A. Sanz, and J. M. Perales, Appl. Microgravity Tech. II, 186 (1990).
[6]A. Sanz, J. Fluid Mech. 156, 101 (1985).
[7]A. Sanz and J. Lopez Diez, J. Fluid Mech. 205, 503 (1989).
[8]N. Ramachadran and C. M. Winter, AIAA Paper No. 90-0654, 1990.

Fluid Column Stability in the Presence of Periodic Accelerations

M. J. Lyell*
West Virginia University, Morgantown, West Virginia 26506

Introduction

THE float zone configuration is used in crystal growth. It may be modeled as a liquid column held by surface tension forces between two end disks. In the case of crystal growth, the thermal and solutal fields as well as those of velocity and pressure are needed to characterize the physics. A compelling reason for crystal growth experiments in a microgravity environment such as that onboard the Space Shuttle is that buoyancy forces are greatly reduced.[1] However, this environment is not quiescent due to the presence of impulse type disturbances from small thruster firings as well as those from periodic vibrations. Given certain "environmental" conditions, such as the presence of a periodic acceleration field, it is possible that a fluid dynamical instability would develop. This would adversely effect the crystal growth.

The crystal growth environment cannot be separated from the fluid dynamics of the liquid column. This latter topic is the focus of the present work. The question of column interface stability in the presence of a periodic acceleration field having a component normal to the longitudinal axis of the isothermal cylinder is investigated. The fluid column is taken to be infinite in length. Floquet theory is used in the stability investigation.

Previous work has determined the natural oscillations of the liquid column. This work was done first for the case of the infinite column[2] and later for the finite length case. In the latter work, both axisymmetric and nonaxisymmetric oscillations were considered.[3,4] Results for the infinite length case were found to be good approximations to those for the finite length column, both numerically and with regard to trends.

Interface behavior of the finite length liquid column in the presence of time-dependent forcing has been investigated for the case in which the forcing was parallel to the longitudinal axis of the column.[5,6] The investigations considered the column behavior subject to a $\sin(t)$ forcing for both the inviscid case of general aspect ratio (within static stability limits[5]) and the viscous case in the slender column limit.[6]

The problem of interface stability of the fluid column in the presence of a periodic acceleration field that has a component normal to the longitudinal axis of the column has not been investigated. Previous work has considered the interface stability of a highly idealized infinite slab-like configuration in the presence of a periodic acceleration field oriented normal to the interface.[7] Interestingly, this study was motivated by experiments in microgravity.

Use of the infinite length configuration in this stability study results in a simplification in that the standard boundary conditions at the solid end disks are not applied, and the focus remains on the interface stability. If an extension of this work to the finite length configuration is of interest, Floquet analysis would be appropriate, although the implementation would be more complicated.

Formulation

The basic configuration is that of an infinite fluid column of circular cross section. The fluid is incompressible, and the surrounding medium is of negligible density. Perturbations are taken to be irrotational. The analysis is linear and inviscid, with the nondimensionalized governing equations those of continuity and conservation of momentum (linearized Euler).

The frequency of the periodic forcing is denoted by ω_f. Pressure and velocity fields are given by p and u, nondimensionalized as follows:

$$R\tilde{x} = x \qquad \omega_f^{-1}\tilde{t} = t \qquad R\omega_f\tilde{u} = u \qquad \rho(R\omega_f)^2\tilde{p} = p \tag{1}$$

Tildes indicate nondimensional quantities.

The continuity and Euler equations are then

$$\tilde{\nabla}\cdot\tilde{u} = 0 \tag{2a}$$

$$\frac{\partial\tilde{u}}{\partial\tilde{t}} + \tilde{u}\cdot\tilde{\nabla}\tilde{u} = -\tilde{\nabla}\tilde{p} - Fr\cos(\tilde{t})\tilde{\nabla}[(1-\tilde{r})\sin\theta] \tag{2b}$$

with $Fr = (Go/R\omega_f^2)$ a Froude type number. Go is the amplitude of the periodic acceleration field. The functional form of the time-dependent forcing is selected to be $\cos(\tilde{t})$.

Received Sept. 21, 1992; revision received Jan. 20, 1993; accepted for publication Jan. 24, 1993.

*Associate Professor, Mechanical and Aerospace Engineering Department. Senior Member AIAA.

The mean state is one of zero velocity; however, the mean pressure is time dependent. Consider a wave-like perturbation propagating on the interface. The governing equations for the perturbation are developed as follows. Expand in the small perturbation parameter ϵ

$$\hat{p} = p_{m(can)} + \epsilon p \qquad \hat{u} = \epsilon u = \epsilon \nabla \phi \tag{3}$$

Substitution of Eq. (3) into Eqs. (2) yields the mean system

$$\nabla p_{m(can)} = -Fr \cos(t) \nabla [(1 - r)\sin\theta] \tag{4}$$

(with the parameter Fr of order one) and the (order ϵ) perturbation equations

$$\nabla^2 \phi = 0 \tag{5a}$$

$$\frac{\partial(\nabla \phi)}{\partial t} = -\nabla p \tag{5b}$$

The spatial dependence of the velocity potential can be determined via solution of Eq. (5a), which is

$$\phi(r, \theta, z, t) = \sum A(t) I_m(kr) \exp(ikz) \exp(im\theta) \tag{6}$$

I_m is the mth modified Bessel function. Clearly, the solution involves a superposition of the azimuthal modes.

It is through the boundary conditions that the free interface can be determined and the stability characteristics investigated. Let the equilibrium interface be given by

$$Fe = r - 1 - \epsilon\eta(\theta, z, t) = r - 1 - \epsilon \sum C(t) \exp(ikz + im\theta) \tag{7}$$

The kinematic condition and the normal force balance at the free interface must be satisfied. In addition, the requirement of conservation of mass, which reduces to a conservation of volume condition, must hold.

The linearized kinematic condition (at order ϵ) is

$$-\frac{\partial \eta}{\partial t} + u_r = 0 \tag{8a}$$

at $r = 1$ with $u_r = \partial\phi/\partial r$. This results in

$$\sum \left(\frac{dC}{dt}\right) \exp(ikz + im\theta) = \sum [I_m(k)]' A(t) \exp(ikz + im\theta) \tag{8b}$$

The normal force balance requires that the difference in pressure across the interface be equal to the curvature multiplied by the surface tension force. In nondimensional form, this is given by

$$Bo \times \Delta(p_{m(can)} + \epsilon p) = \nabla \cdot \mathbf{n} \tag{9a}$$

with $\mathbf{n} = \nabla Fe / \| \nabla Fe \|$. Bo is the nondimensional parameter $(\rho R^3 \omega_f^2 / \gamma)$, with γ the surface tension and ρ the density. At order ϵ, the linearized form of this interfacial condition can be expressed as

$$\eta + \eta_{zz} + \eta_{\theta\theta} + [Bo \cos(t) \sin\theta]\eta = Bo\left(\frac{\partial \phi}{\partial t}\right) \tag{9b}$$

Fr, required to be of order one, has been set equal to unity. The subscripts indicate partial differentiation. This yields

$$\sum [(1 - m^2 - k^2) + Bo \cos(t) \sin\theta] \times C(t) \exp(ikz + im\theta)$$
$$= \sum A(t) I_m(k) \exp(ikz + im\theta) \tag{9c}$$

The sin θ dependence can be re-expressed as an exponential function. Then

$$C_m(t)(1 - m^2 - k^2) + \left(\frac{Bo}{2}\right)(-i)\cos(t)[C_{m-1}(t) - C_{m+1}(t)] = Bo I_m(k)\left(\frac{dA_m}{dt}\right) \tag{9d}$$

and azimuthal mode coupling occurs. Use of Eqs. (8c) and (9d) yields a nonautonomous second-order equation in $C_m(t)$, with mode coupling (as indicated by the subscripts m)

$$\ddot{C}_m - [(1 - m^2 - k^2)/Bo]\,|I_m'/I_m|\,C_m = |I_m'/2I_m|\cos(t)(-i)[C_{m-1}(t) - C_{m+1}(t)] \tag{10}$$

Keep in mind that $\cos(t)$ can be rewritten in exponential form. It is at this juncture that Floquet analysis is applied. For convenience, let $E_m(t) = [dC_m(t)/dt]$. Then take

$$[C_m(t), E_m(t)] = \sum_{l=-\infty}^{\infty} [C_{m,l}, E_{m,l}] \times \exp[(\lambda + il)t] \tag{11}$$

The constant coefficients $C_{m,l}$ and $E_{m,l}$ are unknown. The Floquet exponent is denoted by the eigenvalue λ, which is in general a complex number, and which is also unknown. The nonautonomous differential system is thus transformed into a homogeneous algebraic system for $(C_{m,l}, E_{m,l})$ with the unknown parameter (eigenvalue) λ. If Real(λ) is greater than zero, the interface of the cylindrical column is unstable to the growing wave-like perturbation. Of course, the milieu in which this disturbance is propagating includes the periodic base state pressure.

Use of Eq. (11) in Eq. (10) (rewritten as two first-order modes) yields the infinite algebraic system given by

$$(\lambda + il)C_{m,l} = E_{m,l} \tag{12a}$$

$$(\lambda + il)E_{m,l} = [(1 - m^2 - k^2)/(Bo)](I_m'/I_m)C_{m,l} + (\tfrac{1}{4} I_m'/I_m)(-i)(C_{m-1,l-1} + C_{m-1,l+1} - C_{m+1,l-1} - C_{m+1,l+1}) \tag{12b}$$

Note that the harmonic modes (indicated by l) as well as the azimuthal modes (indicated by m) are coupled to both their preceding and successive modes.

Several remarks are in order concerning the truncation. Once the truncation in m is done, the number of azimuthal modes that contribute are fixed. It is to this truncated system that Floquet analysis is actually applied. To obtain numerical values for λ, it is necessary to truncate the number of harmonic modes in time, i.e., the range of l values. The eigenvalue problem is, therefore, a problem of the truncated system.

Results

The results pertain to the eigenvalue solutions of system (12a) and (12b). NAG library routines were used in determining the eigenvalues. Truncation values of $L = 11|1$, that is, $-15 \le l \le 15$, and $M = 14$ were found to be sufficient. Wave number values ranged from $k = 0.10$ to $k = 3.00$. The parameter Bo was varied from 0.01 to 10.00.

For $k < 1.0$, the interface is unstable to the wave-like perturbation in the presence of a mean periodic acceleration field

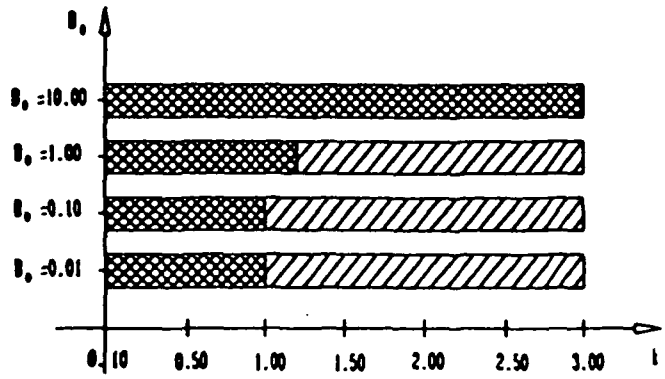

Fig. 1 Stability diagram: the stability of the configuration to wave-like perturbations for a range of Bo parameter values vs wave number k is shown. The cross-hatched area indicates unstable regions in which disturbances are growing in time. The remaining area corresponds to that of the marginal stability state.

over the range of *Bo* values considered. (Note that this range encompasses four orders of magnitude; see Fig. 1.)

As k is increased, such that $1.00 \le k \le 1.20$, the interface remains unstable to the perturbation for the two larger *Bo* values, equal to 10.00 and 1.00. However, marginal stability [Real(λ) = 0] ensues at the smaller *Bo* values. A decrease in *Bo* can be interpreted physically as an increase in the surface tension. So, as the surface tension increases, the restoring force is sufficient to result in marginal stability over this range of wave numbers.

Perturbations corresponding to the larger wave numbers (smaller wavelengths) that were considered, $2.0 \le k \le 3.0$, were found not to grow in time for *Bo* = 0.01-1.00. That is, instability [with Real(λ) > 0] of the interface to perturbations of these larger wave numbers (and smaller wavelengths) occurs only for *Bo* = 10.00; otherwise, Real(λ) = 0. An alternative physical interpretation to that involving a variation in surface tension for differing *Bo* values can be developed. Since *Fr* was taken to be unity, ω_f^2 (the forcing frequency) is proportional to *Go*, the amplitude of the periodic acceleration field. Utilizing this relation in the definition for *Bo* yields $Bo \alpha (Go/\gamma)$. For fixed surface tension (and, of course, density and column radius) values, an increase in *Bo* would result from an increase in forcing amplitude. It is at the highest such amplitude considered that the interface was found to be unstable [with Real(λ) > 0] to the perturbation.

It is noted that the range of *Bo* values used corresponds to values of *Go* and ω_f that would be of interest in a microgravity environment for certain ranges of surface tension values. (Roughly, $10^{-4} g_{earth} \le Go \le 10^{-2} g_{earth}$, and 0.5 Hz < ω_f < 5 Hz for γ values of 1-100 dynes/cm.)

Acknowledgment

NASA support (NAG8-149, JOVE) is acknowledged.

References

[1]Kassemi, S. A., and Ostrach, S., "Nature of Buoyancy-Driven Flows in a Reduced Gravity Environment," *AIAA Journal*, Vol. 30, No. 7, 1992, pp. 1815-1818.

[2]Bauer, H., "Coupled Oscillations of a Solidly Rotating Liquid Bridge," *Acta Astronautica*, Vol. 9, No. 9, 1982, pp. 547-563.

[3]Sanz, A., "The Influence of the Outer Bath in the Dynamics of Axisymmetric Liquid Bridges," *Journal of Fluid Mechanics*, Vol. 156, July 1985, pp. 101-140.

[4]Sanz, A., and Lopez Diez, J., "Non-Axisymmetric Oscillations of Liquid Bridges," *Journal of Fluid Mechanics*, Vol. 205, Aug. 1989, pp. 503-521.

[5]Lyell, M. J., "Axial Forcing of an Inviscid Finite Length Fluid Cylinder," *Physics of Fluids A*, Vol. 3, No. 7, 1991, pp. 1828-1831.

[6]Meseguer, J., and Perales, J. M., "A Linear Analysis of g-Jitter Effects on Viscous Cylindrical Liquid Bridges," *Physics of Fluids*, Vol. 3, No. 10, 1992, pp. 2332-2336.

[7]Jacqmin, D., and Duval, W. M. B., "Instabilities Caused by Oscillating Accelerations Normal to a Viscous Fluid-Fluid Interface," *Journal of Fluid Mechanics*, Vol. 196, Nov. 1988, pp. 495-511.

SECTION C

Finite Length Liquid Column Stability in the Presence of a Periodic Acceleration Field Oriented Normal the Longitudinal Axis

BACKGROUND -

There have been several studies of both forced and free oscillations of fluid cylinders. In previous studies which incorporated forcing into the problem formulation, the forcing has been directed parallel to the longitudinal axis of the fluid column. Although those problems are highly relevant, another important problem is the case of forcing directed so as to have a component perpendicular to the longitudinal axis.

Therefore, this investigation addresses the stability of the fluid column interface in the presence of an acceleration field which is directed perpendicular to the longitudinal axis of the column. Moreover, this periodic acceleration field gives rise to a periodic pressure field as the base state.

APPROACH

The analysis is linear and inviscid. Governing equations are those of conservation of mass and momentum. The nondimensionalization is chosen to be such that the acceleration field forcing term will balance the mean pressure field. The mean pressure field gradient will then be found to depend on both time (t) and theta (the angular dependence).

The solution for Φ is obtained in the standard fashion. It is a solution to Laplace's equation, and since it has been listed in previous reports, it will not be repeated here.

In the solution, there is a dependence of the mean pressure field on theta; it is this not possible to consider disturbances

which are strictly even or odd in theta. Thus, an additional summation should be present, with $\exp(im\theta)$ the functional form in theta.

In the case of the finite length column, the velocity normal to the end disks must be zero. Also, the anchored triple contact line condition is imposed at each of the end disks.

At the free interface, the kinematic condition and the normal force balance must be imposed. The normal force balance will contain a term which represents the presence of the forcing, and it will multiply the free surface perturbation, which itself is a dependent variable.

Thus, the normal force balance will be non-autonomous due to the presence of the sinusoidal forcing function, and a "$\sin\theta$" factor will be introduced, reflecting the mean pressure form.

The goal is to obtain ordinary differential equations in time. The stability of such a system can then be investigated.

Ideally, the z and θ dependencies could be eliminated. For example, the z-dependence could be eliminated via introduction of a set of expansions in z which would satisfy the anchored triple contact line conditions. This is essentially a galerkin method approach, and would require use of the orthogonality properties of the selected expansion functions.

The previous difficulties associated with the presence of theta have been overcome. Elimination of theta results in an infinite system of ordinary differential equations with respect to time. Inspection of this infinite system reveals that the even and

odd azimuthal modes are coupled.

It was realized during the implementation of these considerations that the original basic formulation did not allow for the static deformation of the column, independent of any wave-like perturbation on the surface. That is, the first formulation does not reflect the physical reality as closely as it must.

This was remedied in recent work. The incorporation of the static deformation into the formulation is now complete. This has had the effect of adding coupling between the longitudinal modes as well as the azimuthal modes.

Floquet theory is then utilized to transform the system of differential equations into an infinite set of algebraic equations in a parameter, (lower case) lambda. This parameter is the eigenvalue. Determination of the eigenvalues will give the stability results; if, for all λ, Real(λ) < 0, then the system is stable. The case of marginal stability is given by Real(λ) = 0. This determination of the eigenvalues must be done numerically. In order to effect the numerical investigation, the system must be truncated.

In principle, the finite length and infinite length column stability cases could both be done in this manner. However, the computer system which is being utilized has restrictions on memory and running time which is making the solution of the finite problem difficult.

The aforementioned solution method involves the generation of

a large matrix representing the truncated system, with an assumed Fourier representation in time. The truncations to the solutions are done in the summations representing the solution form in θ, z, and time, t. For low frequency forcing , the number of terms required to for the temporal truncation can be prohibitive. Such a matrix can grow so large that it is difficult to utilize an eigenvalue solver due to computer limitations. An alternative method is sought.

It is noted that the matrix which is generated is much less sparse than it would be if static deformation did not contribute.

Such an alternative method is in the process of being implemented. This involves retaining the derivatives in time; ie, assuming no fourier expansion in time, and constructing a fundamental matrix which represents the system (itself truncated in indices corresponding to θ and z). The eigenvalues of this fundamental matrix are related to those of the system, allowing for calculation of those of the system. Construction of the fundamental matrix proceeds via integration of the system for suitably chosen sets of independent initial conditions to the end of the first forcing period. The solution vector represents a column vector in the fundamental matrix.

SECTION D

publications

Axial forcing of an inviscid finite length fluid cylinder

M. J. Lyell
Department of Mechanical and Aerospace Engineering, West Virginia University, Morgantown, West Virginia 26506-6101

(Received 8 August 1990; accepted 7 March 1991)

Current interest in microgravity materials processing has focused attention upon the finite fluid column. This configuration is used in the modeling of float zones. In this Brief Communication, the incompressible inviscid finite length fluid column is subjected to an axial, time-dependent disturbance. The response of the fluid system and the resulting interface location are determined via Laplace transform methods.

The presence of vibrations will affect the fluid dynamical environment in which materials processing occurs. Experiments performed on Spacelab D1 investigated the effect of g-jitter on the stability of finite fluid columns. It was found that long columns are particularly sensitive to residual accelerations and impulses.[1] The analytical effort has been concerned with the *axial* forcing of *slender* liquid bridges.[2-5] In these analyses, a one-dimensional "slice" model has been used. Such a restriction is invalid in the situation in which the liquid column is not slender, yet whose height and radius are within the static stability limits for fluid columns. The work of Sanz[6,7] has addressed the problem of the *unforced* modes of oscillation of a nonslender finite fluid column.

In this work, the problem of the *axially forced* finite fluid column is investigated, with the axial forcing considered periodic in time. The analysis is linear, inviscid, incompressible, and axisymmetric. It utilizes Laplace transform techniques. The direction of the imposed body force is taken parallel to the longitudinal axis, and in the negative $\hat{e}_z$ direction. The undisturbed column is cylindrical, and is surrounded by an inert gas.

Quantities will be nondimensionalized as follows:

$$R\tilde{\mathbf{x}}=\mathbf{x},\quad \omega_f^{-1}\tilde{t}=t,\quad R\omega_f\tilde{\mathbf{u}}=\mathbf{u},\quad \rho\omega_f^2R^2\tilde{p}=p, \tag{1}$$

and R is the radius of the column. The forcing frequency is ω_f. Pressure and velocity fields are indicated by p and $\mathbf{u}$, respectively. The density of the column is given by ρ. A tilde indicates dimensionless quantities.

Equations are to be rendered nondimensional through the use of (1). This results in

$$\nabla\cdot\mathbf{u}=0, \tag{2a}$$

$$\frac{\partial\mathbf{u}}{\partial t}+\mathbf{u}\cdot\nabla\mathbf{u}=-\nabla p-\mathrm{Fr}\,g(t)\hat{e}_z \tag{2b}$$

and the nondimensional interface equation is

$$f_e=r-1-\mathrm{Fr}\,f(z,t) \tag{2c}$$

with $f(z,t)$ representing the functional form of the perturbation to the interface. The tildes have been dropped for convenience. The nondimensional parameter Fr is a Froude type number, and is given by $(G_0/R\omega_f^2)$. It is taken to be a small parameter. Pressure and velocity are expanded in terms of Fr about a state of zero mean motion. This results in the linearized system of governing equations

$$\nabla\cdot\mathbf{u}=0, \tag{3a}$$

$$\frac{\partial(\nabla\phi)}{\partial t}=-\nabla p-g(t)\hat{e}_z \tag{3b}$$

with $\mathbf{u}=\nabla\phi$. For definiteness, $g(t)$ is chosen to be $\sin(t)$.

The boundary conditions at the upper and lower disks are that the normal component of the velocity be zero. Also, an anchored triple-contact line assumption at both disks will further restrict the interface behavior. These are

$$\left.\frac{\partial\phi}{\partial z}\right|_{z=\Lambda}=0,\quad \left.\frac{\partial\phi}{\partial z}\right|_{z=-\Lambda}=0, \tag{4a}$$

$$f(\Lambda,t)=f(-\Lambda,t)=0. \tag{4b}$$

The constant Λ acts as a slenderness parameter, and is given by $(L/2R)$. As the fluid is incompressible, volume must be conserved, and so

$$\int_{-\Lambda}^{\Lambda}f(z,t)\,dz=0. \tag{4c}$$

Because of axisymmetry

$$u_r\Big|_{r=0}=0,\quad \left.\frac{\partial w}{\partial r}\right|_{r=0}=0. \tag{4d}$$

At the fluid column/inert gas interface, both the kinematic and normal force balance conditions must be imposed. These are given by

$$\frac{-\partial f}{\partial t}+\frac{\partial\phi}{\partial z}=0, \tag{4e}$$

$$\Delta p=\left(\frac{-1}{B_0}\right)\left(\frac{\partial^2 f}{\partial z^2}+f\right), \tag{4f}$$

and are evaluated on $r=1$ (Δp indicates the change in pressure across the interface). The nondimensional parameter B_0 is given by $(\rho R^3\omega_f^2/\gamma)$. Gamma denotes the surface tension. Note that Eqs. (4e) and (4f) have been linearized [and are at $O(\mathrm{Fr})$].

Both the system of equations (3) and the boundary/interface conditions (4) are Laplace-transformed with respect to time. The time dependence is replaced by a pa-

 0899-8213/91/071828-04$02.00

rameter s. The initial velocity perturbation is taken to be zero. The initial position of the interface is taken to be that of the undisturbed cylindrical column $f_e = 1$. This is realistic for the case of a zero mean gravity, which is the case in the present investigation. This yields

$$sU = -\nabla P - [1/(s^2+1)]\hat{e}_r \tag{5a}$$

$$sF = \frac{\partial \Phi}{\partial r}. \tag{5b}$$

The upper-case representation indicates the Laplace transformed variables.

The velocity potential is found to be

$$\Phi(r,z,s) = \sum_{n=1}^{\infty} A_n(s) I_0(k_n r)\cos[k_n(z+\Lambda)], \tag{6}$$

with $k_n = (n\pi/2\Lambda)$. Here, $A_n(s)$ indicates the unknown coefficients and I_0 represents the modified Bessel function.

Use of the kinematic condition yields

$$sF = \sum_{n=1}^{\infty} A_n(s) k_n I_1(k_n)\cos[k_n(z+\Lambda)] \quad \text{on} \quad r=1. \tag{7a}$$

However, use of the normal force balance condition yields a forced ordinary differential equation for $F(z,s)$ at $r = 1$,

$$\frac{\partial^2 F}{\partial z^2} + F = \left(\frac{B_0}{(s^2+1)}\right) z + B_0 K(s) + \sum_{n=1}^{\infty} B_0 s A_n(s) I_0(k_n)\cos[k_n(z+\Lambda)]. \tag{7b}$$

Note that s appears as a parameter. Also, $K(s)$ is a constant of integration. The solution of Eq. (7b) is

$$F(z,s) = a(s)\cos(z) + b(s)\sin(z) + B_0 K(s) + \left(\frac{B_0}{(s^2+1)}\right) z + \sum_{n=1}^{\infty} B_0\left(\frac{s A_n(s) I_0(k_n)\cos[k_n(z+\Lambda)]}{(1-k_n^2)}\right). \tag{7c}$$

Both forms given for $F(z,s)$ must be consistent, and must allow for the remaining boundary conditions to be satisfied. In order to determine the forms of the coefficients "$a(s)$" and "$b(s)$," it is advantageous to expand the functions $\sin(z)$, $\cos(z)$, and (z) in terms of $\cos[k_n(z+\Lambda)]$. These are found in the literature;[6,7]

$$A_{2m} = [2\sin(\Lambda)/\Lambda]\{s/[(1-k_{2m}^2)k_{2m} I_1(k_{2m}) - B_0 I_0(k_{2m}) s^2]\} a(s), \tag{8}$$

$$A_{2m+1} = \left[\left(\frac{2\cos(\Lambda)}{\Lambda}\right) s b(s) + B_0\left(\frac{-2}{\Lambda}\right)\left(\frac{s}{(s^2+1)}\right) \times \left(\frac{(1-k_{2m+1}^2)}{k_{2m+1}^2}\right)\right] (D_{2m+1})^{-1}, \tag{9}$$

with

$$D_{2m+1} = [(1-k_{2m+1}^2)k_{2m+1} I_1(k_{2m+1}) - B_0 I_0(k_{2m+1}) s^2].$$

The conservation of volume requires that

$$a(s)[\sin(\Lambda)/\Lambda] + B_0 K(s) = 0. \tag{10a}$$

Finally, the anchored triple-contact line condition is imposed. This yields a forced set of algebraic equations in the coefficients "$a(s)$" and "$b(s)$," of the form

$$(a11)a(s) + (a12)b(s) = c1, \tag{10b}$$

$$(a21)a(s) + (a22)b(s) = c2, \tag{10c}$$

with $a11 = a21$, $a22 = -a12$, and $c2 = -c1$, and with

$$(a11) = \cos(\Lambda) - \frac{\sin(\Lambda)}{\Lambda} + s^2\left(\frac{2\sin(\Lambda)}{\Lambda}\right) \times \sum_{m=0}^{\infty} \frac{B_0 I_0(k_{2m})}{[(1-k_{2m}^2)D_{2m}]}, \tag{10d}$$

$$(a12) = -\sin(\Lambda) + s^2\left(\frac{2\cos(\Lambda)}{\Lambda}\right) \times \sum_{m=0}^{\infty} \frac{B_0 I_0(k_{2m+1})}{[(1-k_{2m+1}^2)D_{2m+1}]}, \tag{10e}$$

$$(c1) = \left(\frac{B_0}{(s^2+1)}\right)\Lambda\left[1 + \left(\frac{2s^2}{\Lambda^2}\right) \times \sum_{m=0}^{\infty} \frac{B_0 I_0(k_{2m+1})}{(k_{2m+1}^2 D_{2m+1})}\right], \tag{10f}$$

and with

$$D_q = [k_q(1-k_q^2)I_1(k_q) - B_0 I_0(k_q)s^2].$$

It is found that

$$a(s) = 0 \text{ and } b(s) = (c1/a12). \tag{10g}$$

Recall that the expression for A_{2m} contained the factor $a(s)$. Thus A_{2m} will be identically zero, and only the odd modes will contribute to the motion. This reflects the nature of the forcing, i.e., "z" is an odd function with respect to the mean plane between the disks.

The form of the Laplace-transformed perturbation interface $F(z,s)$ is given by

$$F(z,s) = b(s)\sin(z) + B_0\left(\frac{1}{(s^2+1)}\right) z + \sum_{m=0}^{\infty} \frac{s A_{2m+1}(s) B_0 I_0(k_{2m+1})\cos[k_{2m+1}(z+\Lambda)]}{(1-k_{2m+1}^2)}, \tag{11}$$

with the A_{2m+1} as previously determined. Taking the inverse Laplace transform of Eq. (11) will yield the expression for $f(z,t)$.

In order to gain insight into the form of the perturbation interface in the presence of a periodic body force directed along the longitudinal axis of the column, the series will be severely truncated. Only one term in each series will be retained. The inversion will then be done analytically.

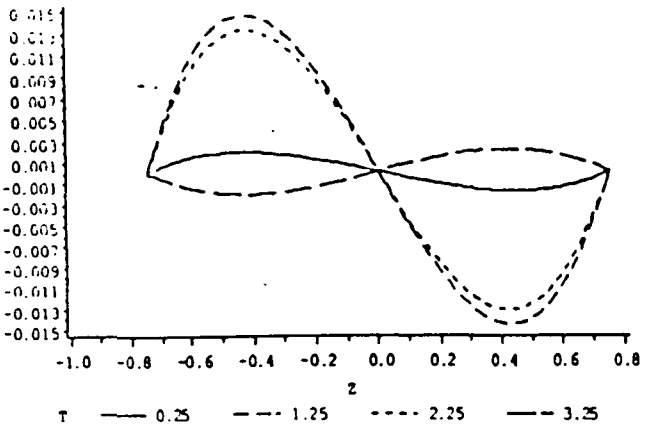

FIG. 1. Deformation $f(z,t)$ versus time, for time = 0.25, 1.25, 2.25, 3.25. $B_0 = 0.50$ and $\Lambda = 0.75$.

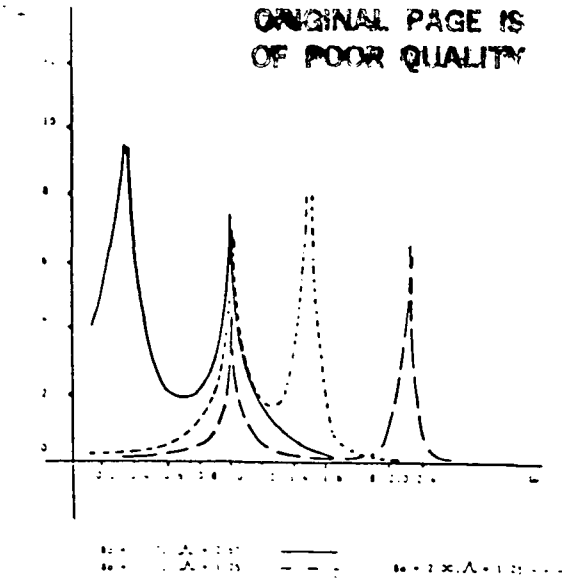

FIG. 2. Transfer function $F(z^*,\omega)$, $z^* = -\Lambda/2$, for the cases ($\Lambda = 2.60$, $B_0 = 1.00$), ($\Lambda = 1.25$, $B_0 = 1.00$), and ($\Lambda = 1.25$, $B_0 = 2.00$).

Then

$$f(z,t) = \sin(z)b(t) + B_0(z)\sin(t) + \cos[k_1(z+\Lambda)] \times \left(\frac{-2\cos\Lambda}{\Lambda(1-k_1^2)}\right)\left(\alpha \int_0^t b(\tau)\sinh[\alpha(t-\tau)]d\tau + b(t)\right) + \cos[k_1(z+\Lambda)]\left(\frac{2B_0}{\alpha\Lambda k_1^2}\right) \times \left(\int_0^t \sin(\tau)\sinh[\alpha(t-\tau)]d\tau + \alpha\sin(t)\right), \quad (12)$$

with

$$\alpha^2 = \left(\frac{k_1(1-k_1^2)I_1(k_1)}{B_0 I_0(k_1)}\right), \quad b(t) = \mathcal{L}^{-1}(b(s)),$$

$$\delta^2 = \left[1 + \left(\frac{2\,\text{cotan}\,\Lambda}{\Lambda(1-k_1^2)}\right)\right], \quad \text{and } \beta^2\delta^2 = \alpha^2.$$

The inverse Laplace transform for $F(z,s)$ [see Eq. (11)] was taken numerically for different values of (B_0,Λ). Graphical results are presented in Fig. 1. for the case $(B_0 = 0.5, \Lambda = 0.75)$ at successive (nondimensional) times of 0.25, 1.25, 2.25, and 3.25. The maximum value of $f(z,t)$ at each of these times is 0.0019, 0.0145, 0.0131, and 0.002, respectively. The value of the parameter Λ indicates that the column is not slender. Note the sinusoidal form of the interface deformation. This is observed for the case of the axially directed forcing.[1]

The equation for $F(z,s)$ [Eq. (11)] can be viewed as a transfer function. Setting $s = i\omega$, values of F may be plotted in frequency space. This is done, and the results are shown in Fig. 2 for $\Lambda = 2.60$, $B_0 = 1.00$, and $\Lambda = 1.25$ with $B_0 = 1.00$ and 2.00. The curve for the slender column ($\Lambda = 2.60$) may be compared with a similar type graph found in Ref. 4 (Fig. 3 in that work). It is seen that a spike in both graphs occur about the resonant frequency at $\omega = 0.34$. The long column is shown to be sensitive to lower-frequency disturbances ($\omega < 1$), as indicated by the relatively large functional values [for $F(z,s)$] in this work and in Ref. 4. Note that the numerical value of $F(z^*,\omega)$ (with $z^* = -\Lambda/2$) compares well with that of the defined transfer function perturbation amplitude in Ref. 4.

It was found that nonslender columns are not similarly sensitive to these low-frequency disturbances. This is shown graphically in Fig. 2 for $\Lambda = 1.25$, $B_0 = 1.00$, and $B_0 = 2.00$. Note the low numerical values of $F(z^*,\omega)$ as compared with that of the case $\Lambda = 2.60$, $B_0 = 1.00$.

The work of Sanz[6] determined the nondimensional natural frequency $\tilde{\omega}_{nat}$ of the fluid column for a range of Λ values. In that work, time was nondimensionalized by $(\rho R^3/\gamma)^{1/2}$. It can be shown that this results in the following equivalence $(\omega_f^2/\omega_{nat}^2) = B_0(1/\tilde{\omega}_{nat}^2)$.

The perturbation interface was determined (numerically) in a number of cases for which the (B_0,Λ) values corresponded to eigenvalues of the unforced system. In these cases, the inviscid finite length fluid column was found to be very sensitive to forcing.

Various orders of magnitude for the vibration level have appeared in the literature.[8] The range of interest of parameter B_0 can be constructed for fluid cylinders of a given density and radius. The interface shape can be obtained for specific values of B_0 and Λ.

ACKNOWLEDGMENTS

The author would like to thank Dr. F. Leslie, Dr. N. Ramachandran, and Ms. C. M. Winter for helpful discussions.

This work was performed as part of Project JOVE (NAG8-149) for NASA Marshall Spaceflight Center.

J. Martínez, Acta Astron. 15, 449 (1987).
[2] J. Meseguer, J. Cryst. Growth 62, 577 (1983).
[3] Y. Zhang and J. I. D. Alexander, Phys. Fluids A 2, 1966 (1990).
[4] J. Meseguer, Appl. Microgravity Tech. I, 136 (1988).
[5] J. Meseguer, A. Sanz, and J. M. Perales, Appl. Microgravity Tech. II, 156 (1990).
[6] A. Sanz, J. Fluid Mech. 156, 101 (1985).
[7] A. Sanz and J. Lopez Diez, J. Fluid Mech. 205, 503 (1989).
[8] N. Ramachadran and C. M. Winter, AIAA Paper No. 90-0654, 1990.

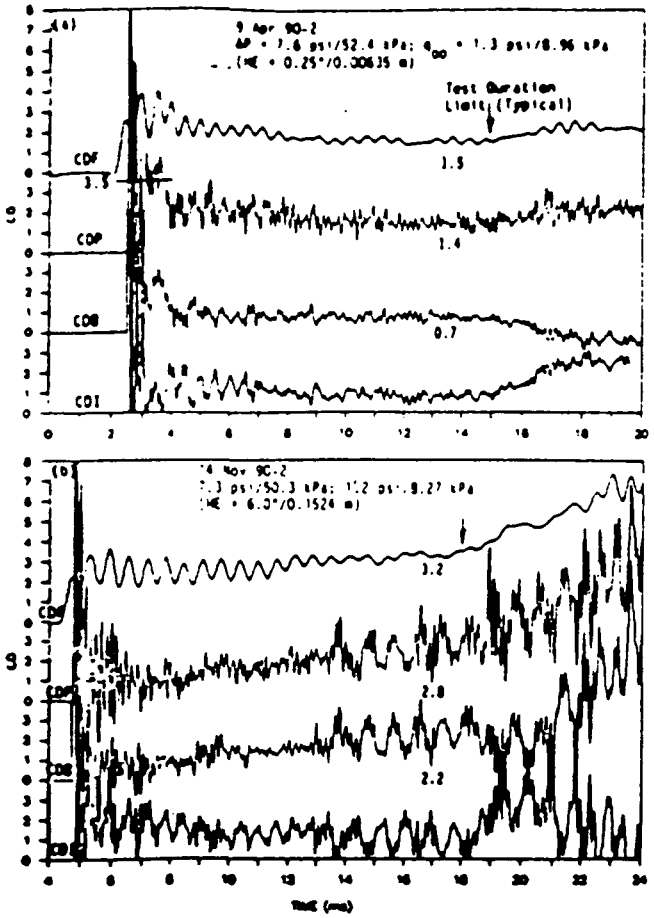

Fig. 2. Typical CD coefficient time histories (ΔP = 7.5 psi/51.7 kPa; clean; without berm).

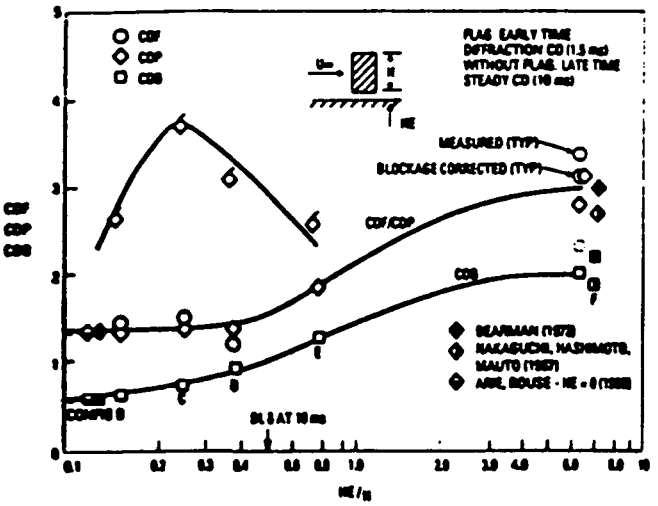

Fig. 3. Dependence of drag coefficient on elevation (ΔP = 7.5 psi/51.7 kPa; clean; without berm).

critical to loads evaluation studies as fineness ratio, Reynolds number, and corner rounding considerations. Note the favorable comparison between the current steady-state data for the two elevation limit cases, $HE \to 0$ and $HE \to \infty$, with earlier results.[3,9,10] Apparently the influence of boundary-layer buildup ($\delta_{10\,mm} \approx 0.5$ in./0.0127 m) on measured CD results is "small" as demonstrated by the favorable agreement of the low *HE* data with established splitter-plate results. Also, the effects of vortex shedding (evidenced by the presence or absence of periodicity in the CDB data), as already discussed and reviewed by Bearman[3] and Vickery,[11] can be seen to play a major role in maintaining low base pressures (high CDB) at high elevation (HE/H = 6, Fig. 2b) and low CDB at low elevation where base scavenging due to vortex shedding is substantially reduced (HE/H = 0.25, Fig. 2a).

Because of the sensitivity of base pressure to the vortex shedding phenomena, investigators have pointed out that reduction in base drag can be achieved by modest geometric changes that interfere with the vortex generating mechanism. Such configuration modifications include fineness ratio,[3] corner rounding,[2] splitter-plate length,[3-5] trailing-edge spoiler,[3] and surface proximity (current results). Note, for example, the onset at late time of periodicity in the CDB signal at HE/H = 6 in Fig. 2b (the vortex shedding "signature") and the absence of any periodicity for the data for HE/H = 0.25 (e.g., Fig. 2a). Since the drag "beat" frequency is typically twice that of the corner shedding frequency,[10] an estimate can be made as to the Strouhal number (S) for the current study

$$S = fH/u_\infty$$

where f represents the Strouhal frequency (= 0.5 × drag periodicity), H the model height, and u_∞ the local freestream velocity. The computed value so derived is seen to be somewhat higher (0.15) than previous measurements (0.13) (Ref. 3). The onset of CDB periodicity is also consistent with the observed increase in base drag as would be expected since base scavenging is controlled by the establishment of the von Kármán vortex street.[3,4]

References

[1]Lindsey, W. F., "Drag of Cylinders of Simple Shapes," NACA Rept. 619, 1938.

[2]Delany, N. K., and Sorensen, N.E., "Low-Speed Drag of Cylinders of Various Shapes," NACA TN 3038, Nov. 1953.

[3]Bearman, P. W., and Trueman, D. M., "An Investigation of the Flow Around Rectangular Cylinders," *Journal of Aeronautical Quarterly*, Vol. 23, Pt. 3, Aug. 1972, pp. 229-237.

[4]Roshko, A., "On the Wake and Drag of Bluff Bodies," *Journal of the Aeronautical Sciences*, Vol. 22, No. 2, 1955, pp. 124-132.

[5]Bearman, P. W., "Investigation of the Flow Behind a Two-Dimensional Model with a Blunt Trailing Edge and Fitted with Splitter Plates," *Journal of Fluid Mechanics*, Vol. 21, Pt. 2, 1965, pp. 241-255.

[6]Batt, R. G., and Peabody, S. A., II, "Rail Garrison Instrumentation Development," Defense Nuclear Agency, DNA-TR-91-126, Dec. 1991.

[7]Bleakney, W., White, D. R., and Griffith, W. C., "Measurements of Diffraction Shock Waves and Resulting Loading of Structures," *Journal of Applied Mechanics*, Vol. 17, No. 4, 1950, pp. 439-445.

[8]Maskel, E.C., "A Theory of the Blockage Effects on Bluff Bodies and Stalled Wings in a Closed Wind Tunnel," Aeronautical Research Council, Great Britain, Repts. and Memoranda No. 3400, Nov. 1965.

[9]Nakaguchi, H., Hashimoto, K., and Muto, S., "An Experimental Study on Aerodynamic Drag of Rectangular Cylinders," *Journal of the Japan Society of Aeronautical and Space Sciences*, Vol. 16, No. 1, 1968, pp. 1-5.

[10]Arie, M., and Rouse, H., "Experiments on Two-Dimensional Flow over a Normal Wall," *Journal of Fluid Mechanics*, Vol. 1, Pt. 2, 1956, pp. 129-141.

[11]Vickery, B. J., "Fluctuating Lift and Drag on a Long Cylinder of Square Cross-Section in a Smooth and in a Turbulent Stream," *Journal of Fluid Mechanics*, Vol. 25, Pt. 3, 1966, pp. 481-494.

Fluid Column Stability in the Presence of Periodic Accelerations

M. J. Lyell*
West Virginia University, Morgantown, West Virginia 26506

Introduction

THE float zone configuration is used in crystal growth. It may be modeled as a liquid column held by surface ten-

Received Sept. 21, 1992; revision received Jan. 20, 1993; accepted for publication Jan. 24, 1993.

*Associate Professor, Mechanical and Aerospace Engineering Department. Senior Member AIAA.

sion forces between two end disks. In the case of crystal growth, the thermal and solutal fields as well as those of velocity and pressure are needed to characterize the physics. A compelling reason for crystal growth experiments in a microgravity environment such as that onboard the Space Shuttle is that buoyancy forces are greatly reduced.[1] However, this environment is not quiescent due to the presence of impulse type disturbances from small thruster firings as well as those from periodic vibrations. Given certain "environmental" conditions, such as the presence of a periodic acceleration field, it is possible that a fluid dynamical instability would develop. This would adversely effect the crystal growth.

The crystal growth environment cannot be separated from the fluid dynamics of the liquid column. This latter topic is the focus of the present work. The question of column interface stability in the presence of a periodic acceleration field having a component normal to the longitudinal axis of the isothermal cylinder is investigated. The fluid column is taken to be infinite in length. Floquet theory is used in the stability investigation.

Previous work has determined the natural oscillations of the liquid column. This work was done first for the case of the infinite column[2] and later for the finite length case. In the latter work, both axisymmetric and nonaxisymmetric oscillations were considered.[3,4] Results for the infinite length case were found to be good approximations to those for the finite length column, both numerically and with regard to trends.

Interface behavior of the finite length liquid column in the presence of time-dependent forcing has been investigated for the case in which the forcing was parallel to the longitudinal axis of the column.[5,6] The investigations considered the column behavior subject to a $\sin(t)$ forcing for both the inviscid case of general aspect ratio (within static stability limits[5]) and the viscous case in the slender column limit.[6]

The problem of interface stability of the fluid column in the presence of a periodic acceleration field that has a component normal to the longitudinal axis of the column has not been investigated. Previous work has considered the interface stability of a highly idealized infinite slab-like configuration in the presence of a periodic acceleration field oriented normal to the interface.[7] Interestingly, this study was motivated by experiments in microgravity.

Use of the infinite length configuration in this stability study results in a simplification in that the standard boundary conditions at the solid end disks are not applied, and the focus remains on the interface stability. If an extension of this work to the finite length configuration is of interest, Floquet analysis would be appropriate, although the implementation would be more complicated.

Formulation

The basic configuration is that of an infinite fluid column of circular cross section. The fluid is incompressible, and the surrounding medium is of negligible density. Perturbations are taken to be irrotational. The analysis is linear and inviscid, with the nondimensionalized governing equations those of continuity and conservation of momentum (linearized Euler).

The frequency of the periodic forcing is denoted by ω_f. Pressure and velocity fields are given by p and u, nondimensionalized as follows:

$$R\tilde{x} = x \qquad \omega_f^{-1}\tilde{t} = t \qquad R\omega_f\tilde{u} = u \qquad \rho(R\omega_f)^2\tilde{p} = p \tag{1}$$

Tildes indicate nondimensional quantities.

The continuity and Euler equations are then

$$\tilde{\nabla}\cdot\tilde{u} = 0 \tag{2a}$$

$$\frac{\partial\tilde{u}}{\partial\tilde{t}} + \tilde{u}\cdot\tilde{\nabla}\tilde{u} = -\tilde{\nabla}\tilde{p} - Fr\cos(\tilde{t})\tilde{\nabla}[(1-r)\sin\theta] \tag{2b}$$

with $Fr = (Go/R\omega_f^2)$ a Froude type number. Go is the amplitude of the periodic acceleration field. The functional form of the time-dependent forcing is selected to be $\cos(\tilde{t})$.

The mean state is one of zero velocity; however, the mean pressure is time dependent. Consider a wave-like perturbation propagating on the interface. The governing equations for the perturbation are developed as follows. Expand in the small perturbation parameter ϵ

$$\tilde{p} = p_{m(can)} + \epsilon p \qquad \tilde{u} = \epsilon u = \epsilon\nabla\phi \tag{3}$$

Substitution of Eq. (3) into Eqs. (2) yields the mean system

$$\nabla p_{m(can)} = -Fr\cos(t)\nabla[(1-r)\sin\theta] \tag{4}$$

(with the parameter Fr of order one) and the (order ϵ) perturbation equations

$$\nabla^2\phi = 0 \tag{5a}$$

$$\frac{\partial(\nabla\phi)}{\partial t} = -\nabla p \tag{5b}$$

The spatial dependence of the velocity potential can be determined via solution of Eq. (5a), which is

$$\phi(r,\theta,z,t) = \sum A(t)I_m(kr)\exp(ikz)\exp(im\theta) \tag{6}$$

I_m is the mth modified Bessel function. Clearly, the solution involves a superposition of the azimuthal modes.

It is through the boundary conditions that the free interface can be determined and the stability characteristics investigated. Let the equilibrium interface be given by

$$Fe = r - 1 - \epsilon\eta(\theta,z,t) = r - 1 - \epsilon\sum C(t)\exp(ikz + im\theta) \tag{7}$$

The kinematic condition and the normal force balance at the free interface must be satisfied. In addition, the requirement of conservation of mass, which reduces to a conservation of volume condition, must hold.

The linearized kinematic condition (at order ϵ) is

$$-\frac{\partial\eta}{\partial t} + u_r = 0 \tag{8a}$$

at $r = 1$ with $u_r = \partial\phi/\partial r$. This results in

$$\sum\left(\frac{dC}{dt}\right)\exp(ikz + im\theta) = \sum[I_m(k)]'A(t)\exp(ikz + im\theta) \tag{8b}$$

The normal force balance requires that the difference in pressure across the interface be equal to the curvature multiplied by the surface tension force. In nondimensional form, this is given by

$$Bo \times \Delta(p_{m(can)} + \epsilon p) = \nabla\cdot\mathbf{n} \tag{9a}$$

with $\mathbf{n} = \nabla Fe/\|\nabla Fe\|$. Bo is the nondimensional parameter $(\rho R^3\omega_f^2/\gamma)$, with γ the surface tension and ρ the density. At order ϵ, the linearized form of this interfacial condition can be expressed as

$$\eta + \eta_{zz} + \eta_{\theta\theta} + [Bo\cos(t)\sin\theta]\eta = Bo\left(\frac{\partial\phi}{\partial t}\right) \tag{9b}$$

Fr, required to be of order one, has been set equal to unity. The subscripts indicate partial differentiation. This yields

$$\sum[(1 - m^2 - k^2) + Bo\cos(t)\sin\theta] \times C(t)\exp(ikz + im\theta)$$

$$= \sum A(t)I_m(k)\exp(ikz + im\theta) \tag{9c}$$

The $\sin\theta$ dependence can be re-expressed as an exponential function. Then

$$C_m(t)(1 - m^2 - k^2) + \left(\frac{Bo}{2}\right)(-i)\cos(t)[C_{m-1}(t) - C_{m+1}(t)] = BoI_m(k)\left(\frac{dA_m}{dt}\right) \tag{9d}$$

and azimuthal mode coupling occurs. Use of Eqs. (8b) and (9d) yields a nonautonomous second-order equation in $C_m(t)$, with mode coupling (as indicated by the subscripts m)

$$C_m'' - [(1 - m^2 - k^2)/Bo][I_m'/I_m]C_m = [I_m'/2I_m]\cos(t)(-i)[C_{m-1}(t) - C_{m+1}(t)] \quad (10)$$

Keep in mind that $\cos(t)$ can be rewritten in exponential form. It is at this juncture that Floquet analysis is applied. For convenience, let $E_m(t) = [dC_m(t)/dt]$. Then take

$$[C_m(t), E_m(t)] = \sum_{l=-\infty}^{\infty}[C_{m,l}, E_{m,l}] \times \exp[(\lambda + il)t] \quad (11)$$

The constant coefficients $C_{m,l}$ and $E_{m,l}$ are unknown. The Floquet exponent is denoted by the eigenvalue λ, which is in general a complex number, and which is also unknown. The nonautonomous differential system is thus transformed into a homogeneous algebraic system for $(C_{m,l}, E_{m,l})$ with the unknown parameter (eigenvalue) λ. If Real(λ) is greater than zero, the interface of the cylindrical column is unstable to the growing wave-like perturbation. Of course, the milieu in which this disturbance is propagating includes the periodic base state pressure.

Use of Eq. (11) in Eq. (10) (rewritten as two first-order modes) yields the infinite algebraic system given by

$$(\lambda + il)C_{m,l} = E_{m,l} \quad (12a)$$

$$(\lambda + il)E_{m,l} = [(1 - m^2 - k^2)/(Bo)](I_m'/I_m)C_{m,l} + (\tfrac{1}{4}I_m'/I_m)(-i)(C_{m-1,l-1} + C_{m-1,l+1} - C_{m+1,l-1} - C_{m+1,l+1}) \quad (12b)$$

Note that the harmonic modes (indicated by l) as well as the azimuthal modes (indicated by m) are coupled to both their preceding and successive modes.

Several remarks are in order concerning the truncation. Once the truncation in m is done, the number of azimuthal modes that contribute are fixed. It is to this truncated system that Floquet analysis is actually applied. To obtain numerical values for λ, it is necessary to truncate the number of harmonic modes in time, i.e., the range of l values. The eigenvalue problem is, therefore, a problem of the truncated system.

Results

The results pertain to the eigenvalue solutions of system (12a) and (12b). NAG library routines were used in determining the eigenvalues. Truncation values of $L = 11$, that is, $-15 \le l \le 15$, and $M = 14$ were found to be sufficient. Wave number values ranged from $k = 0.10$ to $k = 3.00$. The parameter Bo was varied from 0.01 to 10.00.

For $k < 1.0$, the interface is unstable to the wave-like perturbation in the presence of a mean periodic acceleration field over the range of Bo values considered. (Note that this range encompasses four orders of magnitude; see Fig. 1.)

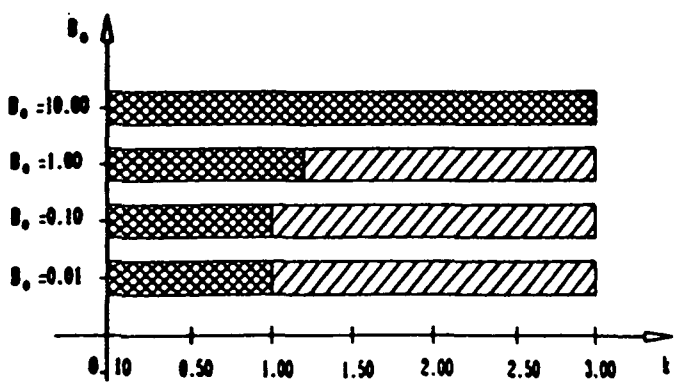

Fig. 1 Stability diagram: the stability of the configuration to wave-like perturbations for a range of Bo parameter values vs wave number k is shown. The cross-hatched area indicates unstable regions in which disturbances are growing in time. The remaining area corresponds to that of the marginal stability state.

As k is increased, such that $1.00 \le k \le 1.20$, the interface remains unstable to the perturbation for the two larger Bo values, equal to 10.00 and 1.00. However, marginal stability [Real(λ) = 0] ensues at the smaller Bo values. A decrease in Bo can be interpreted physically as an increase in the surface tension. So, as the surface tension increases, the restoring force is sufficient to result in marginal stability over this range of wave numbers.

Perturbations corresponding to the larger wave numbers (smaller wavelengths) that were considered, $2.0 \le k \le 3.0$, were found not to grow in time for $Bo = 0.01$-1.00. That is, instability [with Real(λ) > 0] of the interface to perturbations of these larger wave numbers (and smaller wavelengths) occurs only for $Bo = 10.00$; otherwise, Real(λ) = 0. An alternative physical interpretation to that involving a variation in surface tension for differing Bo values can be developed. Since Fr was taken to be unity, ω_f^2 (the forcing frequency) is proportional to Go, the amplitude of the periodic acceleration field. Utilizing this relation in the definition for Bo yields $Bo \alpha (Go/\gamma)$. For fixed surface tension (and, of course, density and column radius) values, an increase in Bo would result from an increase in forcing amplitude. It is at the highest such amplitude considered that the interface was found to be unstable [with Real(λ) > 0] to the perturbation.

It is noted that the range of Bo values used corresponds to values of Go and ω_f that would be of interest in a microgravity environment for certain ranges of surface tension values. (Roughly, $10^{-4} g_{earth} \le Go \le 10^{-2} g_{earth}$, and 0.5 Hz < ω_f < 5 Hz for γ values of 1-100 dynes/cm.)

Acknowledgment

NASA support (NAG8-149, JOVE) is acknowledged.

References

[1]Kassemi, S. A., and Ostrach, S., "Nature of Buoyancy-Driven Flows in a Reduced Gravity Environment," *AIAA Journal*, Vol. 30, No. 7, 1992, pp. 1815-1818.

[2]Bauer, H., "Coupled Oscillations of a Solidly Rotating Liquid Bridge," *Acta Astronautica*, Vol. 9, No. 9, 1982, pp. 547-563.

[3]Sanz, A., "The Influence of the Outer Bath in the Dynamics of Axisymmetric Liquid Bridges," *Journal of Fluid Mechanics*, Vol. 156, July 1985, pp. 101-140.

[4]Sanz, A., and Lopez Diez, J., "Non-Axisymmetric Oscillations of Liquid Bridges," *Journal of Fluid Mechanics*, Vol. 205, Aug. 1989, pp. 503-521.

[5]Lyell, M. J., "Axial Forcing of an Inviscid Finite Length Fluid Cylinder," *Physics of Fluids A*, Vol. 3, No. 7, 1991, pp. 1828-1831.

[6]Meseguer, J., and Perales, J. M., "A Linear Analysis of g-Jitter Effects on Viscous Cylindrical Liquid Bridges," *Physics of Fluids*, Vol. 3, No. 10, 1992, pp. 2332-2336.

[7]Jacqmin, D., and Duval, W. M. B., "Instabilities Caused by Oscillating Accelerations Normal to a Viscous Fluid-Fluid Interface," *Journal of Fluid Mechanics*, Vol. 196, Nov. 1988, pp. 495-511.

Coherent Structure Interactions in Excited Coaxial Jet of Mean Velocity Ratio of 0.3

S. K. Tang* and N. W. M. Ko†
University of Hong Kong, Hong Kong

Nomenclature

D = outer diameter of outer nozzle
d = inner diameter of inner nozzle

Received April 7, 1992; revision received Dec. 21, 1992; accepted for publication Dec. 28, 1992.

*Graduate Student, Department of Mechanical Engineering.
†Professor, Department of Mechanical Engineering.

Effect of Periodic Accelerations on Interface Stability in a Multilayered Fluid Configuration

M. J. Lyell* and Michael Roht
West Virginia University, Morgantown, West Virginia 26505

The increasing number of research opportunities in a microgravity environment will benefit not only fundamental studies in fluid dynamics, but also technological applications such as those involving materials processing. In particular, fluid configurations that involve fluid-fluid interfaces would occur in a variety of experimental investigations. This work investigates the stability of a configuration involving fluid-fluid interfaces in the presence of a time-dependent (periodic) forcing. The fluid configuration is multilayered and infinite in extent. The analysis is linear and inviscid, and the acceleration vector is oriented perpendicular to each interface. A Floquet analysis is employed, and the resulting algebraic eigensystem is truncated. Nondimensional parameters appear in the algebraic system. A numerical study is performed to elucidate the regions of instability and the effect of parameter variation on the fluid configuration stability.

Nomenclature

A, B = matrices representing final system
$A(t)$ = time-dependent coefficient, nondimensional
Bo = nondimensional parameter, $= (\rho_{II} H^2 G_o/\gamma)$
Fe = equilibrium interface, nondimensionalized
Fr = nondimensional parameter, $= [G_o/(H\omega_f^2)]$
G_o = peak value of forcing, dimensional
$g(t)$ = forcing term, nondimensionalized
H = height of middle slab, dimensional
k = wave number of perturbation, nondimensional
$\hat{n}$ = outward pointing unit normal to interface
p = pressure field, nondimensionalized
u = velocity field, nondimensionalized
t = time, nondimensionalized
γ = surface tension
λ = Floquet exponent, eigenvalue
ρ = density
ϕ = velocity potential, nondimensionalized
ω_f = frequency of periodic acceleration (forcing)

Subscripts

I = (finite) middle layer fluid region of height H
II = upper layer (unbounded) fluid region
III = lower layer (unbounded) fluid region
2 = upper interface
3 = lower interface

Superscripts

$(\dot{})$ = differentiation
$(\hat{})$ = unit vector (e.g., $\hat{e}_x$, $\hat{e}_y$, $\hat{e}_z$, $\hat{n}$ or part of vector definition (e.g., $\hat{k}$)
$(\tilde{})$ = dimensional quantities

Introduction

CURRENT interest in microgravity materials processing has focused attention upon certain relevant aspects of fluid mechanics in this environment. In particular, a number of materials processing applications involve fluid-fluid interfaces.

The environment onboard the Space Shuttle is not strictly a microgravity environment. Rather, residual accelerations exist that could affect any ongoing materials science or space processing experiments. A recent summary[1] indicates that accelerations include those in the frequency range of <10 Hz, with acceleration levels ranging from $10^{-6}\, g_{earth}$ to $10^{-3}\, g_{earth}$. In addition to periodic forcing, residual accelerations may be of impulse type, due to such causes as stationkeeping maneuvers and astronaut motion.[2]

This work investigates the effect of periodic accelerations on the interface stablity of an idealized fluid configuration. The fluid configuration is multilayered and infinite in extent (see Fig. 1). The accelerations are periodic about a zero mean g level and are oriented normal (in the $\hat{e}_z$ direction) to each interface.

Previous work has investigated the stability of a single planar free surface subject to periodic forcing in the direction perpendicular to the interface.[3,4] These studies were both done

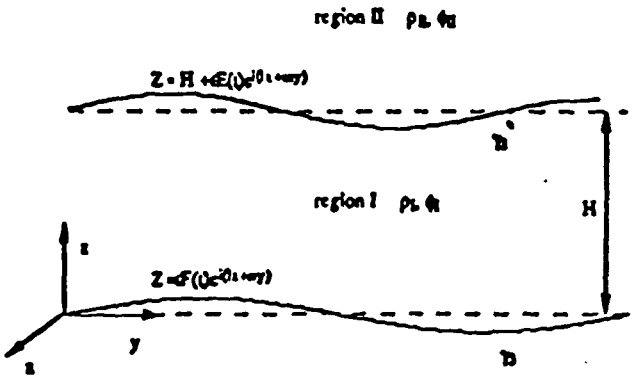

Fig. 1 Multilayer fluid configuration geometry schematic.

Received Aug. 27, 1990; revision received Dec. 6, 1990; accepted for publication Jan. 28, 1991.

*Assistant Professor, Mechanical and Aerospace Engineering Department, Box 6101. Senior Member AIAA.

†Graduate Student, Mechanical and Aerospace Engineering Department, Box 6101.

in a terrestrial environment and required the use of a container. In the work of Benjamin and Ursell,[1] the container was cylindrical in shape. Their analysis resulted in a Mathieu equation that governed the time dependent amplitude of the disturbance. They were able to make statements concerning the interface stability based on known mathematical properties of Mathieu equations. The case of a rectangular container has been addressed recently,[2] and the results extended into the nonlinear regime. Both of these investigations utilized an inviscid analysis.

The effect of viscosity on the stability properties has been studied recently in idealized infinite or semi-infinite configurations that had one fluid-fluid interface.[3,4] Again, the periodic forcing was directed normal to the interface. One theoretical investigation was done assuming a zero mean g level and pertains to the microgravity environment.[5] Results were obtained for different regions of parameter space, and some stability boundaries were determined.

The present work will study the stability of an idealized multiple-layer fluid configuration that is infinite in the $\hat{e}_x$ and $\hat{e}_y$ directions (as well as unbounded in the $\hat{e}_z$ direction) and is subjected to periodic forcing normal to each interface. The height of the middle layer is finite. In general, the densities in each region differ, as do the surface tension values at the upper and lower interfaces. The analysis is linear and inviscid. A Floquet analysis is employed. Details of the analysis are presented in the next section.

The configuration is idealized, as was the case in previous work. However, the use of nondimensional parameters in the stability investigation will enable trends to be discerned and parameter regions (of instability) to be identified.

Equation Development

Governing Equations

The governing equations are those of conservation of mass and momentum applied to an inviscid and incompressible fluid, and are

$$\nabla \cdot \bar{u} = 0 \tag{1}$$

$$\rho\left\{\left(\frac{\partial \bar{u}}{\partial t}\right) + \bar{u}\cdot\nabla\bar{u}\right\} = -\nabla p - \rho G_o g(\omega_f t)\hat{e}_z \tag{2}$$

The time-dependent body force term is indicated in Eq. (2). G_o represents the peak value of the acceleration due to the periodic forcing. The function $g(\omega_f t)$ is periodic and will be taken to be a cosine function. The fluid system is linearized about a state of zero mean motion, and quadratically small terms (after expansion in a small parameter ϵ) are neglected. Use of nondimensionalizations

$$z = H z, \qquad t = \omega_f^{-1} t \tag{3a}$$

$$\bar{u} = H\omega_f \bar{u}, \qquad p = \rho_m H^2 \omega_f^2 p \tag{3b}$$

yields

$$\nabla \cdot \bar{u} = 0 \tag{4}$$

$$\left(\frac{\rho}{\rho_m}\right)\left\{\frac{\partial \bar{u}}{\partial t}\right\} = -\nabla p - \left(\frac{\rho}{\rho_m}\right)\left(\frac{G_o}{H\omega_f^2}\right) g(t)\hat{e}_z \tag{5}$$

The parameter $Fr = (G/H\omega_f^2)$ is taken to be roughly of order 1. Note that the mean pressure field will be periodic in time. (Also, p is expanded into both a mean and perturbation contribution.) A potential function ϕ with $\bar{u} = \nabla\phi$, is defined. Substitution into Eq. (4) yields Laplace's equation. Perturbations are taken to be wavelike in the (xy) plane. That is, they are oscillatory. The resulting differential equations (in z) are solved in the three upper and lower regions to yield

$$\phi_u = \{A(t)\exp(kz) + B(t)\exp(-kz)\}\exp(i[lx + my]) \tag{6a}$$

$$\phi_m = \{C(t)\exp(-kz)\}\exp(i[lx + my]) \tag{6b}$$

$$\phi_m = \{D(t)\exp(kz)\}\exp(i[lx + my]) \tag{6c}$$

Note that A, B, C, and D are time-dependent coefficients. The wave number k is given by $\sqrt{(l^2 + m^2)}$.

Equations representing the upper and lower equilibrium interfaces are

$$Fe_2 = z - 1 - \epsilon E(t)\exp(i[lx + my]) \tag{7}$$

$$Fe_1 = z - \epsilon F(t)\exp(i[lx + my]) \tag{8}$$

Note that E and F are time-dependent coefficients. Thus, for example, the functional form of the perturbation to the mean interface at $z = 0$ is given by the expression $E(t)\exp(i[lx + my])$. At this stage, the time-dependent coefficients are unknowns.

Boundary Conditions

The kinematic condition, which holds at each interface, requires that

$$\left(\frac{\partial Fe}{\partial t}\right) + \bar{u}\cdot\nabla Fe = 0 \tag{9a}$$

After linearization, only the u_z velocity component will contribute. This results in

$$\dot{E}(t) + k\,C(t)\,e^{-k} = 0 \qquad \text{on } z = 1 \tag{9b}$$

$$-\dot{F}(t) + k\,D(t) = 0 \qquad \text{on } z = 0 \tag{9c}$$

In addition to the kinematic condition, the normal component of the velocity is continuous across an interface, which yields

$$\left(\frac{\partial \phi_u}{\partial z}\right) = \left(\frac{\partial \phi_m}{\partial z}\right) \qquad \text{on } z = 1 \tag{10a}$$

$$\left(\frac{\partial \phi_l}{\partial z}\right) = \left(\frac{\partial \phi_m}{\partial z}\right) \qquad \text{on } z = 0 \tag{10b}$$

or

$$A(t)\,e^{2k} - B(t) = -C(t) \qquad \text{on } z = 1$$

$$A(t) - B(t) = D(t) \qquad \text{on } z = 0$$

The remaining boundary condition is the (linearized) normal force balance across an interface. In nondimensional form, it is

$$(Bo/Fr)(\Delta\rho) = \nabla \cdot \hat{n} \tag{11}$$

The unit vector $\hat{n}$ is the linearized outward pointing normal to the interface. After substitution, Eq. (11) yields

$$\{(\rho_u - \rho_l)/\rho_m)\,Fr\,g(t)\,E(t) - (\rho_l/\rho_m)[\dot{A}(t)e^k + \dot{B}(t)e^{-k}]$$

$$+ (\rho_m/\rho_m)\dot{C}(t)e^{-k}\} = (Fr/Bo_2)k^2 E(t) \qquad \text{on } z = 1 \tag{12a}$$

$$\{(\rho_u - \rho_m)/\rho_m)\,Fr\,g(t)\,F(t) + (\rho_l/\rho_m)[\dot{A}(t) + \dot{B}(t)]$$

$$- (\rho_m/\rho_m)\dot{D}(t)\} = (Fr/Bo_1)k^2 F(t) \qquad \text{on } z = 0 \tag{12b}$$

with

$$Bo_2 = (\rho_{ref} H^2 G/\gamma_2)$$

$$Bo_3 = (\rho_{ref} H^2 G/\gamma_3)$$

$$Fr = G/(H\omega_f^2)$$

The term $\gamma_2(\gamma_3)$ indicates the surface tension at the upper (lower) interface.

Final System of Equations

Through the utilization of Eqs. (10c) and (10d), the $C(t)$ and $D(t)$ coefficients can be eliminated to yield the following system:

$$\dot{A}(t)\{-3(1+\rho_{21})/(1+\rho_{21}+\rho_{31})\}e^{t} + \dot{B}(t)\{3(\rho_{21}-1)/(1+\rho_{21}+\rho_{31})\}e^{-t} + E(t)\{3(\rho_{21}-1)/(1+\rho_{21}+\rho_{31})\}Fr\,g(t) = (Fr/Bo_2)k^2 E(t) \quad (13a)$$

$$\dot{A}(t)\{3(1-\rho_{31})/(1+\rho_{21}+\rho_{31})\} + \dot{B}(t)\{3(1+\rho_{31})/(1+\rho_{21}+\rho_{31})\} + F(t)\{3(1-\rho_{31})/(1+\rho_{21}+\rho_{31})\}Fr\,g(t) = (Fr/Bo_3)k^2 F(t) \quad (13b)$$

$$\dot{E}(t) = k\{A(t)e^{t} - B(t)e^{-t}\} \quad (13c)$$

$$\dot{F}(t) = k\{A(t) - B(t)\} \quad (13d)$$

with $\rho_{21} = (\rho_{II}/\rho_I)$ and $\rho_{31} = (\rho_{III}/\rho_I)$.

The governing system of equations has been reduced to four ordinary differential equations (in time) with nonconstant coefficients and with four unknowns. It remains to determine the stability of this system for various values of the parameters Fr, Bo_2, Bo_3, ρ_{21}, ρ_{31}, and k. As was mentioned previously, $g(t)$ is chosen to be $\cos(t)$.

Floquet theory[7] can be applied to system (13). Let the time-dependent coefficients be expressed as

$$\{A(t), B(t), E(t), F(t)\} = \sum_{n=-\infty}^{\infty} \{A_n, B_n, E_n, F_n\} e^{int} e^{\lambda t} \quad (14)$$

The system of four ordinary differential equations in time is now re-expressed as an infinite algebraic system, with the Floquet exponent appearing as another parameter. That is,

$$e^{t}(\lambda+in)\{-3(1+\rho_{21})/(1+\rho_{21}+\rho_{31})\}A_n + e^{-t}(\lambda+in)\{3(\rho_{21}-1)/(1+\rho_{21}+\rho_{31})\}B_n - (Fr/Bo_2)k^2 E_n + \{3(\rho_{21}-1)/(1+\rho_{21}+\rho_{31})\}(Fr/2)(E_{n-1}+E_{n+1}) = 0 \quad (15a)$$

$$(\lambda+in)\{3(1-\rho_{31})/(1+\rho_{21}+\rho_{31})\}A_n + (\lambda+in)\{3(1+\rho_{31})/(1+\rho_{21}+\rho_{31})\}B_n - (Fr/Bo_3)k^2 F_n + \{3(1-\rho_{31})/(1+\rho_{21}+\rho_{31})\} \times (Fr/2)(F_{n-1}+F_{n+1}) = 0 \quad (15b)$$

$$(\lambda+in)E_n + k e^{-t} B_n - k e^{t} A_n = 0 \quad (15c)$$

$$(\lambda+in)F_n + k B_n - k A_n = 0 \quad (15d)$$

The value of n varies from $-\infty$ to ∞. The infinite set of homogeneous equations can be written in matrix form as

$$[\underline{B}^{-1}(\underline{A}) - \lambda \underline{I}]\underline{\ell} = 0 \quad (16a)$$

or

$$\underline{A}\,\underline{\ell} = \lambda \underline{B}\,\underline{\ell} \quad (16b)$$

The latter representation is in the form of a generalized eigenvalue problem. The Floquet exponent λ serves as the eigenvalue. The infinite column vector $\underline{\ell}$ contains $(A_n, B_n, E_n, F_n)^T$. For details concerning the form of matrices $\underline{A}$ and $\underline{B}$, and column vector $\underline{\ell}$, see the Appendix.

The sign on the Floquet exponent/eigenvalue λ indicates the stability. If λ is a positive value, then the disturbance will grow and the interface configuration will be unstable. As this is a linear analysis, no information can be obtained concerning the finite amplitude (nonlinear) form of the configuration. Numerical methods are used to determine the value of λ for different values of the parameters. These are discussed in the next section along with various results.

Results

Comments on Numerical Method

The linear algebraic system given by Eqs. (16) is truncated. Results are presented for a truncation value of $n = |25|$, which involves a system of 204 equations. This resulting system forms a generalized eigenvalue problem, with the matrices $\underline{A}$ and $\underline{B}$ having complex entries. At this level of truncation, both $\underline{A}$ and $\underline{B}$ are sparse.

Eigenvalue techniques were used to determine λ values. An IMSL routine (DGVLCG), based on an LZ algorithm,[8] was utilized. In particular, we are interested in the value of the largest Real(λ), which gives the fastest growing mode. If Real(λ) is positive, the perturbation is growing exponentially. Hence, the fluid configuration is then unstable with respect to the perturbations in the presence of the unsteady periodic acceleration (forcing) field.

Several checks were made to insure that the eigenvalues obtained were correct. Higher truncations yielded the same largest Real(λ) value. As an additional check, the generalized eigenvalue problem was reformulated as a standard eigenvalue problem of the form $(\underline{B}^{-1}\underline{A} - \lambda \underline{I})\underline{\ell} = 0$ and the eigenvalues of this new system were determined. This was done by utilizing an alternate IMSL routine (DEVLCG) based on a different numerical algorithm. Again, the values of Real(λ) were in agreement with those obtained previously. As a final check, a limit case was run (for various parameter values). The value of Bo_2 was set to infinity, which is equivalent to setting the surface tension at the upper interface to zero. In addition, the densities in regions I and II were set to the same value. This limit case represents the one interface case. The actual one interface case was developed separately. Results obtained from using the two interface system (and code developed for it) in the aforementioned limit case and from solving directly the one interface system agreed quite closely.

Discussion of Results

A parametric study was performed to investigate the effects of variation in Bo_2, Bo_3, Fr, and the density ratios with wave number. Because of space limitations, a subset of results that were obtained are presented. (These are illustrative and typical.) In each case, if the periodic forcing function $g(t)$ were to be set to zero, and with the mean gravity level zero, the configuration would be stable to the wave-type small amplitude disturbances. That is, the interface would simply oscillate. It is only with the forcing, and in the indicated parameter regions, that instability does result.

The values of the wave numbers vary between 0.10 and 5.00. Although not all results are presented, the investigation

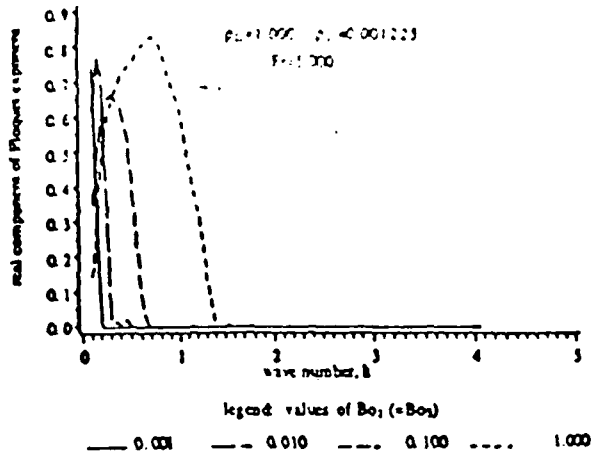

Fig. 2 Effect of Bo on stability: $\rho_{21} = 1.00$; $\rho_{31} = 0.001225$; $Fr = 5.00$.

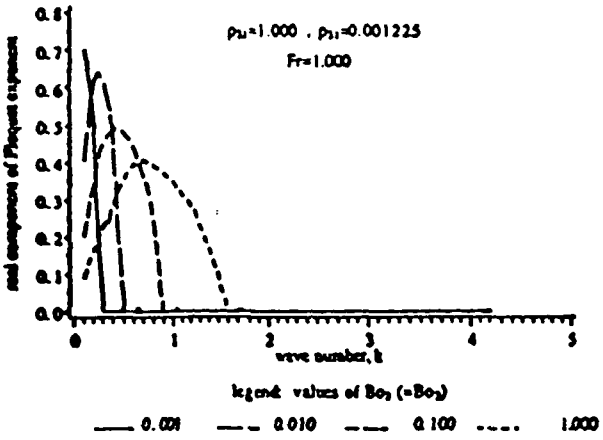

Fig. 3 Effect of Bo on stability: $\rho_{21} = 1.00$; $\rho_{31} = 0.001225$; $Fr = 1.00$.

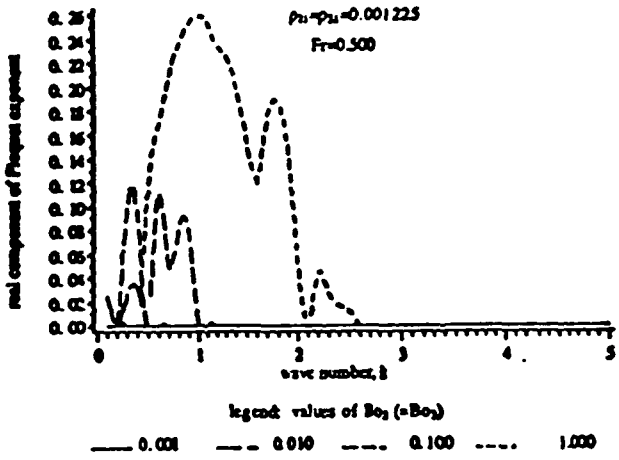

Fig. 4 Effect of Bo on stability: $\rho_{21} = \rho_{31} = 0.001225$; $Fr = 0.50$.

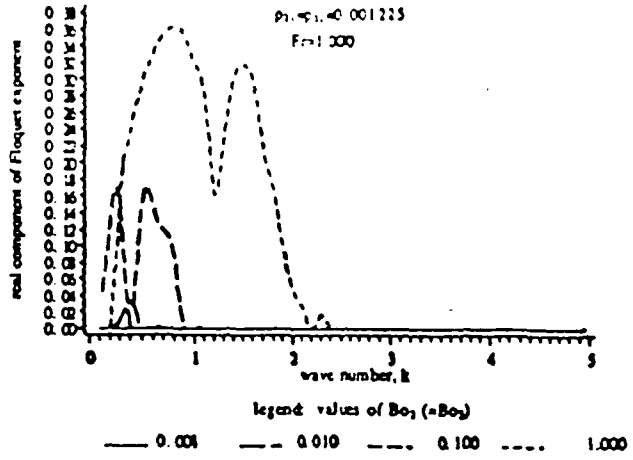

Fig. 5 Effect of Bo on stability: $\rho_{21} = \rho_{31} = 0.001225$; $Fr = 1.00$.

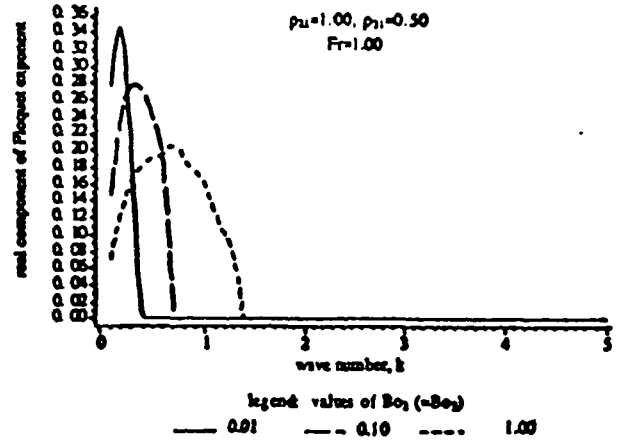

Fig. 6 Effect of Bo on stability: $\rho_{21} = 1.00$; $\rho_{31} = 0.50$; $Fr = 1.00$; $Bo_3 = Bo_2$.

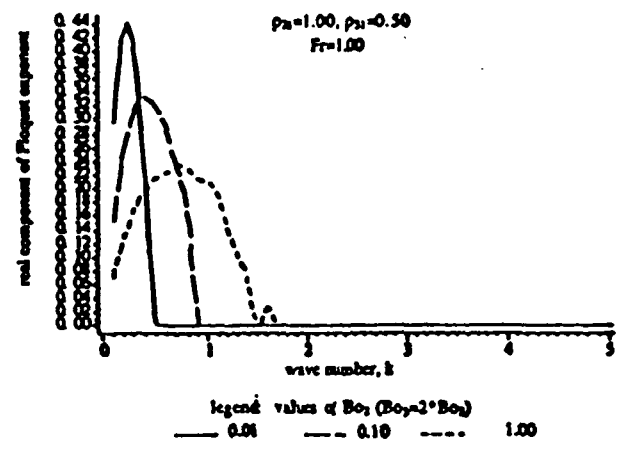

Fig. 7 Effect of Bo on stability: $\rho_{21} = 1.00$; $\rho_{31} = 0.50$; $Fr = 1.00$; $Bo_3 = 2 \times (Bo_2)$.

considered Bo_2 values of (1.0, 0.1, 0.01, 0.001). The values of Bo_3 were set equal to Bo_2, or were twice those of Bo_2 in different studies.

Figures 2–10 show graphs of Real(λ) vs wave number for various values of Bo_2, Bo_3, Fr, ρ_{21}, and ρ_{31}. Note that Real(λ) is the largest eigenvalue and represents the fastest growing (unstable) wave if positive. Regions for which Real(λ) ≤ 0 are indicated by being set equal to zero in the graphs. That is, the value of Real(λ) < 0 is not of interest.

In Figs. 2–7, the effect of Bo_2 and Bo_3 on stability for different Fr and density ratos is elucidated. In Fig. 2, Bo_2 is set equal to Bo_3 for the density ratios $\rho_{21} = 1.0$ and $\rho_{31} = 0.001225$ and for $Fr = 5.00$. The unstable wave number region is broadest for the largest $Bo_2(Bo_3)$ values. As $Bo_2(Bo_3)$ is decreased, the unstable wave number region shrinks to encompass fewer k values and tends toward the lower k region. For low $Bo_2(Bo_3)$ values, this two interface configuration is unstable to the longer wavelength disturbances in the presence of periodic forcing. The effect of a decrease in Fr, keeping the other parameter values the same, is seen in Fig. 3. The range of unstable wave numbers broadens, with smaller wavelengths falling into the unstable region.

The density ratios indicated in Figs. 4 and 5 pertain to a gas-liquid-gas configuration. As was the situation in the preceding two figures, the broadest range of unstable wave number values occurs for the largest $Bo_2(Bo_3)$ value. As Fr is decreased, the unstable wave number band encompasses larger values (corresponding to smaller wavelength disturbances). Inspection of Fig. 5 shows a slight separation in unstable wave number bands near $k = 2.175$. This k value falls into an unstable region at the smaller Fr value given in Fig. 4. Note that the configuration represented in Figs. 4 and 5 is stable when $Bo_2(Bo_3)$ is 0.001. That is, Real(λ) > 0 only for the larger $Bo_2(Bo_3)$ values in the indicated k ranges.

The effect of Bo_2 not equal to Bo_3 on the configuration stability is shown in Figs. 6 and 7 (for the given values of Fr and density ratios). In Fig. 6, the Bo values are equal. This is changed in Fig. 7, with Bo_3 twice Bo_2. Physically, the increase of Bo_3 while keeping Fr fixed can be interpreted as a change (decrease) in the surface tension value at the lower interface. The predominant effect is to broaden the range of unstable wave numbers for each set of Bo_2, Bo_3 values. Note that the numerical value of the real part of the Floquet exponent λ is increased for Bo_3 twice the value of Bo_2, indicating a faster growing "fastest growing" disturbance at the lower Bo_2 values.

In Fig. 8, the effect of holding the (Bo_2, Bo_3) values fixed (for the specified density ratios) and varying Fr is shown. As Fr is decreased, the range of unstable wave numbers increases. Physically, this can be interpreted as a decrease in configuration stability with respect to the wavelike disturbances for somewhat larger frequencies of the periodic forcing.

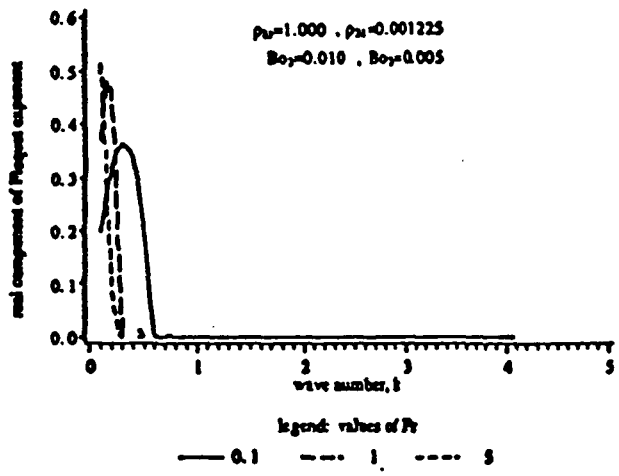

Fig. 8 Effect of Fr on stability: $\rho_{21} = 1.00$; $\rho_{31} = 0.001225$; $Bo_2 = 0.01$; $Bo_3 = 0.005$.

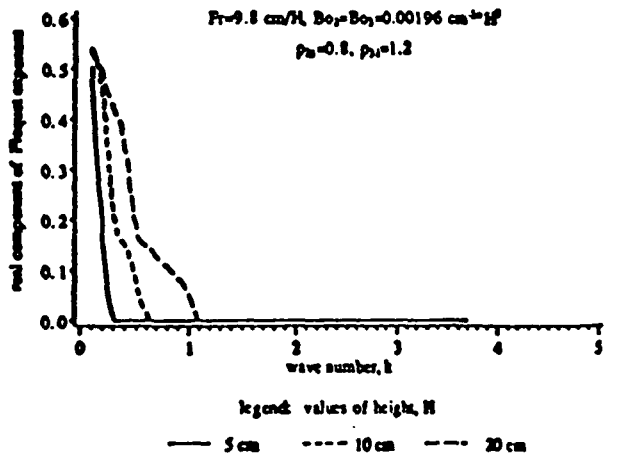

Fig. 9 Effect of height variation: $Fr = 9.8$ cm/H; $Bo_2 = Bo_3 = 0.00196 \times H^2 cm^{-2}$; $\rho_{21} = 0.80$; $\rho_{31} = 1.20$.

The height of the finite middle slab is a physical quantity that appears in both the Bo and Fr nondimensional parameters. In particular, Fr is inversely proportional to the height, whereas Bo depends on the square of the height. An increase in height H implies a decrease in Fr and an increase in Bo. As was seen in Figs. 2-7, the region of instability in wave number space becomes larger as Bo increases. From Fig. 8, it is seen that the broadest region of instability (with respect to k) corresponds to the smallest Fr values. It is anticipated that an increase in H will result in an unstable configuration for a broader range of k values. This is borne out in Fig. 9. Results are presented graphically for the case $G_e = (10^{-4} g_{earth})$, $\omega_f = 0.1$ Hz, and $\gamma_2 = \gamma_3 = 50$ dynes/cm. In addition, $\rho_{21} = 0.8$ and $\rho_{31} = 1.2$.

The effect of density ratio difference on stability is presented in Fig. 10. Values of ρ_{21} and ρ_{31} represent the density ratios of the upper and lower regions to that of the middle layer, respectively. Among cases indicated, the largest magnitude difference in the density ratios is $(\rho_{31} - \rho_{21} = 9)$. This corresponds to the case having the largest range of unstable wave numbers. Note that all three cases belong to a family with $\rho_{21} = 1.0$. In addition, the case in which both density ratios were set to 1, indicating equal densities in all three regions, was addressed. Under the action of periodic forcing, lack of density differences among the layers results in lack of instability.

The wave number at which the subharmonic occurs is plotted in Fig. 11 for a range of Fr values at the indicated Bo values and density ratios. It is seen that there is a shift of the subharmonic to lower wave numbers as Fr increases, i.e., as the forcing frequency decreases.

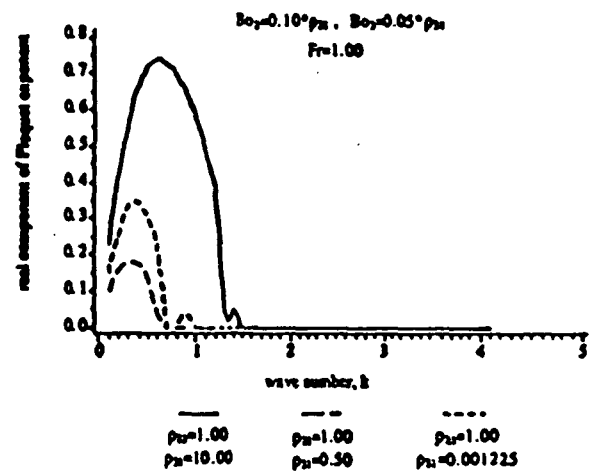

Fig. 10 Effect of density ratios on stability: $Bo_2 = 0.10 \times \rho_{21}$; $Bo_3 = 0.05 \times \rho_{31}$; $Fr = 1.00$.

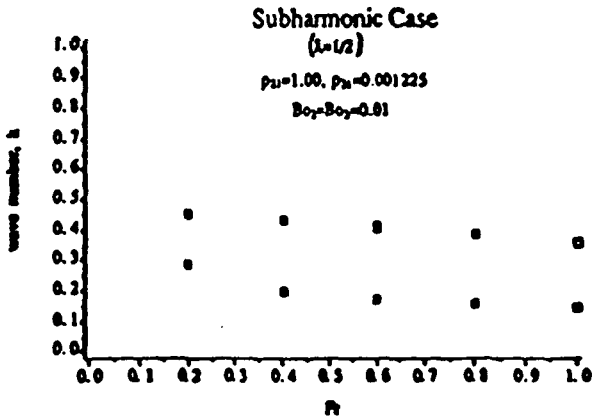

Fig. 11 Subharmonic mode at (Fr,k) values for $Bo_2 = Bo_3 = 0.01$; $\rho_{21} = 1.00$; $\rho_{31} = 0.001225$.

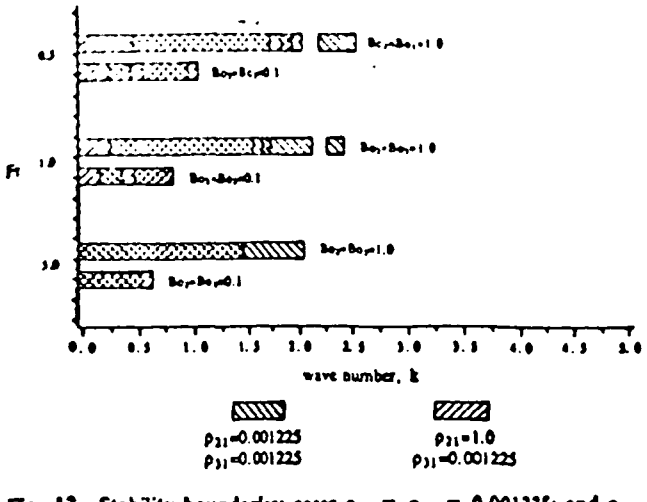

Fig. 12 Stability boundaries: cases $\rho_{21} = \rho_{31} = 0.001225$; and $\rho_{21} = 1.00$, $\rho_{31} = 0.001225$.

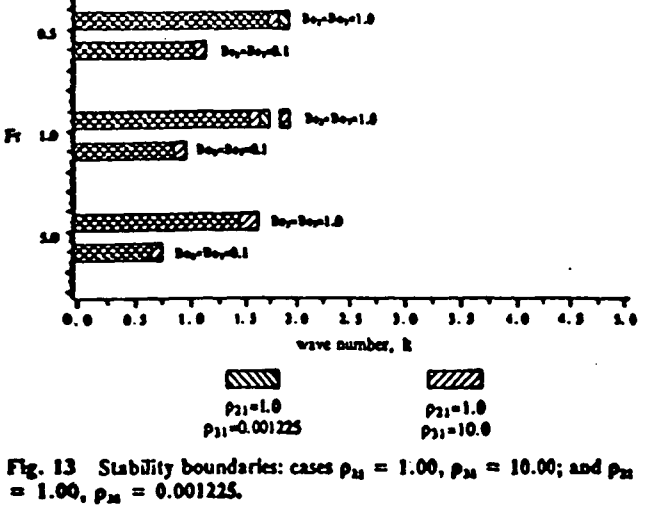

Fig. 13 Stability boundaries: cases $\rho_{21} = 1.00$, $\rho_{31} = 10.00$; and $\rho_{21} = 1.00$, $\rho_{31} = 0.001225$.

Stability boundaries of Fr vs k are plotted in Figs. 12 and 13. (Recall that Fr is inversely proportional to the square of ω_f.) This is done for configurations of different density ratios (as indicated by the different area fill patterns). Moreover, on each graph, multiple values of Bo_2, Bo_3 are represented. The unstable regions are indicated by the rectangular filled regions. No meaning is ascribed to the width of the rectangles.

Conclusions

The effect of periodic accelerations on the stability of a multilayered, two interface, unbounded fluid system has been studied using Floquet analysis. In addition to the wave number, five parameters appear in the problem: Bo_2, Bo_3, Fr, ρ_{21}, and ρ_{31}. Fr is inversely proportional to the square of the forcing frequency, and $Bo_2(Bo_3)$ is inversely proportional to $\gamma_2(\gamma_3)$.

Several trends were discerned in the parameter study. For fixed density ratios ρ_{21} and ρ_{31}, as well as fixed Fr, the range of unstable wave numbers increases as $Bo_2(Bo_3)$ increases. If it is only the parameter Fr that is varied, it is found that the range of unstable wave numbers increases as Fr is decreased. (Note that the variation in Fr values is very limited.) Physical interpretation of these trends has been presented in the preceding section.

Although the comparison is not presented graphically, the multilayered fluid system was found to be, in general, more unstable than the one interface fluid configuration. That is, the range of unstable wave numbers is smaller in the one interface case. In particular, the greatest contrast was in the low k region. This conclusion was determined through consideration of a limit case that involved setting Bo_3 to infinity and ρ_{31} to 1 in order to study the effect of having only one interface using the code developed for the two interface configuration. In this way, the parameters are consistent in both problems.

In the stability boundary diagrams of Figs. 12 and 13, the rectangular filled regions indicate instability. It is clear that, over the indicated range of $Bo_2(Bo_3)$ and Fr values, the configuration is generally unstable at lower wave numbers ($k < 1$). An exception is the gas-liquid-gas configuration ($\rho_{21} = \rho_{31} = 0.001225$) at lower Fr values. Note also that the regions of instability are punctuated by stable regions for the range of Bo values and all but the highest Fr value.

The configuration used in this study was idealized. In an actual space processing application, the fluid configuration would not be infinite in extent. Boundary conditions pertinent to the specific application would have to be taken into account. Nevertheless, the results obtained in this study can be used in a qualitative manner when considering a specific materials processing geometry.

For example, it has been determined that the multilayered fluid system is, in general, unstable over a broader range of k values than the one interface fluid configuration. This has implications for a float zone processing technique in which the fluid cylinder is multilayered. Also, the investigation into the important subharmonic case shows that it occurs at wave numbers that increase with decreasing Fr values. That is, in the more unstable Fr range, the subharmonic (Floquet exponent $\lambda = i$) will occur at smaller values of the perturbation wavelength. A materials processing fluid configuration then could be susceptible to instability due to small wavelength fluctuations in the presence of periodic forcing. The nondimensional idealized system has been studied over the range of parameter values relevant to a microgravity environment (including the Space Shuttle), as can be seen from the Introduction. Configurations involving fluids of specific interest can be investigated at greater length using this methodology.

Appendix

The form of the column vector $\underline{\ell}$ is given by

$$\underline{\ell} = (\ldots E_{n-1}, F_{n-1}, A_{n-1}, B_{n-1}, E_n, F_n, A_n, B_n, \ldots)^T \quad \text{(A1)}$$

The form of matrix $\underline{B}$ is given by

$$\begin{array}{llll} \ldots & -1 & 0 & 0 \\ \ldots & 0 & -1 & 0 \\ \ldots & 0 & 0 & -1 \\ \ldots & 0 & 0 & \{(\rho_{31}-1)/(\rho_{31}+1)\} \end{array} \quad \begin{array}{l} 0\ldots\ldots \\ 0\ldots\ldots \\ \{(\rho_{21}-1)/(1+\rho_{21})\}e^{-2k} \\ -1\ldots\ldots \end{array} \quad \text{(A2)}$$

The form of matrix $\underline{A}$ is given by

$$\begin{array}{llllllllll} \ldots & 0 & 0 & 0 & 0 & in & 0 & -ke^{k} & ke^{-k} & 0 & 0 \ldots \\ \ldots & 0 & 0 & 0 & 0 & 0 & in & -k & k & 0 & 0 \ldots \\ \ldots & \beta 1 & 0 & 0 & 0 & \beta 2 & 0 & in & \beta 3 & \beta 4 & 0 \ldots \\ \ldots & 0 & \beta 5 & 0 & 0 & 0 & \beta 6 & \beta 7 & in & 0 & \beta 8 \ldots \end{array} \quad \text{(A3)}$$

with

$$\alpha 1 = (1 + \rho_{21} + \rho_{31}), \quad \alpha 2 = (1 - \rho_{21})/(1 + \rho_{21})$$

$$\alpha 3 = (1 - \rho_{31})/(1 + \rho_{31}), \quad \alpha 4 = (1 + \rho_{21})$$

$$\alpha 5 = (1 + \rho_{32}), \quad \beta 1 = (Fr/2)e^{-k}\alpha 2$$

$$\beta 2 = (Fr/3Bo_2)k^2 e^{-k}\alpha 1/\alpha 4, \quad \beta 3 = (in)e^{-2k}\alpha 2$$

$$\beta 4 = (Fr/2)e^{-k}\alpha 2, \quad \beta 5 = (Fr/2)\alpha 3$$

$$\beta 6 = -(Fr\,3B\sigma_3)(Ca)^{1/3}\alpha 5, \quad \beta 7 = (in)\,\alpha 3$$

$$\beta 8 = (Fr\,2)\alpha 3$$

Acknowledgments

This work was performed as part of Project JOVE (NAG8-149) for NASA Marshall Spaceflight Center. The authors would like to thank F. Leslie, N. Ramachandran, and C. M. Winter for helpful discussions.

References

[1]Ramachandran, N., and Winter, C. M., "The Effects of G-Jitter and Surface Tension Induced Convection on Float Zones," AIAA Paper 90-0654, Jan. 1990.

[2]Walter, H., *Fluid Sciences and Materials Sciences in Space: A European Perspective*, 1st ed., Springer-Verlag, New York, 1987, pp. 2–13.

[3]Benjamin, T. B., and Ursell, F., "The Stability of the Plane Free Surface of a Liquid in Vertical Periodic Motion," *Proceedings of the Royal Society of London*, Vol. A225, No. 1163, 1954, pp. 505–515.

[4]Gu, X. M., Sethna, P. M., and Narain, N., "On Three-Dimensional Nonlinear Subharmonic Resonant Surface Waves in a Fluid. Part 1—Theory," *Journal of Applied Mechanics*, Vol. 55, No. 1, 1988, pp. 213–219.

[5]Jacqmin, D., and Duval, W. M., "Instabilities Caused by Oscillating Accelerations Normal to a Viscous Fluid-Fluid Interface," *Journal of Fluid Mechanics*, Vol. 196, 1988, pp. 495–511.

[6]Hasewaga, E., "Waves on the Interface of Two Liquid Layers in Vertical Periodic Motion," *Bulletin of the JSME*, Vol. 26, No. 211, 1983, pp. 51–56.

[7]Drazin, P. G., and Reid, W. H., *Hydrodynamic Stability*, 1st ed., Cambridge University Press, London, England, UK, 1982, pp. 353–363.

[8]Kaufman, L., "The LZ Algorithm to Solve the Generalized Eigenvalue Problem," *SIAM Journal of Numerical Analysis*, Vol. 11, No. 5, 1974, pp. 997–1024.

INVESTIGATIONS OF INTERFACE STABILITY IN A MULTI-LAYER FLUID CONFIGURATION UTILIZING WVNET COMPUTATIONAL RESOURCES

Michael Roh
M.J. Lyell
Mechanical & Aerospace
Engineering Dept.
West Virginia University
UOBA0@WVNVM

Abstract

With the increasing opportunities for research in a microgravity environment, there arises a need for understanding fluid mechanics under such conditions. In particular, a number of material processing configurations involve fluid-fluid interfaces which may experience Rayleigh-Taylor type instabilities due to external forcing. Ultimately, the stability of a multi-layer fluid configuration in a microgravity environment subjected to periodic residual forcing,both periodic and non-periodic, is of interest. This forcing may result from various sources, including equipment vibrations and space station maneuvers.

An initial parametric study was performed to investigate the effects of steady forcing due to gravity; in particular, the limit case as gravity goes to zero. Solution of the linearized Euler and continuity equations and imposition of appropriate interface conditions yields a dispersion relation. This was solved using a root finder routine from the IMSL library. The numerical results are presented graphically using SAS/Graph via CMS.

The utilization of a well-integrated system of computational resources is essential for this research.

Introduction

The presence of gravity on earth is so omnipresent a phenomena that its effects often are not realized. In particular, gravity-induced problems arise in manufacturing processes (ie.buoyancy-driven convection in liquids, contamination from vessels that contain samples, and induced stresses that cause defects in crystals).[1,2] An idealized laboratory would be free of gravity "contamination".

(In Proceedings of the 1990 WVNET User Conference
WV Network for Educational Telecomputing
Morgantown, WV)

The effect of gravity has been greatly reduced in low-gravity aircraft flights and drop tubes which provide short periods of microgravity, sufficient for some research, but certainly too brief for most processing experiments. The advent of extended spaceflight has dramatically increased the opportunities for long-duration research and development in a microgravity environment. Space manufacturing can eliminate the gravity-induced problems which are experienced in a terrestrial environment.

The growth of crystals as electronic materials has not reached theoretical performance limits due to defects caused in part by gravity. During the spacelab missions, scientists were able to monitor crystal growth through each stage of its formation. In earth-grown crystals, it can be observed where the seed crystal stops and the new growth begins. The introduction of such a defect was not detected in space due to the lack of gravity-induced convection.[15]

The absence of convection is also pertinent to metallurgical manufacturing. A microgravity environment provides greater understanding of how liquified metals diffuse through each other prior to solidification. Such knowledge is important for the production of improved and novel alloys.

Containerless processing makes possible the production of much improved glasses and ceramics. In such a process, the sample is suspended and manipulated by acoustical and electromagnetic forces without the contamination of a container. Large samples can only be dealt with in a microgravity environment.[10]

Biological processing also benefits from space. Large, pure crystals allow analysis of many unknown protein structures which are essential to the design of new and improved drugs. There is also effort towards the separation and purification of biological substances for pharmaceutical purposes.[9,11]

In the absence of gravity, fluid behavior which might normally be hidden by gravity-driven flows in a terrestrial environment, can be observed and analyzed. Drop and fluid column dynamics in microgravity permit experimentation of basic fluid physics theories.

The environment of board space shuttle is not strictly a microgravity environment. Rather, residual accelerations exist which could affect any ongoing materials science or space processing experiments. A recent summary[12] indicates that accelerations include those in the frequency range of one to ten hertz, with acceleration levels ranging from $10^{-5}*g_{earth}$ to $10^{-3}*g_{earth}$. In addition to periodic forcing (g-jitter), residual accelerations may be of impulse type, due to such causes as station-keeping maneuevers and astronaut motion.[16]

Most processes involve fluid dynamics, and in particular, fluid interfaces. This study does not investigate a specific process per se, but instead considers the stability of fluid interfaces.

Previous work on fluid interfaces in a microgravity has focussed predominantly of the application of fuel slosh in tanks. Most recently, this has included work due to Hung et al[1], which considered g-jitter in a slosh tank. A brief review of earlier work, as well as an extension of the efforts, was given by Gu.[3] These investigations all involved liquid in a container of specified shape with a free surface.

The stability of a single planar free surface subject to periodic forcing in the direction perpendicular to the interface has been investigated[2,3]. Both studies were done in a 1-g ambient environment and required the use of a container. In the work of Benjamin and Ursell[2], the container was cylindrical in shape. The analysis led to a Mathieu equation which governed the time-dependent amplitude of the disturbance. They were able to make statements concerning the interface stability based upon known mathematical properties of Mathieu equations. The case of a rectangular container has been addressed recently bu Gu et al[3], and the results extended into the nonlinear regime. Both of these investigations utilized an inviscid analysis.

Viscous effects of the stability properties has been investigated recently in idealized infinite or semi-infinite configurations which had one fluid-fluid interfaces.[4,5] The forcing was periodic and directed perpendicular to the interface. The work of Jacqmin and Duval[5] assumed a zero mean g-level and pertains to a microgravity environment. A Floquet analysis was applied to the fluid system for the case of sinusoidal forcing.

A multi-layer fluid configuration analysis has been performed by Lyell and Roh.[6] The investigation considers a two-interface configuration in which the middle layer of finite height is situated between two semi-infinite layers of fluid. The analysis is inviscid and incompressible. A zero mean g-level serves as the base state for the study. Two types of time-dependent forcing are investigated, each simulating real microgravity environment accelerations (namely, g-jitter (periodic) and short-duration impulse (non-periodic)).

Prior to investigating the time-dependent forcing on the multi-layer configuration, an analysis was performed for the case of a constant gravitational field. This particular investigation is the subject of this paper.

Problem Description and Equation Development

Fluid configuration stability in the presence of constant acceleration fields is investigated. The limit cases of $1*g_{earth}$ and $0*g_{earth}$ are studied, as well as various intermediate values. Lunar gravity can be approximated by $0.16*g_{earth}$. The $0*g_{earth}$ state will ultimately serve as a basis for investigating the effects of residual accelerations.

The configuration to be considered is comprised of three horizontal fluid layers. No rigid boundaries are present. The layers extend to infinity in the horizontal direction. The top and bottom layers are considered to be semi-infinite in nature, while the middle layer has a finite height. The geometry of the figure is given by Figure 1.

The three fluids are considered quiescent; their mean velocities respectively equal zero. The fluids are immiscible and will be taken as inviscid and incompressible. Surface tension is a property of the interfaces. A normal mode approach to the perturbation is assumed. In a normal mode approach, the disturbance (or perturbation) is assumed to be wavelike. If the wave grows, the fluid system is said to be unstable to the disturbance (perturbation). If the wave decays, the fluid system is stable to the perturbation. This is mathematically represented as follows:

$$\eta = \xi e^{ikx} e^{(-ikc_R t)} e^{(kc_I t)} \qquad (1)$$

where η = interface shape
ξ = amplitude
k = wave number
c_R = real component of propagation speed
c_I = imaginary component of prop. speed

A positive value of c_I will cause growth of the perturbation; and hence, the fluid system will be unstable.

Two cases are investigated:

CASE 1: air/silicone oil/water (region 2/region 1/region 3)
(stable configuration in terrestrial environment)

CASE 2: air/water/air
(unstable configuration in terrestrial environment)

The parameters to be varied include height of middle slab (h), wave number of the perturbation (k), and the value of the

constant gravitational acceleration (g). The propagation speed of the perturbations can be calculated for different parameter conditions. A positive value of the imaginary component of the propagation speed will indicate an instability on the fluid system.

The governing equations of imcompressible fluid mechanics are the continuity equation and the conservation of momentum equation. The analysis is inviscid and linear. Linearization is done about a state of zero mean motion. The following linearized equations govern fluid behavior.

$$\nabla \cdot \underline{u} = 0 \tag{2}$$

$$\rho \frac{\partial \underline{u}}{\partial t} = -\nabla p + \rho g \hat{e}_y \tag{3}$$

where $\underline{u}$ = velocity field
p = pressure

It is straightforward to solve these equations for both the velocity field and pressure. (A velocity potential formulation is utilized in the solution.)

The dispersion relation is obtained by applying three boundary conditions at each interface. These three conditions are: (1) the kinematic boundary condition, which states that a particle of fluid which is at some point on the surface will always remain on that surface, (2) the matching of the normal component of the velocity across each interface, and (3) the normal force balance across each interface.

The boundary conditions are applied to the governing equations, and via manipulation, a dispersion relation is obtained. It is given as follows:

$$\left[(\rho_1+\rho_3)(\rho_1+\rho_2)e^{2kh} + (\rho_2-\rho_1)(\rho_1-\rho_3)\right] c^4$$

$$+ \left[\left\{(\rho_1+\rho_3)\left(\frac{g}{k}(\rho_2-\rho_1)-\tau_2 k\right) + (\rho_1+\rho_2)\left(\frac{g}{k}(\rho_1-\rho_3)-\tau_3 k\right)\right\} e^{2kh} \right.$$

$$\left. + (\rho_2-\rho_1)\left(\frac{g}{k}(\rho_3-\rho_1)+\tau_3 k\right) + (\rho_1-\rho_3)\left(\frac{g}{k}(\rho_2-\rho_1)-\tau_2 k\right)\right] c^2$$

$$+\left[\left\{\left(\frac{g}{k}(\rho_1-\rho_3)-\gamma_3 k\right)\left(\frac{g}{k}(\rho_2-\rho_1)-\gamma_2 k\right)\right\} e^{2kh}\right.$$

$$\left.+\left(\frac{g}{k}(\rho_2-\rho_1)-\gamma_2 k\right)\left(\frac{g}{k}(\rho_3-\rho_1)-\gamma_3 k\right)\right] = 0 \qquad (4)$$

Thus, this propagation speed, c, is the solution of a fourth order polynomial. It is also the eigenvalue of the stability problem which is posed by equations (2) and (3) together with the associated interface conditions. The propagation speed is a complex number, $c = c_R + ic_I$.

An imaginary component equal to zero implies a neutral disturbance. If its value is less than zero, the exponential term decays in time, and the system remains stable. However, if this imaginary component, c_I, is positive, the exponential term grows in time, resulting in an instability.

A limit case which is analytically tractable can be obtained from the full dispersion relation for the special case in which the ratios of the top and bottom densities to the middle density are negligibly small.For such cases, the configuration will remain stable if the following inequality holds true:

$$\frac{\gamma_3 k^2}{\rho_1} \geq g \qquad \text{for} \quad \frac{\rho_2}{\rho_1}, \frac{\rho_3}{\rho_1} \ll 1 \qquad (5)$$

The scope of this study is to analyze the four previously stated cases under various parameter conditions. That is, by allowing the parameters to vary over a specified range, the roots of the dispersion relation can be calculated and, hence, interface stability can be determined. The parameters that are considered are the height of middle layer,the wave number, and the value of the gravitational constant. For our ultimate purposes, we are most interested in the case in which the time-independent gravitational body force is zero.

For a more detailed description of the equation development, see Roh.[13]

The numerical solution and graphical representation of this analytical problem requires a well-integrated host of computer resources. The CMS system was accessed via WVNET on a VT320 terminal. A remote sight at the Engineering Sciences building was used.

The dispersion relation was solved numerically using the DZPORC routine of the IMSL library. The DZPORC routine makes use of the Jenkins-Traub three-stage algorithm[7], in which the roots are computed one at a time for real roots and two at a time for complex conjugate pairs. As the roots are found, the real root or quadratic factor is removed by polynomial deflation.

Two options were explored for graphing the results. Initially the data was downloaded to a diskette via Kermit, which in turn was plotted using Lotus/123 graphics package on a Zenith DS computer. While the output was satisfactory, it was inconvenient and time-consuming to change terminal sites.

The second, and preferred, option was to access CMS directly through a WVNET line connected to a MacIntosh II PC. This was accomplished via VersaTerm and VersaTerm Pro communications. The program calling IMSL routines was run as simply as with a VT320. The data was then transferred to a SAS/Graph routine emulating TEK4014 device, which presented the results graphically. The plots were converted to MacDraw files from which hardcopies were obtained. The advantage to this option is the one-terminal site capabilities.

The numerical results for the time-dependent forcing also accessed several routines from the IMSL library. One solution, in the case of periodic forcing, involved the eigenvalues of a very large complex matrice system. An enormous amount of storage space was required for computation. Temporary disks had to be accessed to provide the necessary space. Details can be found in Roh.[13]

Results and Conclusions

The fourth order polynomial (in c) has four roots. Because of the nature of the dispersion relation, the roots were generated in pairs. That is, for any given solution, there exist two pairs of roots, where each pair consists of the positive and negative values of a number. Physically, for real roots, this means the perturbation may propagate in either the positive or negative direction. For imaginary roots, it implies an instability will occur since these roots

occur in complex conjugate pairs. If all the roots are real, the system will be stable.

Figure 2 shows the four roots of the dispersion relation for Case 1 (air/silicone oil/water). The roots are plotted over a range of gravity ratios (g/g_{earth}) from 0 to 1.0. As might be expected, this case is stable for all parametric conditions. (Note that the non-zero roots are exclusively real.) A less dense fluid above a more dense fluid is stable to small perturbations in the presence of a constant gravitational level.

Figure 3 show the dispersion solution for Case 2. For certain gravity ratios, the presence of a positive imaginary root is revealed, which implies an unstable configuration. This behavior is expected since the configuration has a more dense fluid above a less dense fluid.

Since an instability depends solely on the presence of positive imaginary roots, the subsequent figures will display these particular roots exclusively.

The effect of wave number,(k), on configuration stability is elucidated in Figure 4. As k values increase, the configuration becomes more stable. Thus, since k is inversely proportional to wavelength, the configuration is unstable to long wavelength perturbations. The restoring force required to maintain stability is greater in the long wavelength regime. Note that all cases are stable at $0*g_{earth}$. The results of Case 1 do not appear since the configuration is stable for all parameter space.

From Figure 5, it is tempting to conclude that the middle slab height,(h), has no effect on the stability of the configuration. This conclusion is valid for values of h which are considerably larger than the wavelength (inversely proportional to k). However, as h approaches the order of the wavelength, the effect of the slab height becomes apparent (see Figure 6). The fastest growing instabilities are associated with configurations with the smallest middle layer heights.

The limit case (eq. 5) simulates a liquid layer situated between two layers of a gas, and its accuracy can be verified by comparing it to Figure 4. According to (eq. 5), for Case 2 (air/water/air), and h=1cm, the instability should originate at $g/g_{earth}=0.073$ for k=1, at $g/g_{earth}=0.294$ for k=2, and at $g/g_{earth}=0.661$ for k=3. The results from Figure 4 confirm these values.

It is seen that in the case of zero gravity, each configuration remains stable. Although we might expect Rayleigh-Taylor type instabilities for Case 2, there is no body force which would drive the density difference;hence, the system will remain stable.

This zero gravity state has been taken as the base state for the time-dependent studies. As previously stated, the

presence of g-jitter or manuever type short-duration impulses will play an important role in the stability of multi-interface configurations (see Roh).[13]

References

1) Avduyevsky,V.S. (ed.) Scientific Foundations of Space Manufacturing, MIR Publishers, Moscow, 1984.

2) Benjamin,T.B. and Ursell,F., "The Stability of the Plane Free Surface of a Liquid in Vertical Periodic Motion", Proc. Roy. Soc. Lond., A225, 505, 1954.

3) Gu,X.M., Sethna,P.M., and Narain,N., "On Three-Dimensional Non-linear Subharmonic Resonant Surface Waves in a Fluid: Part 1-Theory", J. Appl. Mech.,55, 213, 1988.

4) Hasewaga, E., "Waves on the Interface of Two Liquid Layers in Vertical Periodic Motion",JSME Bull.,26, 51, 1983.

5) Hung,R., Lee,C., and Wu,J., "Gravity-Jitters and Excitation of Slosh Waves", AIAA Paper 90-0655, 1990.

6) Jacqmin,D. and Duval,W.M., "Instabilities Caused by Oscillating Accelerations Normal to a Viscous Fluid-Fluid Interface", J. Fluid Mech.,196, 495, 1988.

7) Jenkins,M.A., and Traub,J.F., "A Three-Stage Algorithm For Real Polynomials Using Quadratic Iteration, SIAM J.on Num. Anal., 7, 545, 1970.

8) Lyell,M.J. and Roh,M. "Instability of Multi-Layer Configurations in the Presence of Time-Dependent Accelerations in a Microgravity Environment", AIAA Paper 91-0109, 1991.

9) Malacinski,G.M. "Developmental Biology in Outerspace", Bioscience, 39, 314, 1989.

10) NASA. (n.d.) Science in Orbit- The Shuttle and Spacelab Experience: 1981-1986, U.S. Government Printing Office, Washington D.C., 1988.

11) Pool,R. "Zero Gravity Produces Weighty Improvements", Science, 246, 580, 1989.

SECTION E

Copy of Course Syllabus:MAE 399

MAE 399: FREE SURFACE AND INTERFACE FLUID MECHANICS

1. REASON FOR REQUEST FOR MAE 399

The student (Ms. K. Perkins) requires knowledge of free surface fluid mechanics. Moreover, it is necessary that the student learn this material during Fall Semester 1993. This course has information that the student will need to know even before being told of her thesis problem. No other MAE class covers the material which will be taught in this directed study class. As the material has a large mathematical component as well as demanding interdisciplinary fluid physics, it is felt that a structured class is necessary.

The student will be working on a thesis topic in the area of free surface flows in a microgravity environment. The topics covered in this class will provide some (not all!) of the necessary background knowledge.

2. NARRATIVE DESCRIPTION

PREREQUISITES

Co-current registration in MAE 411,
Background of MAE 104 and
Co-current registration in MATH 317.

DESCRIPTION OF COURSE

This is a course in free surface fluid mechanics. It includes both invisicid and viscous flows. The treatment will be equation-based, with both analytical formulations as well as pertinent numerical method approaches to be covered. The conservation of mass, momentum and energy equations will underline the work, of course. In the case of the inviscid formulations, the topics covered will involve traveling surface waves. If the geometry is finite (and the fluid is containerized), the focus will be on standing waves. For the viscous fluid formulation, many practical problems will involve a thermal field and/or a concentration gradient. The analytical formulation becomes much more complex. Marangoni flows become very important, and will be investigated.

Some of the physico-chemical aspects of the free surfaces will be introduced, beyond the basic concept of surface tension. Concepts such as excess surfactants, absorption and desorption, and reaction at the interface will be introduced. This will necessitate the introduction of the diffusion equation (for mass) as another pertinent governing equation. The description of the free surface as an interface will be introduced, along with such concepts as surface viscosity, etc.

The application of free surface flows in microgravity will be covered, also. This will include liquid column (float zone) applications, planar configurations involving Marangoni flows, and a brief introduction to drop dynamics.

Finally, the current state of the art in the computational approaches to resolving wave motion on the interface/free surface and in the determination of bulks flows with a free surface will be elucidated.

3. TOPICAL COVERAGE

I. Free Surface Inviscid Flows

- A. Governing Equations -Inviscid Flows
  Boundary/Interface Conditions: General
- B. Wave Motion - Linearized Problem
  Formulations/Linearization Scheme
  Dispersion Relation - Travelling Waves
  Standing Waves in Finite Containers
  Waves in Forced Containers (Intro)
- C. Nonlinear Wave Motion, Solutions

II. Free Surface Flows/Viscous Effects

- A. Extension of Governing Equations
  Discussion of Restriction to a Newtonian Fluid and Alternative
- B. Boundary/Interface Conditions
- C. Discussion of Physical Examples
- D. Introduction to Computational Methods

III. Free Surface Physico-Chemical Hydrodynamics

- A. Properties Beyond "Surface Tension"
- B. Introduces posibilty of longitudinal waves as well as transverse waves

IV. Free Surface Flows/Thermal Fields

- A. Effect of Thermal Gradient on Surface Tension
- B. Marangoni Flows
- C. Physical Examples, Introduction to Microgravity Applications

V. Free Surface Flows/Concentration Gradients

- A. Surfactants Confined to Interface
- B. Surfactants Absorbing/Desolving in the Bulk
- C. Effect of Concentration Gradient on Surface Tension
- D. Application/Microgravity Examples

VI Additional Computational Methods

- A. Emphasis on Algorithims, Approximations Made (eg. How much does the interface deform?)

REFERENCES

Topic I:

a) I.G. Cupkie
Fundamental Dynamics of Fluids
McGraw-Hill
Chapter 6

b) G.B. Whitman
Linear and Nonlinear Waves
Wiley
Chapter 11, Selected Topics of Chapter 12, Chapter 13, Sections 1-9,10-12

Topic II:

a) Dr. Lyell's Notes

b) Computational Fluid Mechanics
Chow
McGraw-Hill
Sections 2.9, 2.10, 2.11, 3.6, 3.7, 3.8

c) Papers from the Literature including:
H. Bauer's on Natrual Oscillations of Viscoelastic Fluid Drops and/or Cylinders

Topic III:

a) B. Levich
Physico-Chemical Hydrodynamics
Article in the 1963 Annual Reviews of Fluid Mechanics

b) T. Sorensen (Editor)
Dynamics of Fluid Interfaces
Chapters (actually tutorial papers) by Hennenberg and Sanfeld

Topic IV:

a) Dr. Lyell's Notes

b) Sternling and Scriven's Classical Paper

c) Recent Papers from the Literature which Involves Microgravity Formulations (and thus neglect the complicating bouyancy force) including:
* Doi & Koster
Phys. Fluids, 1993
* Myra Carpenter
MS Problem Report/WVU

d) Scientific Foundations of Space Manufacturing
Avdeyevsky
MIR Publishers

Topic V:

a) Scientific Foundations of Space Manufacturing
Avdeyevsky
MIR Publishers

b) JFM Papers by
-Sen & Davis
-Meiburg & Homsy
on Marangoni Flows in Slots with Contamination

Topic VI: papers from the literature: from Physics of Fluids, Int'l J. of Numerical Meth. in Fluids, J. Computational

4. GRADING

HOMEWORK	40%
TEST	25%
COMPUTER PROJECT	10%
REPORT	25%